

A Novel Reactive Distillation Process for the Production of Cyclohexanol from Cyclohexene

Dissertation

zur Erlangung des akademischen Grades

Doktoringenieur

(Dr.-Ing.)

von Dipl.-Ing. Frank Steyer

geboren am 27. Februar 1974 in Göttingen

genehmigt durch die Fakultät für Verfahrens- und Systemtechnik
der Otto-von-Guericke-Universität Magdeburg

Gutachter: Prof. Dr.-Ing. Kai Sundmacher
Prof. Zhiwen Qi

Promotionskolloquium am 14. Dezember 2010

Danksagung

Die Forschungen zu dieser Arbeit wurden während meiner Tätigkeit am Max-Planck-Institut für Dynamik komplexer technischer Systeme in Magdeburg unter der Leitung von Herrn Prof. Dr.-Ing. habil. Kai Sundmacher durchgeführt, dem ich für diese Gelegenheit und die gewährte akademische Freiheit an dieser Stelle zu Dank verpflichtet bin. Herrn Professor Qi, der die Zweitkorrektur übernommen hat und mit dem ich auch einige Zeit zusammenarbeiten durfte, möchte ich für die dafür investierte Zeit und Geduld danken. Ohne meine diversen Kollegen und Mit-Doktoranden wäre diese Arbeit teilweise nur unter wesentlich schwierigeren und insbesondere einsameren Bedingungen möglich gewesen. Vielen Dank für die hilfreichen Diskussionen und die Zusammenarbeit nicht nur an dieser Arbeit. Vielen Dank auch Herrn Prof. Flockerzi - nachdem wir uns verstanden hatten, war die Lösung stets einfacher als gedacht.

Eine experimentelle Arbeit, wie es diese in Teilen ist, profitiert enorm durch die Hilfe der Labor-Mitarbeiter und Studien-, Diplom- und Masterarbeiter, die zusammen mit mir einen großen Teil der erforderlichen Messreihen durchgeführt haben. Insbesondere möchte ich an dieser Stelle Evelin Felsch, Bianka Stein, Beate Seliger und Marianna Savova danken.

Der Bau, Umbau und die Reparatur von experimentellem Gerät, das für die Durchführung dieser Arbeit erforderlich war, wäre ohne die praktische Hilfe der Mechanik- und Elektrowerkstatt schwierig gewesen - insbesondere Herrn Franz und Herrn Könning meinen Dank für ihre stets freundliche und hilfsbereite Art.

Schließlich bin ich meiner Familie und meinen Eltern dankbar für die Geduld und die Bereitschaft, mir die nötige Zeit zur Erstellung dieser Arbeit zu ermöglichen.

Contents

Danksagung	iii
List of Symbols	ix
List of Figures	xvii
List of Tables	xx
Zusammenfassung	xxi
Summary	xxiii
1 Introduction	1
1.1 Reaction System and Process Idea	1
1.2 Reactive Distillation with Liquid Phase Splitting	6
1.3 Brief Literature Overview	7
1.4 Objectives of this Work	10
2 Experimental Methods and Results	11
2.1 Materials	11
2.2 Concentration Measurements	13

2.3	Vapor-Liquid Equilibrium Measurements	14
2.4	Liquid-Liquid Equilibrium Measurements	16
2.5	Reaction Kinetic Measurements	17
2.5.1	Batch Reaction Rate Measurements	17
2.5.2	Continuous Reaction Rate Measurement	18
2.5.3	Concentration Measurement in Reacting Liquid-Liquid Systems .	20
2.5.4	Experimental Setup	21
2.6	Experimental Results and Analysis	22
2.6.1	Vapor Pressure Measurements and Fitted Antoine Parameters . .	22
2.6.2	Vapor Phase Dimerization of Formic Acid	24
2.6.3	Vapor-Liquid Equilibria	25
2.6.4	Liquid-Liquid Equilibria	26
2.6.5	Vapor-Liquid-Liquid Equilibria	27
2.6.6	Reaction Kinetics	32
2.6.6.1	Discussion of Potential Catalysts	34
2.6.6.2	Direct Cyclohexene Hydration	38
2.6.6.3	Cyclohexene Esterification	38
2.6.6.4	Ester Hydrolysis	40
2.6.6.5	Reaction Rate Measurement Results	40
2.6.6.6	Mass Transfer Effects	41
3	Numerical Methods and Results	43
3.1	Global Optimization Algorithm	43
3.1.1	Simulated Annealing & Metropolis Criterion	45

3.1.2	Evolution Strategies	46
3.1.3	Global Evolution Strategy	47
3.2	Objective Functions	50
3.3	Phase Splitting Calculations	53
3.3.1	Homotopy Continuation	53
3.3.1.1	Tie Line Coordinates	55
3.3.1.2	Phase Partitioning Coefficients	58
3.3.2	Rate-Based Approach	59
3.3.3	Numerical Considerations	61
3.3.4	Performance Comparison and Conclusions	62
4	Process Design	71
4.1	Residue Curves	71
4.2	Column Design for Cyclohexene Esterification	74
4.2.1	Residue Curve Map Studies	74
4.2.2	Column Design Consequences	76
4.3	Column Design for FCE Splitting	79
4.3.1	Residue Curve Map Studies	79
4.3.2	Column Design Consequences	82
5	Conclusions and Outlook	85
5.1	Further Work	86
5.2	Process Variations	86
Bibliography		89

Appendices	101
A GC Measurement Method	101
B Sample Chromatogram	115
C Own Publications	121
D Lebenslauf	125

List of Symbols

Greek Variables

α	exponent of φ — $-1, 0$ or 1 with equal likelihood [-]
α_j	product of reactant activities of a reaction j [-]
β	mole fraction of the non-polar phase [-]
γ	activity coefficient [-]
δ	objective function to be minimized [-]
ε	surface fraction on the catalyst [-]
ζ	factor smaller 1 [-]
η	transformed mole fraction in tie-line coordinates [-]
θ	vector of transformed mole fraction variables [-]
ϑ	vector of individual step sizes in global optimization
Θ	matrix of derivatives of linearly independent mole fractions with respect to transformed mole fractions
κ	definition flag [-]
λ	continuation parameter [-]
μ	chemical potential [$\frac{J}{mol}$]
ν	stoichiometric factor [-]
ξ	transformed mole fraction in tie-line coordinates [-]
σ	standard deviation - unit depends on reference base
Σ	analytical Jacobian of the NRTL equation with respect to the x_i
τ	matrix of derivatives of mole fractions with respect to linearly independent mole fractions

List of Symbols

ϕ	vector of normally distributed random numbers
φ	scalar step scaling factor in global optimization [1.4]

Latin Variables

a	Activity [-]
a_{12}	NRTL parameter [-]
A	Antoine coefficient [-]
A_{int}	dimensionless interfacial area between the two phases [-]
B	Antoine coefficient [-]
c_P	molar heat capacity [$\frac{J}{molK}$]
C	Antoine coefficient [-]
dim	dimension of the optimization problem [-]
Da	Damköhler number [-]
E_A	activation energy [$\frac{J}{mol}$]
f	some arbitrary function
g	generation counter in global optimization [-]
g_{12}	NRTL parameter [$\frac{J}{mol}$]
g_{21}	NRTL parameter [$\frac{J}{mol}$]
ΔG_R	molar Gibbs' enthalpy of the reaction [$\frac{J}{mol}$]
h	heterogeneity [-]
$\Delta_f H^0$	molar enthalpy of formation under standard conditions [$\frac{J}{mol}$]
I	individual in global optimization
J	Jacobian matrix
k	kinetic constant - unit depends on kinetic process
K_0	formic acid dimerization equilibrium constant at infinite temperature [$2.4726 \times 10^{-14} Pa^{-1}$]
K_{eq}	equilibrium constant based on mole fractions - unit depends on reaction
K_{SLE}	solid-liquid equilibrium constant [-]
lb	lower bound

m	mass [kg]
n	molar amount [mol]
P	pressure [Pa]
\mathcal{P}	likelihood of acceptance in Metropolis criterion [-]
q	some arbitrary quantity to be fitted
r	specific reaction rate - unit depends on whether it is a homogeneous reaction ($[\frac{1}{s}]$) or a heterogeneous reaction ($[\frac{mol}{kg_{cat}s}]$)
R	Universal Gas Constant [$8.314 \frac{J}{molK}$]
\mathcal{R}	reaction rate [$\frac{mol}{s}$]
S^0	molar entropy of formation under standard conditions [$\frac{J}{molK}$]
t	time [s]
T	temperature [K]
ub	upper bounds
x	liquid mole fraction [-]
y	vapor mole fraction [-]
z	vector of optimization variables in global optimization

Subscripts

$_$	flux - e.g. \underline{n} is a molar flux
0	under standard conditions
γ	activity coefficient
A	reactant A
B	reactant B
cat	catalyst
C	reactant C
D	reactant D
eq	equilibrium
f	forward

List of Symbols

<i>FA</i>	formic acid
<i>FCE</i>	formic acid cyclohexyl ester
<i>i</i>	index for chemical species
<i>in</i>	inflow
<i>int</i>	interfacial
<i>j</i>	index for chemical species
<i>k</i>	iteration counter
<i>l</i>	index for chemical species
<i>LLE</i>	liquid-liquid equilibrium
<i>m</i>	index for chemical species
<i>n</i>	index for individual experimental data
<i>NC</i>	number of chemical components
<i>out</i>	outflow
<i>P</i>	pressure
<i>q</i>	arbitrary quantity to be optimized
<i>r</i>	index for reaction
<i>start</i>	starting conditions
<i>SLE</i>	solid-liquid equilibrium
<i>tot</i>	overall / total
<i>T</i>	temperature
<i>VLE</i>	vapor-liquid equilibrium
<i>x</i>	liquid mole fraction
<i>y</i>	vapor mole fraction

Superscripts

0	under standard conditions
<i>calc</i>	calculated
<i>exp</i>	experimentally measured

<i>het</i>	heterogeneous
<i>hom</i>	homogeneous
<i>nonpolar</i>	non-polar liquid phase
<i>NC</i>	number of chemical components
<i>NLLE</i>	number of liquid-liquid equilibrium measurement points
<i>NP</i>	number of measurement points
<i>NR</i>	number of reactions
<i>NVLE</i>	number of vapor-liquid equilibrium measurement points
<i>polar</i>	polar liquid phase
<i>ref</i>	reference
<i>sat</i>	saturation
<i>t</i>	"true" values
<i>tot</i>	overall / total

List of Figures

1.1	Production routes and use of cyclohexanol.[45]	2
1.2	Asahi production process for cyclohexanol by cyclohexene hydration [42]	4
1.3	Proposed “ideal” column configuration	5
1.4	The indirect reaction scheme suggested for cyclohexanol production.	6
1.5	Suggested two-column configuration for cyclohexanol production with intermediate ester formation.	7
2.1	Vapor-liquid measurement device type FISCHER VLE 602	15
2.2	Reaction kinetic measurement setup	21
2.3	Vapor-liquid equilibrium measurement results and computations	27
2.4	Ternary liquid-liquid measurement results and computations	28
2.5	Effect of catalyst placement on reactant availability at catalyst sites - spherical membranes as ideal catalysts. a: catalyst in aqueous phase, b: catalyst in organic phase, c: catalyst between phases, d: spherical catalyst membrane between organophilic and aqueous phases	35
2.6	REM images of metal column packings coated with HZSM5-type zeolite catalyst particles. a: overview showing accumulations at intersections, b: individual wire with homogeneous, thin coating, c: close-up of coating layer with defects	37

2.7	Comparison between computed (-) and measured reaction rate constants k for the Amberlyst 15 catalyzed direct cyclohexene hydration reaction. Squares denote the measured reaction rate constants for cyclohexanol formation, circles denote the measured values for cyclohexanol splitting.	39
2.8	Comparison between computed (-) and measured reaction rate constants k for the cyclohexene esterification reaction. Squares denote measured Amberlyst 15 catalyzed reaction rate constants (in $\ln(\text{mol}/\text{kgs})$) for the backwards reaction, circles denote the homogeneously catalyzed reaction rate constants (in $\ln(1/\text{s})$) of the forwards reaction.	39
2.9	Comparison between computed (-) and measured reaction rate constants k for the ester splitting reaction. Circles denote measurement values for the uncatalyzed backward reaction rate constant (in $\ln(1/\text{s})$), squares denote the Amberlyst 15 catalyzed measurement values of the rate constant for the forward reaction (in $\ln(\text{mol}/\text{kgs})$).	40
4.1	Non-reactive residue curves for cyclohexene esterification system at $P=100$ kPa and $P=10$ kPa	75
4.2	Reactive residue curve maps for cyclohexene esterification system at $P=10$ kPa and different values of the homogeneous Damköhler number	76
4.3	Changing location of the stable node as a function of Damköhler number for the cyclohexene esterification system at $P=10$ kPa.	77
4.4	Suggested reactive distillation column configuration for cyclohexene esterification. Shown concentration profiles are based on combined residue curve computations and do not consider feed point locations	78
4.5	Non-reactive residue curves for the FCE splitting reaction system at $P=10$ kPa	80
4.6	Residue curves for the FCE splitting reaction system at chemical equilibrium and $P=10$ kPa	81

4.7	Residue curve map for the FCE splitting reaction system at chemical reaction equilibrium using transformed composition variables [2] at P=10 kPa	81
4.8	Suggested reactive distillation column configuration for FCE splitting. Shown concentration profiles are based on combined residue curve computations and do not consider feed point locations.	83
5.1	Suggested flow sheet for a new indirect cyclohexene hydration process for the production of cyclohexanol using two reactive distillation columns.	85
5.2	Column integrating both reaction steps into one column with two catalytic zones. Formic acid as the reactive entrainer is trapped in the column and only needs to be replenished to compensate for losses.	88

List of Tables

2.1	Antoine parameters, valid temperature ranges and standard deviations between measurements and computations for the six components. Parameters for formic acid were fitted to literature data [55, 75].	24
2.2	NRTL parameter set identified for the six-component system and the standard deviations associated with the parameter set. The σ_{LLE} numbers are for the ternary systems according to Figure 2.4, the letter in parentheses denoting the sub-figure meant.	31
2.3	Thermodynamic data and Langmuir sorption constants used for the computation of the temperature dependent equilibrium constants.	41
2.4	Reaction kinetic parameters fitted to experimental data	41
3.1	Parameterizations, number of variables and computation times for the example taken from [70] with the four components propanol, butanol, benzene and water using the NRTL parameters reported there. All algorithms found the same LLE solution. (“BM” - original Bausa & Marquardt algorithm, “Tie” - tie line approach, “Part” - phase partitioning coefficients, “Rate” - rate based approach)	63
3.2	Computation times, overall composition (x^{tot}) and correct two phase solution ($x^{nonpolar}$ and x^{polar}) for the three algorithms (“Tie” - tie line approach, “Part” - phase partitioning coefficients, “Rate” - rate based approach) and the different number of components.	65

3.3 Computation times, and overall composition (x^{tot}) for the three algorithms (“Tie” - tie line approach, “Part” - phase partitioning coefficients, “Rate” - rate based approach) and the different number of components. Correct solution shows only one phase. 66

3.4 Computation times for the three algorithms (“Tie” - tie line approach, “Part” - phase partitioning coefficients, “Rate” - rate based approach) and the different number of components. The overall composition was $x_{Water} = 0.00153$, $x_{Cyclohexene} = 0.99847$, all other components had zero mole fraction. The correct solution found by all algorithms is $x_{Water}^{nonpolar} = 0.0015296$ and $x_{Cyclohexene}^{polar} = 4.6043 \times 10^{-5}$ with a mole fraction of the small phase of less than 4×10^{-7} 67

3.5 Computation times for the three algorithms (“Tie” - tie line approach, “Part” - phase partitioning coefficients, “Rate” - rate based approach) and the different number of components. The overall composition was $x_{Water} = 0.00152$, $x_{Cyclohexene} = 0.99848$, all other components had zero mole fraction. The correct solution found by all algorithms has only one phase with the same composition. 68

Zusammenfassung

Die vorliegende Arbeit befasst sich mit der Entwicklung eines neuen Produktionsprozesses zur Herstellung von Cyclohexanol aus Cyclohexen mittels Reaktivdestillation. Die Hydratisierung des Cyclohexens wird dabei über den Umweg der Veresterung mit Ameisensäure und nachfolgender Esterhydrolyse vorgenommen. Dieser neue Produktionsprozess ist aus ökonomischen und ökologischen Gründen sowie aus Gründen der Anlagensicherheit dem bestehenden, auf der Partialoxidation von Cyclohexan beruhenden Prozess überlegen.

Um den Prozess simulieren und auslegen zu können, werden effiziente Lösungsmethoden für die Berechnung des Flüssigphasenzerfalls benötigt. Diese werden im Rahmen der vorliegenden Arbeit erarbeitet und dargestellt. Weiterhin wird ein neuer Globaloptimierungsalgorithmus entwickelt und vorgestellt, der für die Parameteranpassung der benötigten Modellparameter für die Flüssig-Flüssig-, die Dampf-Flüssig- Gleichgewichte und die Reaktionskinetiken verwendet wird.

Ein wesentlicher Teil der Arbeit widmet sich der Messung der benötigten Modellparameter für den Phasenzerfall im Sechsstoffsystem Cyclohexen, Wasser, Cyclohexanol, Cyclohexan, Ameisensäure und Ameisensäurecyclohexylester. Es werden Parameter für die Berechnung der Aktivitätskoeffizienten, der Dampfdrücke sowie der Reaktionsgeschwindigkeiten ermittelt.

Die Machbarkeit des neuen, aus gekoppelten Reaktivdestillationskolonnen bestehenden, Gesamtprozesses wird anschließend mit Hilfe von Rückstandskurven belegt. Darauf basierend werden erste Prozesskonfigurationen vorgeschlagen.

Summary

This work presents a novel reactive distillation process for the production of cyclohexanol from cyclohexene. Cyclohexanol is produced by indirect hydration of cyclohexene via formic acid cyclohexyl ester (FCE). The proposed route from cyclohexene to cyclohexanol seems advantageous in economic, ecologic and safety aspects when compared to the conventional process based on partial oxidation of cyclohexane.

To be able to simulate this process, efficient algorithms to compute liquid-liquid phase splitting are needed which are developed and presented as part of this thesis.

Also, a global optimization algorithm is developed and presented which was used to determine the necessary parameters for liquid-liquid and vapor-liquid phase equilibria as well as reaction kinetics from experimental data.

An important part of this work are measurements performed to determine liquid-liquid and vapor-liquid phase splitting as well as reaction kinetics within the six component system cyclohexene, water, cyclohexanol, cyclohexane, formic acid and FCE. Parameters for computing activity coefficients, vapor pressures and reaction rates are also presented.

The feasibility of the proposed new process comprised of two coupled reactive distillation columns is demonstrated using reactive residue curve maps. Preliminary process configurations are proposed based on the results obtained.

1 Introduction

Since reactive distillation has first been employed on a large scale for the production of methyl acetate in the middle of the 1980s, interest in this integrated process has dramatically increased. This interest has been both on the academic and industrial sides and has led to several additional bulk chemicals which are produced by way of reactive distillation today. Most notable under these are the fuel ethers of which MTBE (methyl-*tert*-butyl ether) is the most well known and has the largest production capacity installed worldwide. Its use as an anti-knock gasoline additive is the reason for the large capacity installed as it has allowed to replace lead compounds in gasoline. The dispersion of MTBE into the environment where it is non-degradable in ground water on the other hand has led to its use being restricted in some parts of the world today.

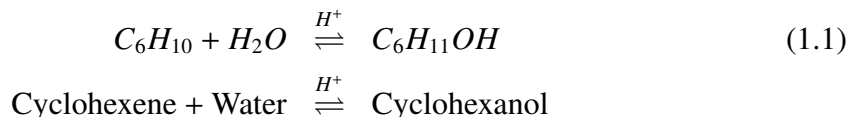
As both the methyl acetate and MTBE production processes have been studied extensively and are understood quite well today a new reaction system was chosen for this work. The reaction system was chosen both for its commercial attractiveness and because it showed an additional challenging feature apart from its reaction and distillation behavior: liquid-liquid phase splitting.

1.1 Reaction System and Process Idea

Of the systems that have frequently been used in the reactive distillation literature most do not exhibit large regions where phase splitting occurs. In fact most do not exhibit phase splitting at all. If liquid phase splitting is to be a focus of this work the system being studied should contain a large phase splitting region to assure that the resulting column designs have at least certain regions in which phase splitting occurs or show phase

splitting as a transient behavior.

For this reason the acid catalyzed production of cyclohexanol from cyclohexene and water was chosen:



The commercial interest in this reaction lies in the fact that cyclohexanol is an intermediate in nylon production as it can be oxidized to cyclohexanone and further to adipic acid or ϵ -caprolactam which is then used in nylon polymerization as can be seen in Figure 1.1. Currently, cyclohexanol / cyclohexanone mixtures are produced by partial oxidation

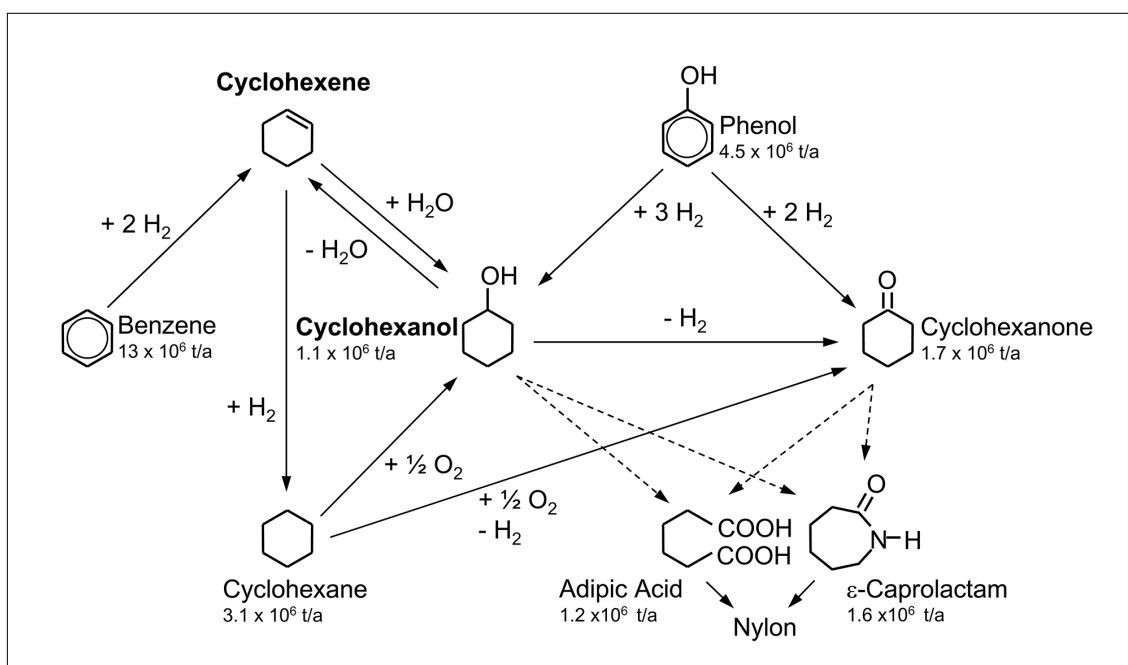


Figure 1.1: Production routes and use of cyclohexanol.[45]

of cyclohexane via cyclohexene (see Fig. 1.1). This process suffers from several drawbacks however. The first is the fact that three hydrogen molecules are needed to produce cyclohexane from benzene. This high hydrogen demand is energy-intensive because the hydrogen consumed by it has to be produced e.g. from natural gas which leads to carbon dioxide emissions. The hydrogen demand of the process could be reduced by one third if cyclohexene were used instead of cyclohexane.

The second drawback lies in the low selectivity of partial oxidation reactions. Even

though air is usually fed stepwise in a reactor cascade and the overall conversion is kept low to avoid formation of subsequent oxidation products the overall selectivity of the conventional process is reported only to be in the range of 70-80% [45]. Considering that the production capacity installed in western Europe alone is more than 1 million tons per year [45] the amount of side products is significant. The cyclohexene hydration reaction however has been reported to show very little amounts of side products, reaching almost 100% selectivity under suitable reaction conditions [28, 42].

The third and most important drawback of the conventional process lies in the inherent risk associated with the direct oxidation route. In this process air is mixed with cyclohexane. During this mixing procedure the region of potentially explosive air / cyclohexane mixtures has to be crossed. If an ignition source is available and active in this mixing region, explosions can occur — as has been the case in at least one incident with several fatalities and the destruction of the facility [76]. The alternative route to cyclohexanol from cyclohexene uses water instead of air making the process inherently safe since explosive air / cyclohexane mixtures are never formed.

As the idea to replace the conventional process with the cyclohexene hydration process seems very attractive, others have previously considered doing so. Especially Asahi Chemical, Japan, has built several plants using the reaction given in Equation 1.1 [28, 42]. Their process uses a slurry reactor filled with the two reactants and large amounts of a very fine-grained HZSM5-type zeolite catalyst. The process is depicted in Figure 1.2. After the slurry reactor a settler separates the two liquid phases. The catalyst is found exclusively in the aqueous phase, which is recycled to the reactor. The organic phase is distilled to separate the product cyclohexanol from unreacted cyclohexene. Due to low equilibrium conversion to cyclohexanol (of only around 14% [6, 45]) the larger part of the organic stream is then recycled back to the reactor. An additional problem encountered in the Asahi process is the fact that the partial hydrogenation of benzene to cyclohexene, which was also developed by Asahi Chemical, can never be completely selective at full conversion. This leads to certain amounts of cyclohexane and benzene in the cyclohexene feed, which are hard to separate from the cyclohexene due to low differences in boiling point. To avoid an accumulation of the inerts in the organic phase beyond an acceptable level, a certain amount of organic phase has to be purged from the plant, also leading to losses of

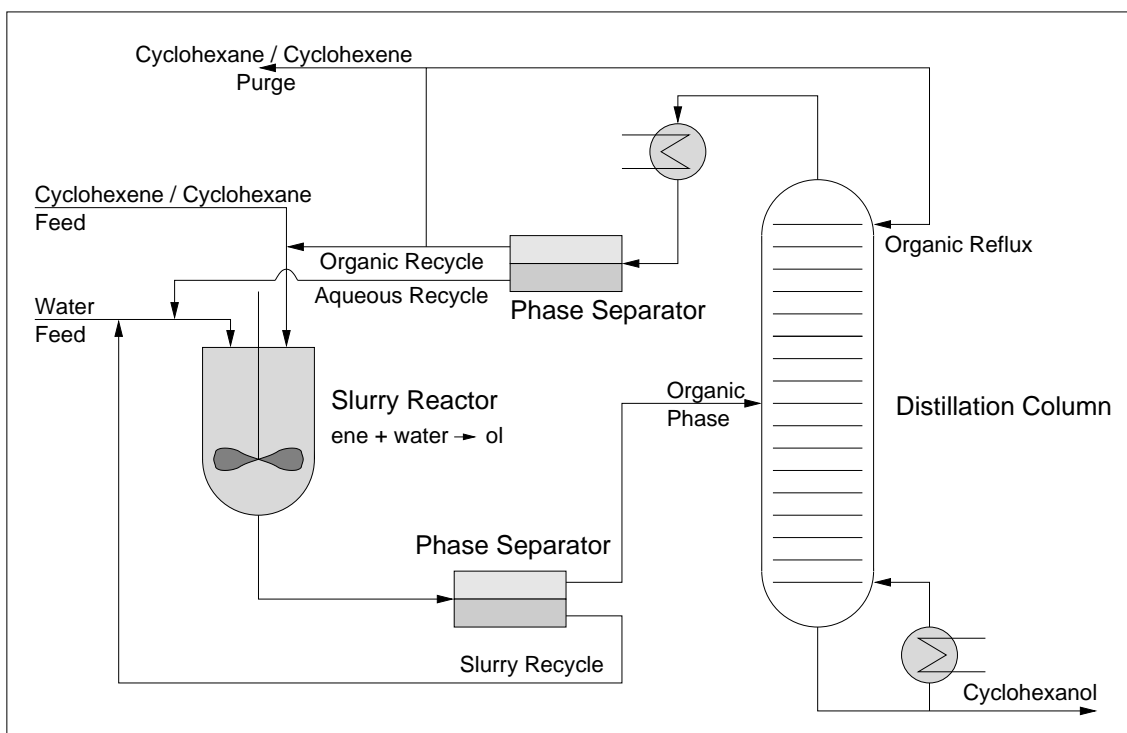


Figure 1.2: Asahi production process for cyclohexanol by cyclohexene hydration [42]

cyclohexene.

As the reaction is slightly exothermic ($\Delta_R H^0 = -28181 \text{ J/mol}$) and equilibrium limited, it seems well suited to be performed in a reactive distillation column, which would also internalize the external recycles mentioned before [64]. Ideally, such a column would be fed with cyclohexene (including the inerts) at the bottom of a reactive zone and with water at the top of the reactive zone. The two reactants would be contacted in a counter-current manner. The pure inerts would leave the column at the top, the cyclohexanol would leave at the bottom. This initial ideal process idea is depicted in Figure 1.3. For this process to work technically, the design procedure has to assure favorable vapor- and liquid-liquid behavior as well as sufficient reaction rates. Unluckily however, the reaction rate is almost nonexistent when uncatalyzed and is still very slow when catalyzed with standard acidic ion exchange resins. The zeolites used by Asahi on the other hand are extremely fine particles [28, 42] that are almost impossible to immobilize within the column making them badly suited for reactive distillation.

Due to the reaction rate limitations, an intermediate step has to be introduced, namely the

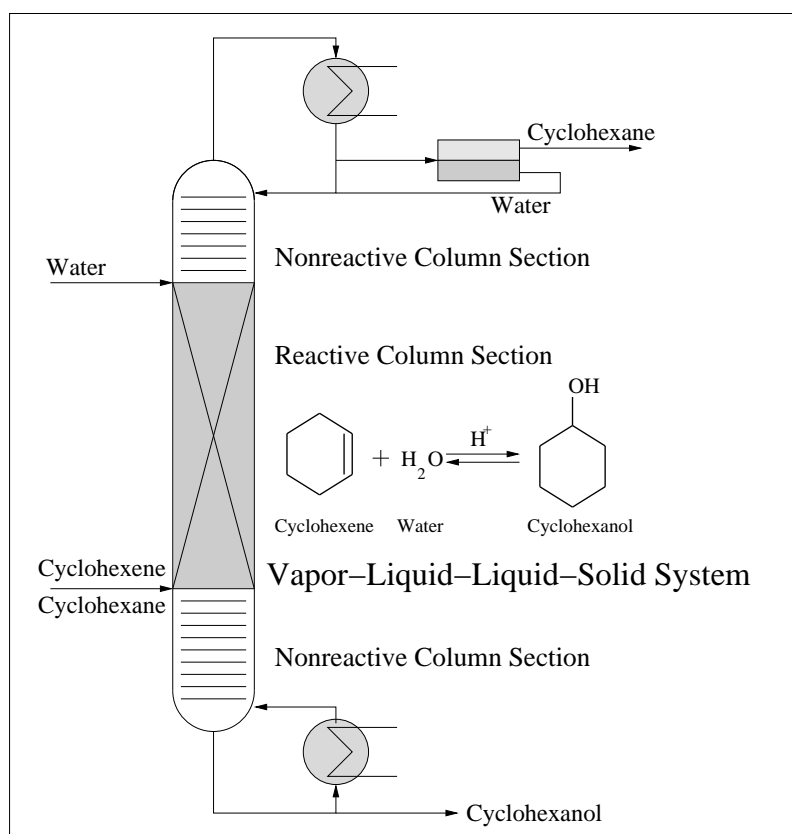
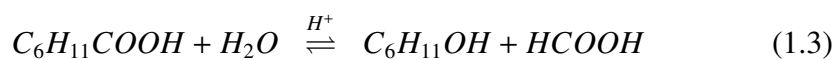
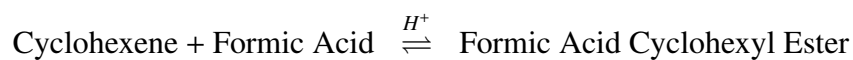


Figure 1.3: Proposed “ideal” column configuration

addition of formic acid to cyclohexene instead of the water addition reaction. The ester formed is then split back with water into the desired product cyclohexanol and into formic acid, which is recycled within the system. The two reactions are as follows:



If one adds the reactions in Equations 1.2 and 1.3, the same overall reaction as given in Equation 1.1 results. The reaction rates in the two reaction schemes will be shown to be much faster [67] so that a technical process consisting of two coupled reactive distillation columns seems possible. Figure 1.4 shows the overall reaction scheme graphically: The according column configuration idea is shown in Figure 1.5.

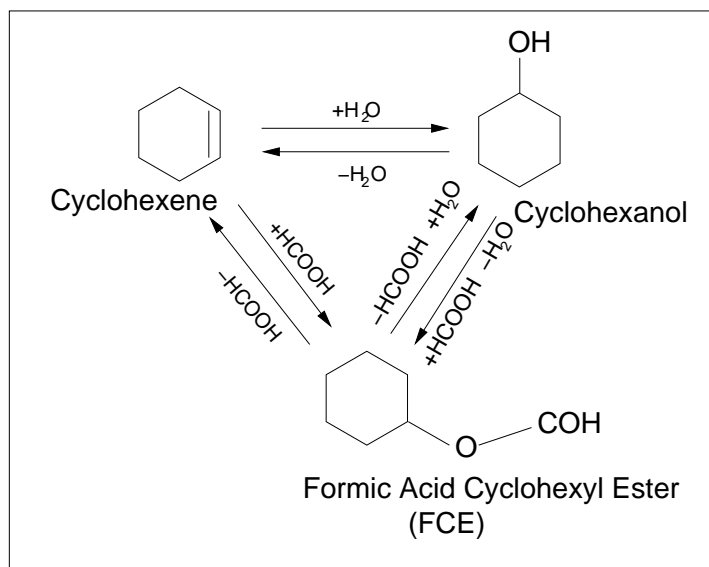


Figure 1.4: The indirect reaction scheme suggested for cyclohexanol production.

1.2 Reactive Distillation with Liquid Phase Splitting

The fundamental investigation of the effect of liquid phase splitting on reactive distillation is interesting as many likely candidate reactions to be carried out in a reactive distillation column show this effect. Examples are esterification reaction systems that are equilibrium limited and contain azeotropes — a combination that made the methyl acetate process so successful. Due to the very high complexity of these processes and their operation, very detailed and thorough investigations are needed to reduce the amount of uncertainties that would otherwise inhibit industrial adoption of such a new combined process.

Part of such initial investigations has to be the development of a simulation model that describes the process. Such a model can both be used to help in scale up and optimization of the process as well as to show the amount of understanding of the process already achieved. Modeling such systems is a challenge, however, since the phase splitting problem has to be solved for every unit that is to be modeled for every time step. As the phase splitting calculation is a search for the global minimum of the Gibbs' enthalpy, when done rigorously the computational costs associated with the highly repetitive phase splitting calculations are very high. In addition to this, one needs accurate model parameters to describe both the vapor-liquid and the liquid-liquid equilibria which are usually not

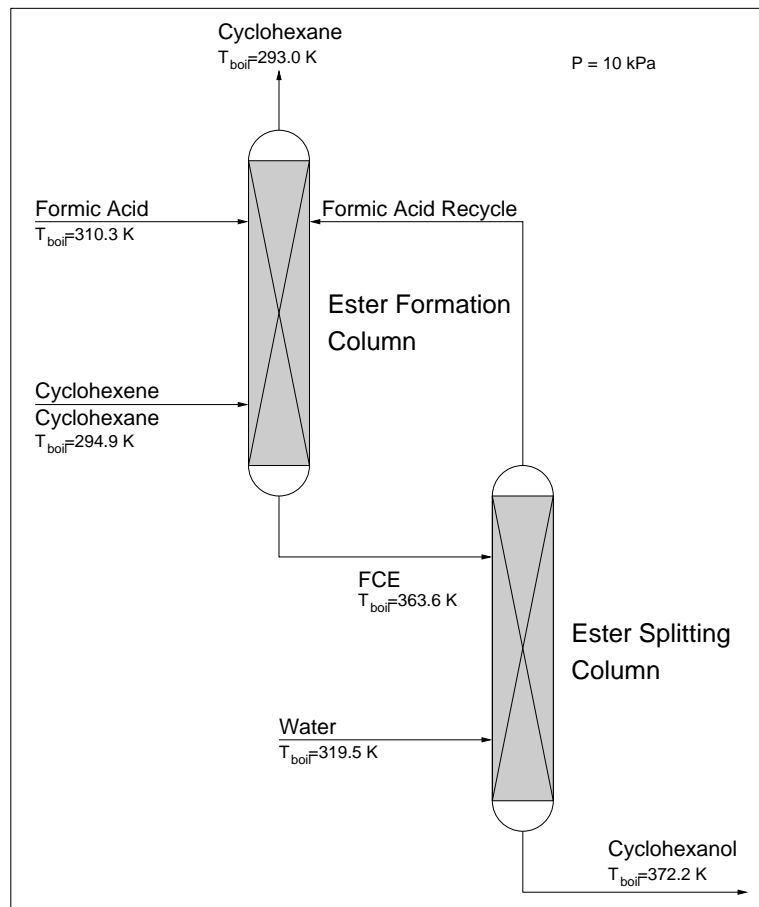


Figure 1.5: Suggested two-column configuration for cyclohexanol production with intermediate ester formation.

available in the literature. Finally, the rates of the reactions to be carried out in the target system have to be known in the two-phase system. Their measurement is a challenge in itself.

1.3 Brief Literature Overview

When designing a new reactive distillation process, an intimate knowledge of the different thermodynamic and reaction kinetic processes is needed. Due to the integrated nature of the process, the distillation and reaction trajectories in composition space will interact which can lead to the disappearance of distillation and reaction boundaries (e.g.

azeotropes and reaction equilibrium points). At the same time, the superposition of reaction and distillation can lead to the formation of new reactive separation boundaries which will often depend on the ratio of reaction and distillation rates which is usually expressed as the Damköhler number.

To allow a better understanding of the overall effects these phenomena have, the group of Doherty [2, 73] has developed a method called “residue curve maps” for plotting feasible column top and bottom products and the ranges within composition space that lead to them. Starting from initial multicomponent distillation feasibility studies, they have added reaction into the method to allow for studying reactive distillation under a certain set of assumptions. Similar work has been performed by the group of Stichlmair [16]. This work was recently extended to include mass transfer considerations imposed e.g. by membrane separation by Huang et. al [27], to include the effects of liquid phase splitting by Qi et. al. [49] and to include the effects of noncondensable reactants by Ivanova et al. [29] all of which are from the group of Sundmacher.

Sundmacher was also the first to consider the effect of mass transfer and non-equilibrium effects in reactive distillation [68]. Later, especially the group of Taylor and Krishna [26, 25] have done extensive analysis of reactive distillation from this perspective and have shown that mass transfer limitations can even allow crossing reactive separation boundaries. As part of the mass transfer issues, an increased amount of work is going into the modeling of fluid holdup, transport and residence time for given column internals and load conditions using computational fluid dynamic (CFD) approaches [74]. CFD modeling of liquid flow in catalytic bales within columns is very computationally intense work and has not been done for systems with two liquid phases undergoing reaction. Some work performed by Repke et al. [54] on non-reactive distillation with two liquid phases suggests that ignoring the presence of two liquid phases can lead to errors in mass transfer computations under certain circumstances.

Based on these more rigorous rate based models we increasingly understand the dynamic behavior of reactive distillation systems. These can be quite nonlinear and complex as e.g. Mohl et al. showed for MTBE synthesis [44, 43] which can exhibit quite some steady state multiplicities. As a reaction to this complexity, Grüner et al. [21] and others have responded with the design of control schemes to be able to safely run these processes.

Of equal importance are startup simulations which allow computing whether the desired steady state is achievable and to determine the trajectory to reach the desired steady state. Simulations of this type for reactive distillation columns have been carried out by Reepmayer et al. [51] and others.

From the perspective of literature on reactive distillation with liquid phase splitting there is not much literature available. Apart from the theoretical work done by Qi et al. mentioned above, Gumus and Ciric [22] have used aniline production, which shows phase splitting behavior, as a numerical challenge for one of their algorithms. Of the many publications on butyl acetate production via reactive distillation (e.g. by Gangadwala et al. [17], Löning et al. [36], Venimadhavan et al. [77]), Zhicai et al. [83]) — a reaction system that can exhibit liquid phase splitting in a small region of composition space — only Brüggemann et al. [8] explicitly include the phase splitting behavior into their computations.

The amount of literature available on the reaction system being considered here is very limited. The direct hydration of cyclohexene to cyclohexanol was studied by Pannemann et al. [46] using large amounts of co-solvents to overcome phase splitting. Due to the change in composition and the resulting change in activities and due to the fact that they chose a very high boiling co-solvent, this data was of little use for a reactive distillation treatment. The group of Sharma [81] has studied the direct hydration of cyclohexene using different catalysts. Their results showed that zeolite catalysts are superior to Amberlyst 15 but unluckily they do not report any reaction kinetic equations based on their measurement results. Sharma's group also studied the esterification of cyclohexene with formic acid [15] — a reference that helped us choose formic acid as the reactive entrainer. Unluckily, they did not publish any reaction rate equation for the reaction catalyzed by Amberlyst 15. However, this is one of the very rare references to FCE we have been able to find in the literature at all.

1.4 Objectives of this Work

The main objective of this work is to show the feasibility of the proposed alternative route from cyclohexene to cyclohexanol. This is seen as the first step towards the development of this new process which seems attractive economically, environmentally and from a plant safety perspective.

As part of this central objective, some first steps are taken into exploring the potential challenges of reactive distillation in reaction systems undergoing liquid-liquid phase splitting. During the development process the necessary tools needed for the numerically efficient treatment of the liquid-liquid phase splitting problem are developed and the parameters needed for simulating reaction rates and phase behavior are measured and extracted from the measurement data.

2 Experimental Methods and Results

Integrating reaction and distillation into one unit operation — a reactive distillation column — can save both investment and operational costs. The price of this integration lies in more complicated operational behavior and in a much more difficult design process. Adding a third effect such as phase splitting makes matters even more challenging. One of the main reasons for the difficulties of designing such processes lies in the fact that very accurate thermodynamic data is needed in the form of vapor-liquid and liquid-liquid equilibria and in the form of reaction kinetics. Without a precise data set that allows to determine the appropriate parameters for the equations describing these phenomena, a model-based design of such a process can lead to significant deviations between simulation and the real process once it has been implemented. As deviations in some design variables can break the real process (e.g. it is very hard to introduce more catalyst after setting up the process when using catalyst bales), precise measurement data is highly desirable to avoid such problems.

For this reason an effort was undertaken to measure a consistent and accurate set of data to be used for identifying the appropriate parameters. The methods and materials used for this purpose are described in this chapter.

2.1 Materials

In the following chapters that describe the experimental setups and methods, chemicals are mentioned frequently. These chemicals were acquired from the following sources and pre-treated as follows:

Cyclohexene, cyclohexane, cyclohexanol and formic acid were bought from VWR International GmbH in synthesis quality (>99%). They were used as delivered except for cyclohexene which was distilled twice using a rotary evaporator at reduced pressure to remove the high boiling stabilizer. Water was drawn from a deionizer type Millipore Milli-Q.

The catalysts used during the experiments were Amberlyst 15 (produced by Rohm & Haas) from VWR and several zeolite catalysts (HMOR-20, HMOR-40, HMOR-90, BETA, and FMI-90) from Südchemie AG. Also some additional experimental zeolite catalysts of the HZSM-5 type were prepared by the group of Schwieger at Erlangen University, Germany.

Formic acid cyclohexyl ester had to be produced in-house as no supplier could be found for it. The synthesis was performed by mixing cyclohexene and formic acid at a slight stoichiometric excess of formic acid. The reaction was catalyzed by Amberlyst 15 with a volume fraction of the overall reaction mixture of approximately 5%. The mixture was then heated in a rotary evaporator to 60 °C for four hours while being agitated by rotation at approximately 90 rpm. After these first four hours the temperature was raised to 80 °C for another two hours. The reaction was carried out at ambient pressure and no distillation effects were seen or desired at this point. During the reaction the second liquid phase that was present initially disappeared.

After the end of the reaction, the catalyst was filtered from the reaction mixture which had turned greenish brown. The catalyst was washed in isopropanol and water to remove any reactants and products from it and then dried in a vacuum oven (80 °C at 10 mbar over night) before being used again in subsequent synthesis runs. The reacted mixture was then washed three times with water to extract the remaining formic acid which is a catalyst itself. This led to the organic mixture turning a clear yellow color while the watery phase stayed colorless. The organic mixture was then distilled three times in a rotary evaporator at reduced pressure.

The first distillation was to remove most of the unreacted cyclohexene. It was done without any reflux at 50 °C bath temperature and 90 mbar pressure until no significant distillate stream was produced any more.

The second distillation was done to remove the high boiling dark side product that was

responsible for the yellow color. To do this, almost the complete remaining mixture was evaporated in the water bath at 90 °C and 20 mbar without permitting any reflux. The condensed mixture was collected in the distillate bottle. The final 2-5 ml (approximately 0.2% of the overall amount) were then disposed of, containing all of the dark side reaction product. At this point, the residue being disposed of was still mainly formic acid cyclohexyl ester. The dark, high-boiling side product was only a trace overall. Its identity was not clarified as we were not able to analyze it via GC-MSD due to its high boiling point (no potential peaks were found even at 360 °C - the maximum temperature of the column being used). The purity of the formic acid cyclohexyl ester in this second distillate was roughly 95%.

This mixture was then distilled again at 65 °C bath temperature and 20 mbar under complete reflux — essentially a closed system except that the condenser was not able to condense the cyclohexene under these conditions completely. The cyclohexene was condensed in a glass spiral condenser behind the vacuum pump and removed this way. After roughly five to six hours this complete-reflux distillation run was stopped when the purity of the formic acid cyclohexyl ester had surpassed 98% in a GC-MSD analysis (percentage based on peak area). The main remaining impurities were traces of cyclohexene and cyclohexanol. Cyclohexanol is formed from minute traces of water in the formic acid and has an azeotrope with formic acid cyclohexyl ester as well as sharing (almost) the same boiling point making a direct separation of these two almost impossible.

2.2 Concentration Measurements

To measure the concentrations within any liquid samples taken, two gas chromatographic preparations were applied. The first one was on a Hewlett Packard 6890 with an FID / TCD combination of detectors behind a 30m x 250 μm x 0.25 μm INNOWAX column. The second one was on an Agilent 6890N equipped with an MSD detector using a 60m x 250 μm x 0.1 μm DB5ms column.

Calibration was done using samples of known composition. These samples were prepared using a Mettler Toledo type AT261 DeltaRange scale with an accuracy of better than 0.01

mass%. To measure the reproducibility of the GC measurements, samples were measured repetitively with the calibrated GC. The standard deviation found this way was below 0.05 mole%. To check the accuracy of the calibration, samples that had been composed gravimetrically were measured. The deviations between the gravimetrically determined composition and that measured with the calibrated GC showed a standard deviation of 0.31 mole%. Thus, the overall uncertainty associated with the gas chromatographic composition analysis can be assumed to lie within a range of ± 0.6 mole% with 95% confidence. All samples analyzed via gas chromatography were at room temperature (295 K) when analyzed. The chromatographic method used and a sample chromatogram can be found at the end of this work.

2.3 Vapor-Liquid Equilibrium Measurements

To measure vapor-liquid equilibria for different compositions, a special vapor-liquid equilibrium device (Type VLE 602, FISCHER process technology GmbH, Bonn, Germany) was used. A picture of the device is shown in Figure 2.1. The device is designed to determine the equilibrium concentrations in both liquid and vapor phases while also measuring temperature and pressure. Temperature measurement is performed in the liquid phase close to the phase boundary between the vapor and liquid phases using a PT100 temperature sensor with a resolution of 0.1K. Pressure was also measured close to the phase boundary using a pressure sensor attached to the vapor sampling outlet. The pressure was measured with a WIKA CPH6200 pressure sensor with a range from 0 to 160 kPa which was calibrated to 0.2% of the upper end of the measurement range (± 320 Pa with 95% confidence). Concentration measurement was performed using gas chromatography.

Samples of the vapor phase are typically withdrawn after the vapor stream has been condensed. If desired, it is also possible to draw vapor samples directly out of the vapor phase before it is condensed. This can be useful in cases in which the distillate stream splits into two liquid phases. This is the case for the mixture cyclohexanol / water where the organic phase can hold quite an amount of water. However, even though this option was used a

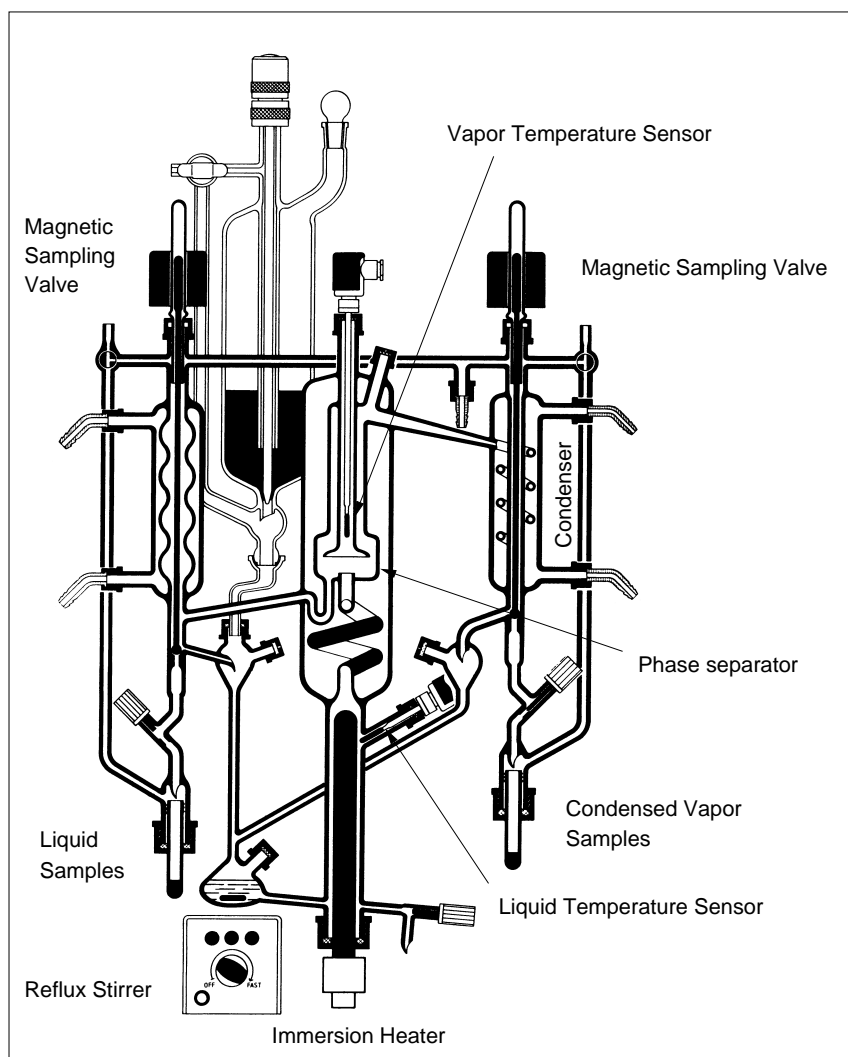


Figure 2.1: Vapor-liquid measurement device type FISCHER VLE 602

large amount of noise was observed in the data gained for this system indicating that the device is not ideal for two-phase measurements.

The six components under study here show six binary mixing gaps. In all cases except cyclohexanol / water these mixing gaps are very wide, leaving only very small one-phase regions in extreme proximity to the pure-component corners. The measurement of vapor-liquid equilibrium (VLE) data in these five binary systems poses a problem since the liquid phase also shows phase splitting even at very low concentrations of the minority compound which leads to an unrepresentative ratio of non-polar to polar phase in the reboiler. This is the reason why no direct measurements of the cyclohexene / water, cy-

clohexene / formic acid, cyclohexane / water, cyclohexane / formic acid and water / formic acid cyclohexyl ester vapor-liquid equilibria were performed.

2.4 Liquid-Liquid Equilibrium Measurements

Measuring liquid-liquid equilibrium (LLE) behavior was generally done by measuring the compositions of both liquid phases at equilibrium via gas chromatography at room temperature (295 K). The composition of the samples was usually adjusted by starting in the middle of a mixing gap of one binary pair and successively adding a third component stepwise. After the mixture composition was adjusted, the mixture was stirred vigorously with an ultra-turrax (Type T25 basic from IKA Werke) at 13,000 rpm to generate very small droplets of one phase in the other. These small droplets lead to a small diffusion distance and large surface area for any mass transfer to take place. A sample of the resulting fine dispersion was then split using a centrifuge (Type Sigma 3K30) at 10,000 g for 2 minutes which always resulted in a good separation. Once the two phases were separated, samples were withdrawn from them and analyzed separately.

The stepwise addition of the third component was continued either until the second phase disappeared or until the third component was the major component. In this latter case, a second series was started at the binary pair between the third component and one of the first components depending which of them formed a mixing gap with it. This approach was used whenever type II mixing behavior was found.

For the LLE measurements between cyclohexanol / water / formic acid this approach had to be modified slightly since cyclohexanol and formic acid slowly react even at room temperature. To avoid this as far as possible, the individual mixtures were composed individually out of the pure components just prior to the measurement. The components were cooled as far as possible without freezing the cyclohexanol. The mixtures were then agitated using an ultrasound tip, type Bandelin electronic UW 2060, which also resulted in a very fine dispersion. This dispersion was then treated like the other samples via centrifugation, separation and subsequent gas chromatographic analysis. The analysis was performed as fast as the gas chromatograph permitted. The amount of formic acid

cyclohexyl ester was monitored for each sample to ascertain that little reaction had taken place. With typical ester contents of around 0.1%, this goal was achieved quite well.

2.5 Reaction Kinetic Measurements

In general, two approaches exist to measure reaction rates. One is based on measuring the composition evolution over time within a batch reactor, the other one is the measurement of steady state conversion in a continuously operated, stirred tank reactor. Both approaches were used during the reaction rate measurements performed.

To be able to compute reaction rates in later simulations, the dependencies the reaction rates show have to be included into the measurement program. One of the main factors influencing reaction rates is the presence or absence of catalysts. In cases in which the reaction mixture shows significant reaction rates without an additional catalyst present, measurements have to be performed with and without catalyst to determine the individual dependencies.

For fast reactions, the mass transfer rate to the catalyst or — in the case of two liquid phases — the droplet size plays an important role which should be clarified prior to other experiments by adjusting different flow regimes. Finally, the reaction rates are strongly dependent on reactor temperature so that measurements have to be performed at different temperatures to be able to determine the temperature dependence.

2.5.1 Batch Reaction Rate Measurements

Batch reactor experiments are very versatile for the measurement of reaction rates, allowing a very wide range of reaction rates to be measured. The measurement is based on the evaluation of the component molar mass balances:

$$\frac{dn_i}{dt} = \sum_{r=1}^{NR} \nu_{i,r} \mathcal{R}_r \quad (2.1)$$

The equation is written for the case of NR reactions with individual reaction rates \mathcal{R}_r for i components. The $\nu_{i,r}$ are the stoichiometric coefficients of the individual components in

the individual reactions. After inserting the overall molar mass balance and rearranging equation 2.1 becomes:

$$\frac{dx_i}{dt} = \sum_{r=1}^{NR} (v_{i,r} - x_i v_{tot,r}) \frac{\mathcal{R}_r}{n_{tot}} \quad (2.2)$$

The interpretation of equation 2.2 becomes much easier in cases in which one of the components participates in only one reaction — as will often be the case. Under these conditions, the reaction rate can easily be computed as:

$$\mathcal{R} = \frac{n_{tot}}{v_i - x_i v_{tot}} \frac{dx_i}{dt} \quad (2.3)$$

To measure the reaction rate in this way, one just has to measure the composition versus time relationship as the total mole number is a function of the extent of reaction(s) and can be computed from the x_i .

In cases in which the reaction under consideration is reversible, \mathcal{R} is time dependent due to the fact that the backwards reaction becomes increasingly faster as the forwards reaction produces increasing amounts of products. To be able to interpret the collected data, one either has to measure the gradient of the mole fraction at time close to 0 (differential approach) when no products are available for the backwards reaction or one has to model both backward and forward reactions and fit the parameters describing \mathcal{R} to the data collected by integrating Equation 2.2 up to the moment in time the measurement was performed (integral approach). Both approaches are being used in this thesis. The choice of the approach was made depending on the rates encountered in the individual reactions.

2.5.2 Continuous Reaction Rate Measurement

If the reactor that is used to measure the reaction rate is operated continuously, this can have the advantage of being able to measure the reaction rate at very low product concentrations accurately. In essence the mole fraction of the product can be adjusted such that the backwards reaction can be ignored as there is only a negligible amount of product to react. To be able to do this adjustment of the product mole fraction, the feed rate into the reactor is changed. To see the effect that this has, the component molar mass balance is

considered:

$$\frac{dn_i}{dt} = \underline{n}_{i,in} - \underline{n}_{i,out} + \sum_{r=1}^{NR} \nu_i \mathcal{R}_r \quad (2.4)$$

Underlined symbols are used for the appropriate streams - e.g. \underline{n} denotes a molar flux. If one considers this equation for a reaction product, the inflow is typically zero. If it is also assumed that there is only one reaction in which the product is formed, that the reactor has reached steady state and that the product mole fraction is small (typically less than 5% of equilibrium mole fraction, allowing to ignore the backwards reaction) the equation reduces to

$$\mathcal{R} = \frac{x_i \underline{n}_{tot,out}}{\nu_i} \quad (2.5)$$

Since the reaction rate is (almost) independent of the flow rate the left side of the equation is left unchanged with a change in flow rate. Since the stoichiometric coefficient is also unchanged, the product mole fraction x_i has to decrease to the same degree that the flow rate is increased allowing to adjust the product mole fraction at will.

Obviously, this is an extremely comfortable way of measuring the reaction rate in cases in which the above assumptions can be fulfilled. The steady state assumption is typically fulfilled after the reactor has been operated for five residence times. In cases in which several different residence times exist — as e.g. in two phase reactors — this requirement refers to the longest residence time of the system.

As the product concentration in the outflow of the reactor can be adjusted by changing the flow rate the question arises as to which product mole fraction is desirable. The ideal product concentration is chosen such that there is minimal backwards reaction rate, while maintaining a well measurable product concentration. In cases in which all reactions are only operated at very low conversions, the effect of an overall increase or decrease in mole number due to the reactions can be ignored such that the flow rate into the reactor can be assumed to be the same as the flow rate out of the reactor, simplifying the overall flow rate measurement.

In some cases in which the reaction rate is very fast or very slow, the feed rate would have to be set so high or low according to the principles just stated that the continuous operation is no longer feasible. In these cases the batch approach has to be chosen.

2.5.3 Concentration Measurement in Reacting Liquid-Liquid Systems

Both Equations 2.3 and 2.5 require accurate measurements of reactor composition to allow to compute the reaction rate. In systems exhibiting only one liquid phase, the determination of the composition is possible by means of drawing samples out of the reactor which will usually be representative of the overall reactor content if the reactor is stirred well. This is not easily possible in case that two liquid phases exist. Extensive experiments have shown that it is impractical to try obtaining samples out of the reactor that are representative with respect to phase ratio.

To overcome this measurement difficulty in the case of two liquid phases, only the non-polar phase was sampled. The samples obtained were analyzed using the FID detector of the gas chromatograph which does not detect water and formic acid. Since the inputs into the reactor were known, the main component of the second phase (water and / or formic acid) was also known. This knowledge allowed using overall component mass balances to compute the composition which would have to be present in the reactor to measure the composition determined in the non-polar phase while at the same time having two liquid phases in equilibrium within the reactor. In the four component case of the ester hydrolysis reaction, the stoichiometric relationships of the reaction also had to be taken into account to be able to solve the equation system. Solving the resulting equation system allowed computing the composition of the outflow.

To determine the outflow rate which is also needed for Equation 2.5, the outflow composition was used to compute the extent of reaction achieved. In cases in which the reaction changes the overall mole number within the reactor, the extent of reaction in combination with the steady state assumption can be used to determine the outflow rate if the inflow rate is known. In most cases these computations were simplified by the fact that the reaction product was not fed into the reactor. Only in the case of the formic acid cyclohexyl ester (FCE) splitting reaction this assumption was not valid as the FCE already contained trace amounts of the desired reaction product cyclohexanol which was measured and taken into account when computing reactor outflow rate.

2.5.4 Experimental Setup

To be able to carry out measurements in both batch and continuous modes, a reactor was set up that allowed both operating conditions. The flow sheet of the experimental set-up can be seen in Figure 2.2. The reactor chosen was a glass 100 ml Miniclave Drive from Büchiglas Uster which can be operated at pressures up to 10 bars. It is equipped with a propeller stirrer with stirring speeds up to 3000 rpm (using a type cc075 device for adjustment), an electronic pressure sensor with a range up to 60 bars and a resolution of 10 mbar (type pr94), a PT 100 temperature sensor with a resolution of 0.1K (type te94) and a hall sensor to measure actual stirrer speed with a resolution of 1 rpm (type sm94). To ensure a safe operation of the device, it was equipped with a burst disc which is set to 10 bars for the glass reactor. Behind the burst disc, the system was coupled to a cyclone venting into a condenser venting into the building exhaust system. The remaining three

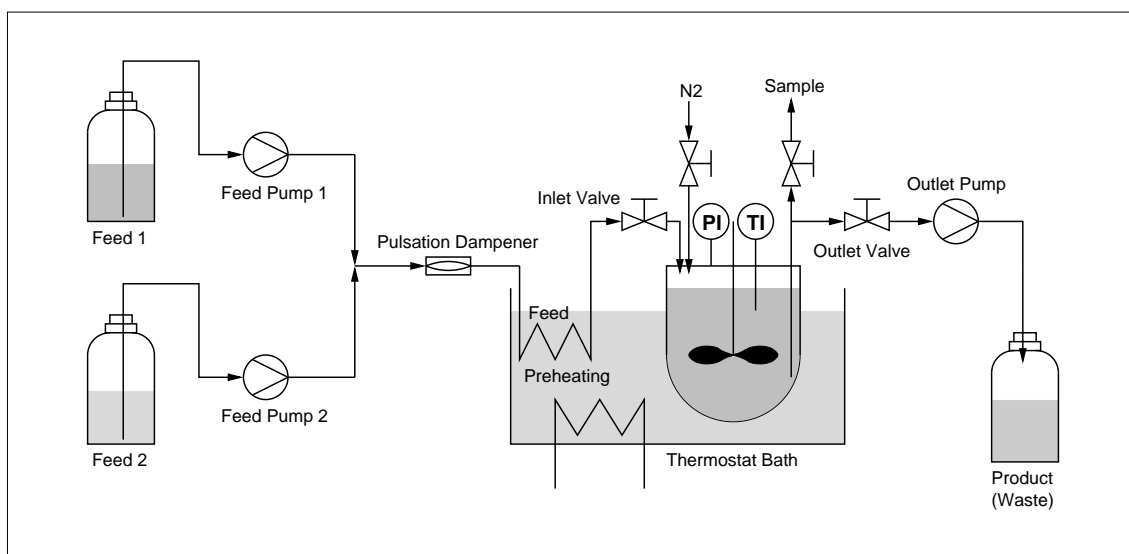


Figure 2.2: Reaction kinetic measurement setup

connections on the reactor lid were used to connect the inlet, outlet and sampling valves. The sampling valve is set up behind a T-junction whose other end was used to connect a nitrogen pressure supply to be able to set the operating pressure by applying nitrogen. Depending on the mode of operation desired, the inlet and outlet can be opened or closed. To assure that the heterogeneous catalyst stayed within the system, the outlet was shielded with the help of a wire mesh with a hole size of 140 μm . The sampling outlet pipe was

only 1/16" in outer diameter and was squeezed flat such that it did not need shielding for Amberlyst 15.

To adjust the reactor temperature, the whole assembly was immersed into an oil or water bath depending on the desired temperature. The bath was of type Haake C40 which can be adjusted to 0.01 K of the desired temperature up to 100 °C and to 0.1 K above that. Before entering the reactor in the continuously operated case, the reactants were passed through a heat exchanger immersed in the same thermostat bath to adjust the inlet temperature. The reactants and the reactor outflow were pumped using Ismatec rotary piston pumps of type ISM321A which use pump heads from Fluid Metering (type RH00) and have a range 0.025 to 45 ml/min. To dampen the flow rate pulsation a Fluid Metering pulse dampener (type PD-06-LF) was used. The pumps were calibrated for the different substances and pressure gradients to within $\pm 1\%$ of the desired value by weighing the fluid volume pumped over a defined amount of time. In the continuously operated cases, samples were withdrawn from the reactor outlet stream.

2.6 Experimental Results and Analysis

As before, the results can be divided between the phase equilibrium measurements and the reaction kinetic measurements. The reaction kinetic experimental results need a valid activity coefficient model for their interpretation so that the phase equilibrium results will be presented before the reaction kinetic results are shown. The interpretation of the vapor-liquid equilibrium measurements depends in turn on accurate data for the pure component saturation pressures at different temperatures. This is why the Antoine parameters are presented first.

2.6.1 Vapor Pressure Measurements and Fitted Antoine Parameters

The relationship between temperature and boiling pressure was evaluated using the same experimental apparatus as was used for the vapor-liquid equilibrium measurements. The only difference being that this time a pure substance was inserted into the device and

that the pressure was systematically varied using a vacuum pump. The according boiling temperatures were recorded after steady state had been reached.

This type of pressure / temperature data was collected for all substances except for formic acid for which an extensive data set was found in [55] and [75] and for which strong precautionary measures would have been necessary to protect the vacuum pump. The pressure / temperature data was especially needed for formic acid cyclohexyl ester as the few data points available for this substance in the literature showed such a significant disagreement that own measurements were needed. For this substance it was also not possible to find any Antoine parameters in the literature.

The data set generated this way (including the literature data [55, 75]) was then used in a sum of least squares fitting procedure that used the global evolution strategy presented in Chapter 3.1 as the minimization algorithm. The Antoine Equation used can be seen in Equation 2.6, pressure is calculated in Pa, Temperature is inserted in K. In this way, an Antoine parameter set was found with which it was possible to compute boiling pressures which showed a standard deviation interval of typically less than 1 mbar between the measurement and the model.

$$\log_{10}\left(\frac{P}{Pa}\right) = A - \frac{B}{\frac{T}{K} + C} \quad (2.6)$$

As the calibrated pressure sensor has a 95 % confidence interval of ± 3.2 mbar, the true value of the pressure can be expected to lie within an interval of ± 3.8 mbar from the computed value. The Antoine parameter set as well as the temperature range for which it is valid and the individual standard deviations of the fit can be found in Table 2.1. The individual data points measured were published previously in [65] and [66] and will not be repeated here. A comparison between the data measured for water and the according data reported in the literature [35], which can be assumed to be very accurate for water, shows an agreement to within the measurement accuracy of our measurements. This is an indication that our measurement approach is suitable for Antoine parameter determination.

Table 2.1: Antoine parameters, valid temperature ranges and standard deviations between measurements and computations for the six components. Parameters for formic acid were fitted to literature data [55, 75].

Component	A	B	C	Temperature Range in K	σ in mbar
Cyclohexene	8.98075	1206.02	-52.7753	310-360	0.6374
Cyclohexanol	9.06566	1258.75	-123.673	320-435	0.3293
Water	10.00749	1605.78	-52.2025	300-375	1.0270
Cyclohexane	8.96959	1191.56	-53.2741	305-355	0.9905
FCE	9.09578	1489.03	-71.4825	305-435	0.3437
Formic Acid	9.57631	1608.22	-21.8974	265-385	1.6700

2.6.2 Vapor Phase Dimerization of Formic Acid

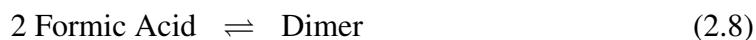
Under the pressures that were used for vapor-liquid equilibrium measurements (typically around 100 kPa), one can usually ignore the very small effect of non-ideal gas phase behavior. The vapor-liquid equilibrium is thus described by:

$$x_i \gamma_i P_i^{sat} = y_i P \quad (2.7)$$

In this equation the γ_i are the activity coefficients, P and P_i^{sat} are the pressure and saturation pressure of component i , respectively, and the y_i are the vapor mole fractions. The mole fraction in the liquid and vapor and the overall pressure and temperature can be measured. Using the Antoine equation, the saturation pressure can be computed and thus Equation 2.7 can be used to determine the γ_i that an appropriate activity coefficient model is to be fitted to. For the sake of this work, the NRTL equation was chosen as the activity coefficient model as it is known to be able to describe both liquid-liquid and vapor-liquid behavior well.

However, there is one substance that shows a dramatically different behavior in the gas phase than is predicted by Eq.2.7: formic acid. Due to its very polar nature and the charge distribution over the molecule surface it tends to dimerize in the vapor phase. This dimerization has been extensively studied (e.g. by [10]) and the dependency of dimerization

can be described as a simple gas phase reaction:



As the reaction reduces the number of moles when forming the dimer it is favored when higher pressures are applied. Also, the temperature plays an important role as the dimer's stability is reduced at higher temperatures. The behavior can be described as:

$$K_{eq}(T) = \frac{P_{Dimer}}{P_{Monomer}^2} \quad (2.9)$$

The equilibrium constant K_{eq} was fitted to the measurement data supplied by Chao and Zwolinski in [10] using the following equation:

$$K_{eq}(T) = K_0 e^{\frac{-\Delta G_R}{RT}} \quad (2.10)$$

Again, the global optimization algorithm described in Chapter 3.1 was used and K_0 was determined to be $2.4726 \times 10^{-14} \frac{1}{Pa}$ and $(-\Delta G_R)$ was determined to be $6.3766 \times 10^4 \frac{J}{mol}$. The computed K_{eq} values based on these parameters were always within 5% of the measured values in the temperature range from 200-500K.

The saturation pressure computed using the Antoine parameters from Chapter 2.6.1 is equal to the sum of the monomer and dimer pressures:

$$P_{FormicAcid}^{sat} = P_{Monomer} + P_{Dimer} \quad (2.11)$$

Combining Equation 2.11 and Equation 2.9 allows computing the monomer and dimer partial pressures. Since the vapor composition is measured after the vapor has been condensed as described in Chapter 2.3, the dimers have dissociated again and are measured as two molecules of formic acid. Equations 2.9 to 2.11 allow compensating for this effect.

2.6.3 Vapor-Liquid Equilibria

The system being studied contains six components which leads to 15 binary pairs. In theory, measuring VLE data for all of these pairs would seem the ideal approach to cover their vapor-liquid phase behavior. Unluckily however, there are some restraints as to which binary pairs can be measured for two reasons.

In some binary pairs, the mixing gap is so large that there does not exist any significant concentration range in which measurements can be performed. This is the case for the five binary systems cyclohexene / water, cyclohexene / formic acid, cyclohexane / water, cyclohexane / formic acid and formic acid cyclohexyl ester / water.

Some further binary systems exhibit reaction at the typical measurement temperatures (which have to exceed the cooling water temperature significantly to assure complete condensation to avoid harming the vacuum pump). This is true for the binary mixtures of cyclohexanol / formic acid and formic acid cyclohexyl ester / formic acid.

Of the remaining eight binary pairs, the vapor-liquid phase equilibrium is very well studied for water / formic acid. For this reason it was decided not to measure this system again and to rely on literature data [18, 69, 71].

The results of the measurements of the remaining seven binary pairs is shown as vapor-liquid equilibrium diagrams as Figures 2.3a to 2.3g (measurement data is shown as circles). The data on the compositions at the individual measurement points has been published in [65] and [66] and will not be repeated here.

2.6.4 Liquid-Liquid Equilibria

Of the potentially 20 three-component mixtures that are possible with six substances, five do not show any liquid-liquid phase splitting at all and were thus not considered for phase splitting measurements.

Of the remaining 15 candidate systems, some also show extreme type II phase behavior (as e.g. cyclohexene / cyclohexane / water). Measurements of such combinations are very hard to perform as the compositions of the two phases are extremely hard to measure accurately due to the extreme trace amounts of the according minority components.

In the end, seven ternary systems were chosen for liquid-liquid equilibrium measurements which allowed to complement the vapor-liquid equilibrium data in a way that all binary pairs are covered either in vapor-liquid or liquid-liquid equilibrium measurements or both. Again, the raw data was previously published in [65] and [66] and will not be repeated here. The plots of the measured ternary liquid-liquid equilibrium data can be seen as Figures 2.4a to 2.4g.

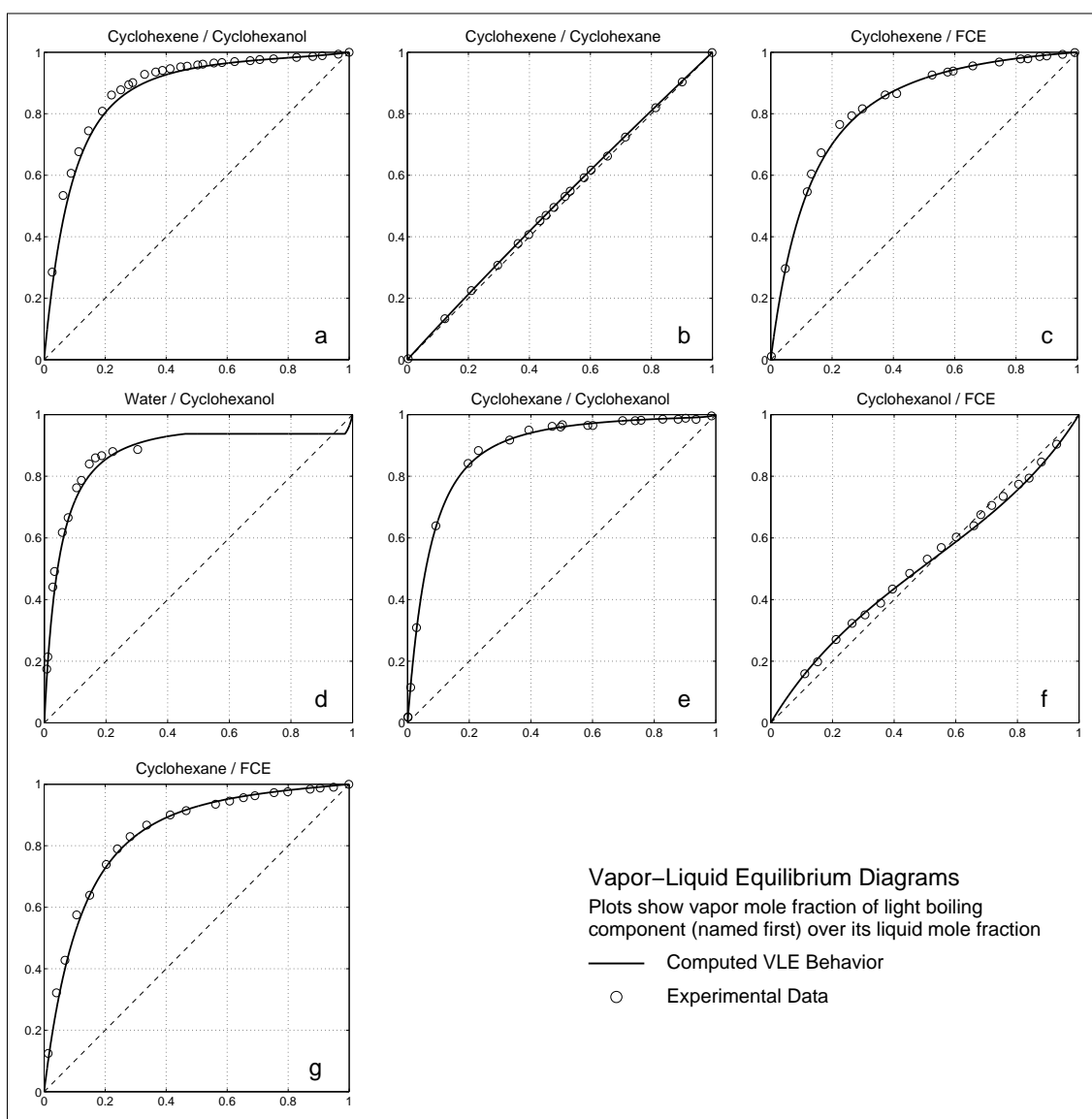


Figure 2.3: Vapor-liquid equilibrium measurement results and computations

2.6.5 Vapor-Liquid-Liquid Equilibria

To be able to compute the vapor-liquid and liquid-liquid equilibria the NRTL model was chosen as it is capable of describing both vapor-liquid and liquid-liquid equilibria [53]. This model has three parameters (g_{ij} , g_{ji} and a_{ij}) for every binary pair resulting in 45 parameters that have to be fitted to experimental data. The same set of parameters were used for the description of both the vapor-liquid and liquid-liquid equilibria.

The fitting procedure was based on a variance-weighted sum of least squares objective function δ which is composed of terms for the vapor-liquid and liquid-liquid equilibria.

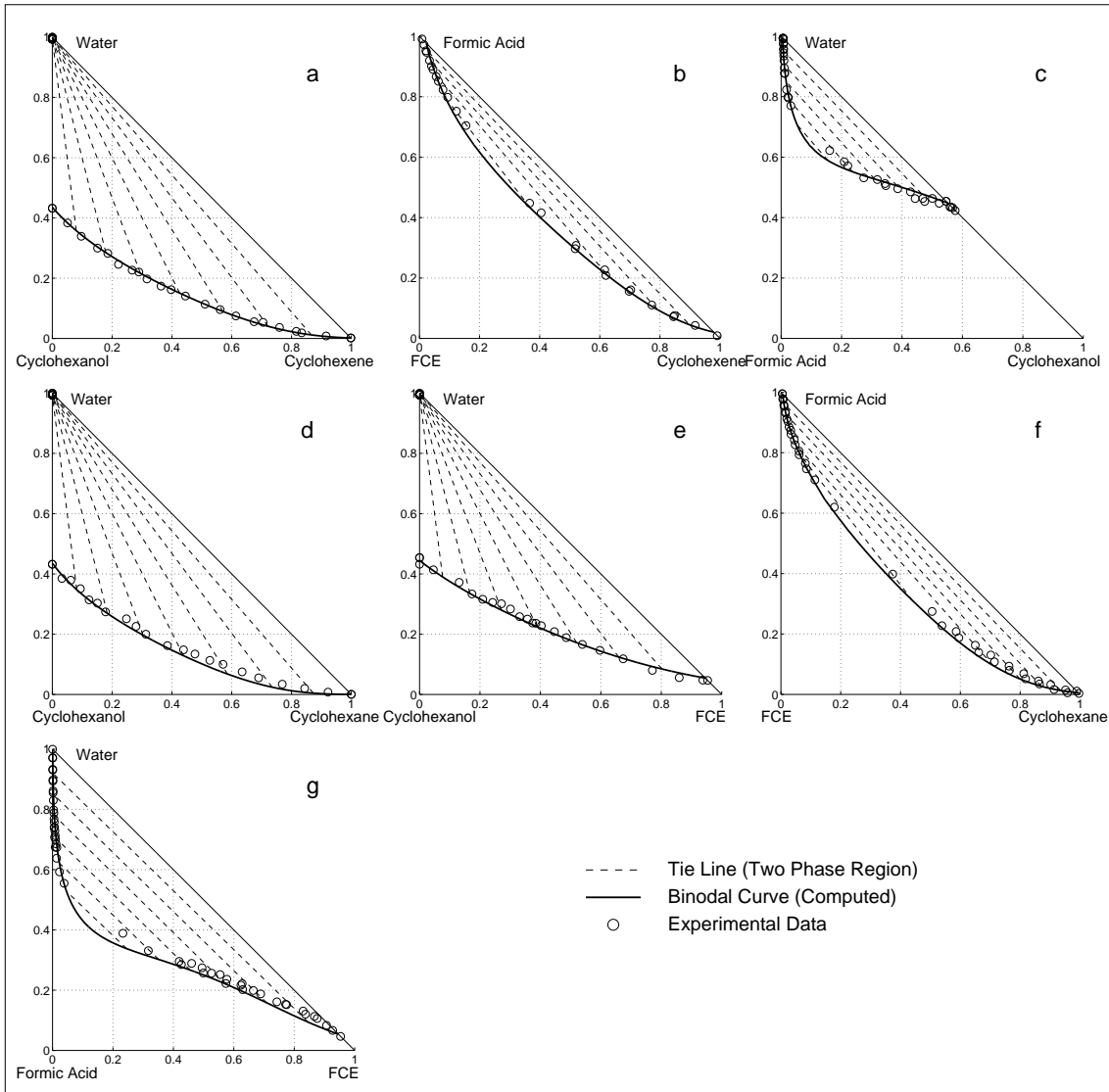


Figure 2.4: Ternary liquid-liquid measurement results and computations

The vapor-liquid equilibrium term also considers the fact that the partial pressures have to add up to the (measured) overall pressure.

$$\begin{aligned}
 \delta &= \delta_{VLE} + \delta_{LLE} & (2.12) \\
 \delta_{VLE} &= \frac{1}{8} \left[\sum_{n=1}^{NVLE} \frac{2}{\sigma_P^2} \left[P_n^{exp} - \sum_{n=1}^{NC} x_{i,n}^{exp} \gamma_{i,n}^{calc} P_{i,n}^{sat} (T_n^{exp}) \right]^2 \right. \\
 &\quad + \sum_{n=1}^{NVLE} \sum_{i=1}^{NC} \frac{1}{\sigma_{x,VLE}^2} \left[x_{i,n}^{exp} - \frac{y_{i,n}^{exp} P_n^{exp}}{\gamma_{i,n}^{calc} P_{i,n}^{sat} (T_n^{exp})} \right]^2 \\
 &\quad \left. + \sum_{n=1}^{NVLE} \sum_{i=1}^{NC} \frac{1}{\sigma_y^2} \left[y_{i,n}^{exp} - \frac{x_{i,n}^{exp} \gamma_{i,n}^{calc} P_{i,n}^{sat} (T_n^{exp})}{P_n^{exp}} \right]^2 \right]
 \end{aligned}$$

$$+ \sum_{n=1}^{NVLE} \sum_{i=1}^{NC} \frac{1}{\sigma_{\gamma}^2} \left[\gamma_{i,n}^{calc} - \frac{y_{i,n}^{exp} P_n^{exp}}{x_{i,n}^{exp} P_{i,n}^{sat}(T_n^{exp})} \right]^2 \quad (2.13)$$

$$\delta_{LLE} = \frac{1}{3} \sum_{n=1}^{NLE} \sum_{i=1}^{NC} \frac{1}{\sigma_{x,LLE}^2} \left[x_{i,n}^{polar,exp} \gamma_{i,n}^{polar,calc} - x_{i,n}^{nonpolar,exp} \gamma_{i,n}^{nonpolar,calc} \right]^2 \quad (2.14)$$

As the expressions for the vapor-liquid and liquid-liquid equilibria have different numbers of terms on their respective right sides, the right sides are divided by 8 or 3 respectively such that each individual measurement is weighted equally. The overall objective function according to Equation 2.12 was minimized using the global evolution strategy as presented in Chapter 3.1.

Additionally to the measurement data shown above, data from the literature on the VLE behavior of water + cyclohexanol [20, 72, 82], cyclohexene + cyclohexane [24, 39] and water + formic acid [18, 69, 71] was included into the fitting procedure. Also LLE data on the binary phase splitting behavior of cyclohexanol + water and cyclohexane + water [3, 61, 58] from the literature as well as data on azeotropes [19] was included into the fitting procedure. The literature data was chosen based on availability, quality and suitable conditions (similar pressure range). Overall, there was a good agreement between the literature data and the measurements presented in Chapters 2.6.3 and 2.6.4.

Unluckily, the resulting 45-dimensional global optimization, when carried out directly, resulted in a computational effort that was not acceptable. For this reason, two other approaches were taken. The first was to split the simultaneous optimization into several sequential optimizations for two- to four-component subsystems for which only those equilibrium measurements were used that have an influence on the according parameters. This approach leads to a significantly lower computational effort and at the same time has the advantage of permitting parallel computations on several computers for different subsets.

The best parameter sets found during these global optimization runs were then used as starting points for local optimization runs. For these local optimizations, new optimization variables in addition to the NRTL parameters, were included for the "true" values. For every vapor-liquid equilibrium measurement point this meant three additional optimization variables - namely the temperature and the two liquid mole fractions - out of

which the "true" pressure and vapor mole fractions were computed. For the liquid-liquid equilibrium data points no additional variables were needed as it was assumed that the average between the compositions of the individual phases is the "true" overall composition. The objective function was then the same as before (Equations 2.12 to 2.14) only that in Equation 2.13 the right sides of the differences were replaced by the "true" values. Theoretically speaking, this would have been the ideal objective function for a global optimization. However, as it has over 500 (!) optimization variables the global optimization would have been infeasible for computation time reasons. Even the local optimization run with this objective function took several days to reach the local minimum.

The results of this second optimization can be seen as the solid lines in Figures 2.3 and 2.4. The resulting NRTL parameter set is shown in Table 2.2 together with the remaining standard deviations between measurement and calculations. As can be seen, the standard deviations are usually quite small such that it can be said that the fitting procedure was successful. The slightly higher standard deviations for the pressure values in some cases can be attributed to the very high sensitivity of the boiling pressure in these systems with respect to the composition of the liquid phase and of the temperature. Even though the parameter set presented here shows a good agreement between measurements and computations, it can be assumed that there might be a parameter set that describes the phase behavior even better as there seems to be some areas where the measurement data does not scatter randomly around the computed curves. These deviations might be attributed to a deficiency of the NRTL equation to be able to describe the according systems. More likely, however, the ideal parameter set has not been found yet.

There are two reasons for this assumption. For one the computation times for the global optimization runs was still very high and the runs were terminated when a (subjectively) acceptable fit was found. As the global optimizer is of stochastic nature, only an infinite amount of computation time would guarantee finding the global optimum. The other reason is that the objective function for the parameter sets for binary systems showing liquid-liquid phase splitting is not continuous as all parameter sets that do not lead to phase splitting will lead to the same function value for the liquid-liquid deviation term (Equation 2.14). Only slightly different parameters that do predict liquid-liquid phase splitting however will have a markedly better function value and a continuous improve-

Table 2.2: NRTL parameter set identified for the six-component system and the standard deviations associated with the parameter set. The σ_{LLE} numbers are for the ternary systems according to Figure 2.4, the letter in parentheses denoting the sub-figure meant.

Binary Pair	g_{12} in J/mol	g_{21} in J/mol	a_{12}	σ_y	σ_P in mbar	σ_{LLE}
Cyclohexene (1) / Cyclohexanol (2)	3568.41	-0.962835	0.802522	0.0279	41.5	
Cyclohexene (1) / Water (2)	14175.4	21695.0	0.267206			0.00497 (a)
Cyclohexene (1) / Cyclohexane (2)	42.4813	60957.2	0.831053	0.00386	9.20	
Cyclohexene (1) / FCE (2)	-2390.29	3308.21	0.215759	0.0120	29.7	
Cyclohexene (1) / Formic Acid (2)	7828.68	7619.60	0.342528			0.0162 (b)
Cyclohexanol (1) / Water (2)	1336.76	10959.4	0.359706	0.0151	131.7	
Cyclohexanol (1) / Cyclohexane (2)	19.9341	4071.64	0.993301	0.0230	91.7	
Cyclohexanol (1) / FCE (2)	1540.33	337.622	0.313377	0.0132	8.28	
Cyclohexanol (1) / Formic Acid (2)	-1778.81	3290.04	0.689468			0.00893 (c)
Water (1) / Cyclohexane (2)	25048.5	17650.0	0.258799			0.00681 (d)
Water (1) / FCE (2)	15899.1	5877.86	0.286963			0.00458 (e)
Water (1) / Formic Acid (2)	3507.57	-4043.93	0.139498			
Cyclohexane (1) / FCE (2)	3627.17	-2134.86	0.315477	0.0154	56.6	
Cyclohexane (1) / Formic Acid (2)	10153.6	9943.91	0.287689			0.0120 (f)
FCE (1) / Formic Acid (2)	-415.705	3158.48	0.765244			0.0162 (g)

ment towards the local minimum. This discontinuity makes the optimization even harder. From an engineering standpoint the fit found is of similar quality as the scattering observed between the individual measurement points. The remaining error due to the limitations of the fitting procedure is thus of a similar order of magnitude as the measurement error so that it can be said to be acceptable even if it can still be improved.

2.6.6 Reaction Kinetics

It was assumed that the overall reaction rate is the sum of homogeneous and heterogeneous reaction rates:

$$\mathcal{R} = \mathcal{R}^{het} + \mathcal{R}^{hom} \quad (2.15)$$

The one exception to this rule is the cyclohexene direct hydration reaction which did not show any measurable reaction rate without the heterogeneous catalyst. To be able to describe the reaction rate analytically, a rate expression was formulated that incorporates both homogeneous and heterogeneous reaction rates.

The Langmuir-Hinshelwood approach was chosen to model the heterogeneous reaction rate. Strictly speaking, this approach is only valid under the assumptions that the adsorption sites are energetically and chemically equivalent, that only a mono-molecular layer of chemical species is adsorbed, that every adsorption site can adsorb only one molecule and that there are no interactions between the adsorbing species.

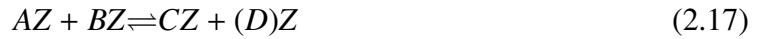
For Amberlyst 15, which quells significantly in water and whose adsorption sites are the acidic sites which dissociate in water, many of these assumptions can be said not to hold. Experimental evidence suggests, however, that the Langmuir-Hinshelwood approach is still fairly well suited to describe this type of solid catalyzed reaction [52].

The Langmuir sorption approach describes the adsorption equilibrium between an arbitrary chemical species A and an active catalytic site Z similar to a reversible reaction as:



The overall amount of adsorption sites was assumed to equal the amount of acidic sites which was measured to be 4.7 mmol/g of catalyst. This is also the figure claimed by

Rohm & Haas (the producer). The reaction rates are then formulated for the adsorbed species:



A , B , C and D are the three or four reactants of the reaction being studied (D appearing only in the ester splitting reaction). Under the assumption that the adsorption equilibrium is reached and that all chemical species compete for the same adsorption sites, the chemical reaction can be reformulated using the surface fraction of the species on the catalyst surface:

$$\varepsilon_i = \frac{K_{SLE,i}a_i}{1 + \sum_{j=1}^{NC} K_{SLE,j}a_j} \quad (2.18)$$

The necessary adsorption equilibrium constants, $K_{SLE,i}$, were fitted simultaneously with the kinetic parameters to the measured kinetic data using a least squares objective function.

Inserting the surface fractions into the overall reaction rate equation (Equation 2.15 and rearranging results in

$$\begin{aligned} \mathcal{R} = & \left(m_{cat} k_{f,0}^{het} e^{-\frac{E_A^{het}}{RT}} \frac{K_{SLE,A} K_{SLE,B}}{(1 + \sum_j a_j K_{SLE,j})^2} + n_{FA} k_{f,0}^{hom} e^{-\frac{E_A^{hom}}{RT}} \right) \\ & \times \left(a_A a_B - \frac{a_C (a_D)}{K_{eq}} \right) \end{aligned} \quad (2.19)$$

As can be seen, Equation 2.19 has two terms in the first bracket – one for the heterogeneous reaction rate containing the heterogeneous catalyst mass and one for the homogeneous reaction including the molar amount of formic acid as the homogeneous catalyst. The second bracket contains the terms describing the thermodynamic driving force of the reaction.

Equation 2.19 leads to four parameters that need to be fitted to experimental data for each reaction, namely the two frequency factors and the two activation energies. Since the direct cyclohexene hydration reaction did not show any homogeneous reaction rate this leads to a total of five frequency factors and five activation energies. Additionally, the adsorption equilibrium constants of the five components and the enthalpy of formation of the ester had to be fitted to the data. The enthalpy of formation of the ester is needed for

the computation of K_{eq} for the reactions containing the ester but there were no literature values available for it.

2.6.6.1 Discussion of Potential Catalysts

As already stated in the Introduction section, the direct reaction of cyclohexene with water to cyclohexanol would be the ideal process if a suitable catalyst can be found for it. The choice or design of a catalyst is always one of the most critical and first steps in the design of a reaction / separation process.

The direct cyclohexene hydration is catalyzed by strong acids which would initially suggest sulphuric acid as a potential homogeneous catalyst. As it shows a high boiling point, it would tend to accumulate at the bottom of the column as shown in Figure 1.3 and in turn especially accelerate the cyclohexanol splitting reaction. This would strongly limit the overall conversion achievable.

Taking these considerations into account, a heterogeneous catalyst that allows limiting the reaction zone to both sides can be said to be advantageous. Measurements of the reaction rates obtainable with different solid acids such as strongly acidic zeolites and Amberlyst 15 are both available in the literature [81] and carried out as part of this work (see Chapter 2.6.6.2). In both cases the reaction rates found for the zeolites were significantly higher than for Amberlyst 15, an ion exchange resin. Additional experiments with heteropoly acids which were initially deemed to be interesting candidates for direct hydration catalysts produced even lower rates than Amberlyst 15.

Between the zeolites there were large differences in reaction rates, however. Even seemingly similar zeolites which showed a similar Al/Si ratio (indicating the amount of acid sites) but which were obtained from different suppliers had vastly different catalytic activity. The interpretation of these results is that the ideal catalyst for reaction systems with extreme liquid-liquid phase splitting behavior is one which is built in a way that it is located between the two liquid phases. Only in such a configuration, both reactants have good access to the catalytic sites without incurring large mass transfer resistances. Figure 2.5 shows these effects. The resulting consequence could be to choose a membrane reactor for this type of reactions. The membrane would be designed to allow the two species

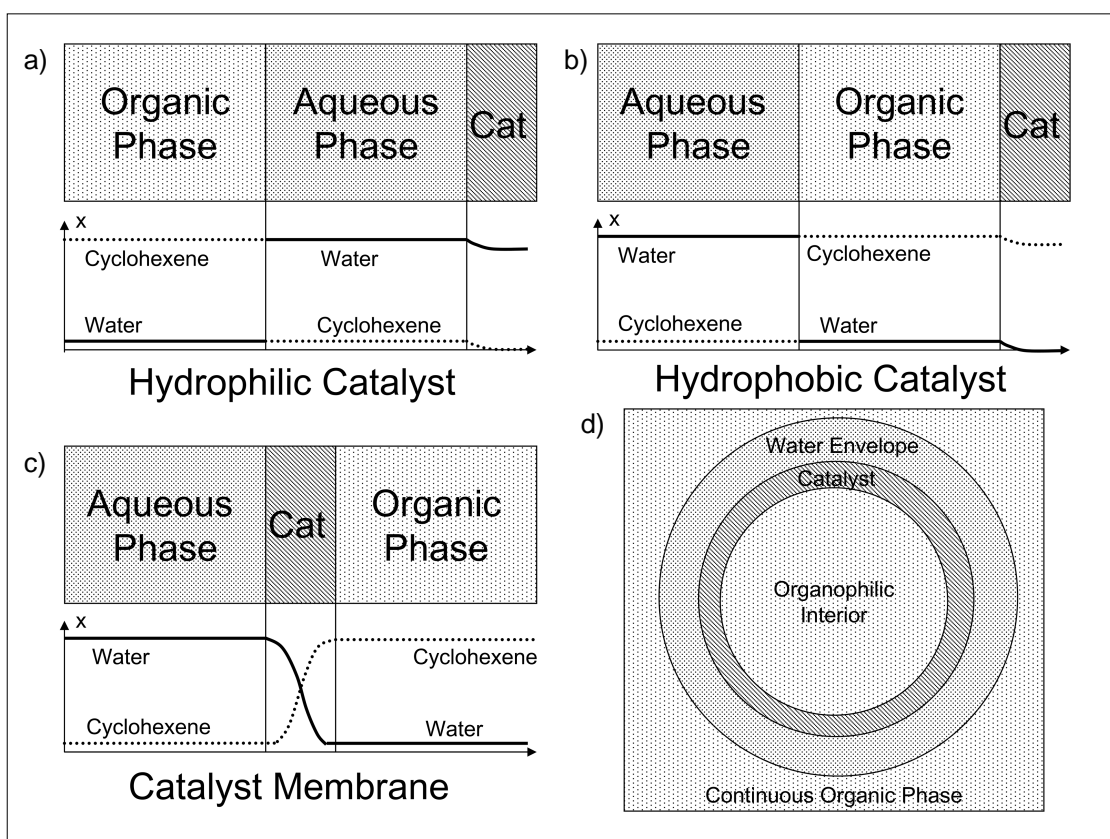


Figure 2.5: Effect of catalyst placement on reactant availability at catalyst sites - spherical membranes as ideal catalysts. a: catalyst in aqueous phase, b: catalyst in organic phase, c: catalyst between phases, d: spherical catalyst membrane between organophilic and aqueous phases

with strongly differing polarities easy access to the catalytic sites. The geometry of such a membrane does not necessarily have to be a sheet, however. The high catalytic activity found when using certain zeolites as catalysts was interpreted to be due to a shell-like catalyst particle structure as shown in Figure 2.5 in which the inside of the catalyst particles contains a sufficiently non-polar core where the non-polar components accumulate and a polar outer shell which leads to the strong preference of the catalyst to be immersed in water as was reported for the Asahi process [42]. This shell catalyst concept would be enhanced even further if part of the outer layer were non-polar, allowing the non-polar phase easy access to the interior. Massive particles without polarity gradients such as Amberlyst 15 cannot compete with such shell structured catalysts.

If this interpretation of the experimental results is correct, there is a need for shell struc-

tured catalyst particles with a strong polarity gradient and especially a very large catalyst surface area to allow operating the direct hydration reaction commercially. Needless to say the requirement for a large surface area results in small catalyst particles — a requirement which once again correlates well with what is known about the zeolites used in the Asahi process which are reported to be smaller than one micrometer [42]. The catalyst slurry within the Asahi process allows both large catalyst quantities of such small particles and an easy separation of the catalyst as it strongly prefers the aqueous phase. Introducing such slurries into reactive distillation columns as suggested e.g. by Wang [78], however, has the drawback of not being able to limit the catalytic zone towards the bottom of the column as was the case with sulphuric acid. Also, operating such a column has the inherent risk of the catalyst adhering to the column internals which would clog the column and spoil fluid dynamics within.

An alternative approach to catalyst optimization was explored by conducting some experiments with zeolite particles grown directly onto the metal mesh of the distillation packings. These catalyst samples were prepared by the group of Schwieger at Erlangen University, Germany, which has extensive experience in coating metal surfaces with zeolites (e.g. [37]). Applying zeolite layers to metallic distillation packings and thus immobilizing the zeolites within the column was shown to be feasible as can be seen in Figure 2.6. The zeolites showed the expected catalytic activity but due to the extremely small amounts introduced into the column by these surface coatings, the catalytic activity was not sufficient for a commercial application. Several alternative approaches to the direct hydration catalysis problem were considered including thermomorphic solvent systems for reaction systems undergoing liquid phase splitting, proposed e.g. by the group of Behr at Dortmund University (e.g. [7]) or the use of micro-emulsions to enlarge the phase boundary area as suggested by the group of Schomäcker from Berlin Technical University (e.g. [84]). These alternative approaches are interesting subjects of research in themselves but had not previously been applied to the reaction system under study. Especially, there was no data available on whether such approaches would work under the changing temperatures and under boiling conditions within a reactive distillation column. As the direct hydration reaction was in consequence unlikely to be feasible commercially, the alternative approach of using a reactive entrainer was chosen as was already men-

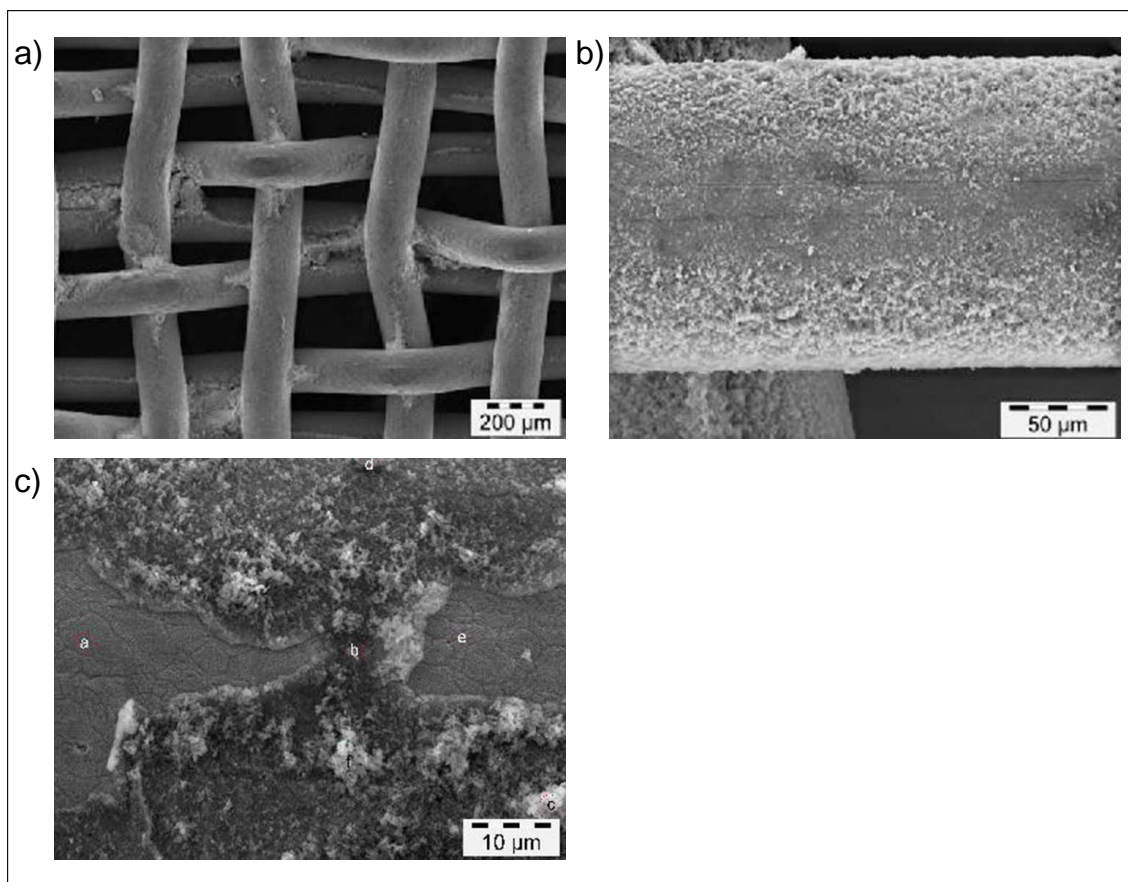


Figure 2.6: REM images of metal column packings coated with HZSM5-type zeolite catalyst particles. a: overview showing accumulations at intersections, b: individual wire with homogeneous, thin coating, c: close-up of coating layer with defects

tioned in the Introduction (Chapter 1). The literature suggested that formic acid reacts at a substantial rate with cyclohexene forming FCE [14] which could — in a second step — be converted to cyclohexanol using a conventional ester splitting reaction. The more common acetic acid was also evaluated with the help of some exploratory experiments but discarded in favor of formic acid which showed a higher rate of reaction.

Advantages of this reaction route are that no significant amounts of side products were formed using the conventional Amberlyst 15 as the catalyst. Only at elevated temperatures beyond 333 K did we encounter a slow but continuous increase in pressure within the reactor used to measure the reaction rates which was identified to be due to the formic acid decomposing into water and carbon monoxide in the presence of the catalyst [55]. As a consequence of this side reaction, it was decided to conduct further experiments that

included formic acid only at temperatures up to 333 K where no pressure increase was observed. The reactive distillation column should thus be operated at e.g. 10 kPa to move the boiling point range of the mixtures to lower temperatures.

2.6.6.2 Direct Cyclohexene Hydration

As was stated before, the direct hydration of cyclohexene is a very slow reaction which was only observed in the presence of catalyst even at temperatures up to 393K. For this reason, the homogeneous reaction rate was ignored.

Even with Amberlyst 15 as a catalyst, the reaction rate was slow at the temperatures at which Amberlyst 15 is stable which was the reason for the choice of the indirect hydration route.

For measuring the direct hydration, the reactor setup was used in CSTR mode with residence times of up to 50 minutes to achieve the amount of conversion needed to be able to reliably measure the cyclohexanol mole fraction. The reactor was fed with equal volumetric amounts of cyclohexene and water and large amounts of catalyst were used.

Cyclohexanol decomposition was also studied using a reactor feed of pure cyclohexanol and wetted catalyst to avoid water accumulation in the catalyst from prolonging the time needed to reach steady state. The residence times adjusted in these experiments were even longer, but the experiments were carried out at lower temperatures. The results of these measurements can be seen in Figure 2.7.

2.6.6.3 Cyclohexene Esterification

The cyclohexene esterification reaction with formic acid showed measurable reaction rates both in the presence and absence of Amberlyst 15 as a heterogeneous catalyst. This is due to the fact that formic acid acts both as a reaction partner and as a homogeneous catalyst (even though it shows liquid phase splitting behavior when in contact with pure cyclohexene).

Since both reaction rates were not negligible, the homogeneous rate was measured first followed by experiments that also contained the heterogeneous catalyst Amberlyst 15.

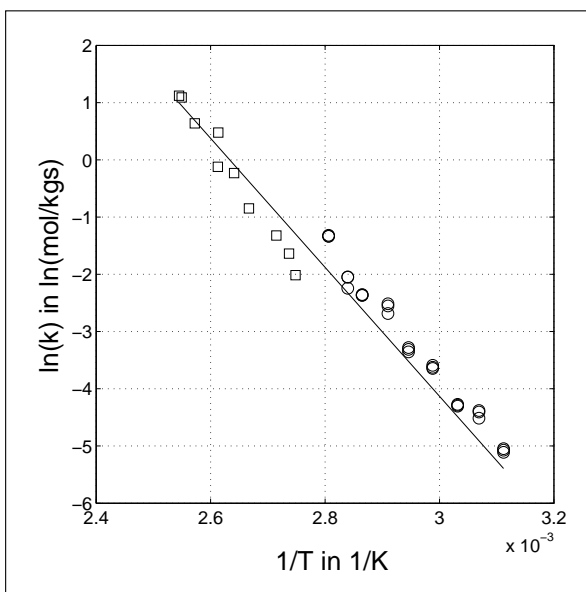


Figure 2.7: Comparison between computed (-) and measured reaction rate constants k for the Amberlyst 15 catalyzed direct cyclohexene hydration reaction. Squares denote the measured reaction rate constants for cyclohexanol formation, circles denote the measured values for cyclohexanol splitting.

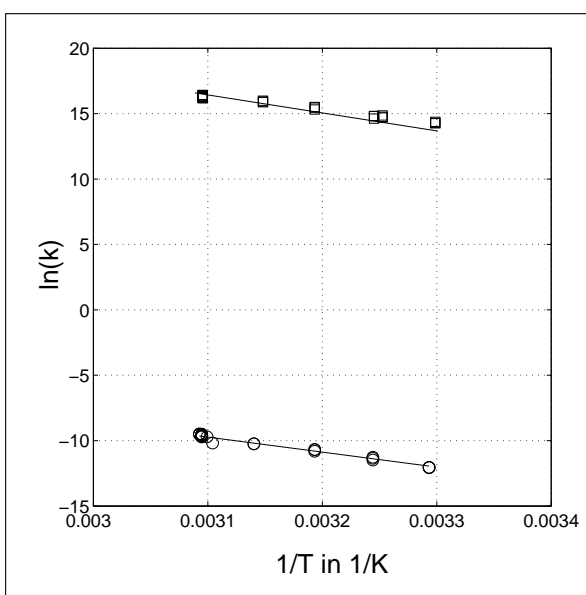
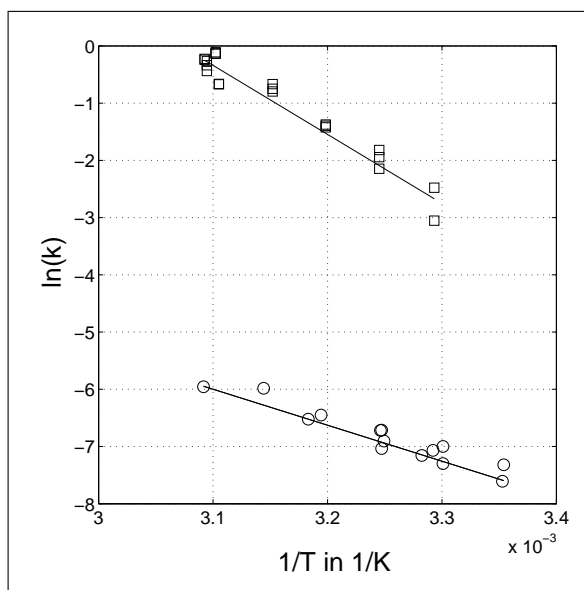


Figure 2.8: Comparison between computed (-) and measured reaction rate constants k for the cyclohexene esterification reaction. Squares denote measured Amberlyst 15 catalyzed reaction rate constants (in $\ln(\text{mol}/\text{kgs})$) for the backwards reaction, circles denote the homogeneously catalyzed reaction rate constants (in $\ln(1/\text{s})$) of the forwards reaction.

The heterogeneous reaction rate was then easily computed by subtracting the homogeneous rate from the overall rate of reaction measured.

The reaction rates encountered enabled measurements in CSTR mode of the reaction setup at moderate residence times of around 10 minutes. The reverse reaction was observed to take place only in the presence of a catalyst which is why it was studied in the presence of Amberlyst 15 only – pure FCE was seen to be stable even at its boiling temperature of 434 K. The measurement results can be seen in Figure 2.8.

Figure 2.9: Comparison between computed (-) and measured reaction rate constants k for the ester splitting reaction. Circles denote measurement values for the uncatalyzed backward reaction rate constant (in $\ln(1/s)$), squares denote the Amberlyst 15 catalyzed measurement values of the rate constant for the forward reaction (in $\ln(\text{mol}/\text{kg}\cdot\text{s})$).



2.6.6.4 Ester Hydrolysis

The reaction rates encountered when studying the ester hydrolysis reaction were again amenable to be measured with the CSTR reaction setup. The reverse reaction of ester formation from cyclohexanol and formic acid however was so fast that the residence time needed for an accurate measurement was not achievable with the reaction setup available. Additionally, the sampling times that would have been necessary for sample handling until samples would have been analyzed would have significantly influenced the results. For this reason, the reverse reaction was studied in batch reactor mode.

The reaction was mainly studied using the heterogeneous catalyst in the ester hydrolysis direction and without catalyst in the reverse reaction as formic acid acts as a very capable homogeneous catalyst in itself. Measurement results are shown in Figure 2.9.

2.6.6.5 Reaction Rate Measurement Results

The thermodynamic data that was used when fitting the reaction rate measurement results can be found in Table 2.3. Included in this table is the enthalpy of formation of the ester and the adsorption equilibrium constants which were fitted to the experimental data points. To fit the parameters to the measured reaction rate data, the global optimizer described in Chapter 3.1 was used again. Table 2.4 reports the frequency factors and

Table 2.3: Thermodynamic data and Langmuir sorption constants used for the computation of the temperature dependent equilibrium constants.

Substance	$\Delta_f H^0$ in $\frac{J}{mol}$	S^0 in $\frac{J}{molK}$	c_P in $\frac{J}{molK}$	K_{SLE}
Cyclohexene	-37820 [59]	216.33 [5]	148.83 [59]	0.055396
Cyclohexanol	-351831 [80]	203.87 [1]	213.59 [1]	0.92793
Water	-285830 [12]	69.95 [12]	75.39 [11]	19.878
FCE	-487129	275.5 [33]	219.5 [47]	3.7942
Formic Acid	-425379 [23]	129 [30]	99.84 [55]	2.8568×10^{-7}

activation energies found during the data fitting procedure. The measurement data are compared to the computed values in Figures 2.7 to 2.9.

Table 2.4: Reaction kinetic parameters fitted to experimental data

Reaction	$k_{f,0}^{hom}$ in $\frac{1}{s}$	E_A^{hom} in $\frac{J}{mol}$	$k_{f,0}^{het}$ in $\frac{mol}{kg_{cat}s}$	E_A^{het} in $\frac{J}{mol}$
Cyclohexene Hydration	–	–	7.7083×10^{12}	93687
Cyclohexene Esterification	1.7089×10^{11}	95467	4.5701×10^{25}	114395
Ester Hydrolysis	7.2738×10^5	52287	1.2148×10^{16}	100240

2.6.6.6 Mass Transfer Effects

The use of heterogeneous catalysts can lead to reaction rate limitations which are due to the limited mass transfer rates to and from the catalytic sites. In case there are two liquid phases and an uneven distribution of a homogeneous catalyst between the phases, mass transfer effects can also play an important role. Knowing the observed reaction rate and making certain assumptions about catalyst grain size and reactant concentration within the catalyst particle, the criterion formulated by Weisz and Prater [79] allows evaluating whether internal mass transfer effects play a significant role for a given reaction. For

the direct hydration route this evaluation was done by Seliger [57] and shows that mass transfer effects do not play any role for this reaction. For both other reactions, inner mass transfer effects were found to play a significant role. To validate these results and to determine whether external diffusion limitations were at all significant some simple experiments were carried out.

In the first set of these experiments, the stirrer speed within the reactor was varied to change the flow field around the catalyst particles. These experiments indicated that indeed the direct cyclohexene hydration is not mass transfer limited with respect to the outer mass transfer to and from the catalyst particles as was to be expected. This can be attributed to the very slow chemical micro-kinetics of this reaction. The changes in reaction rate observed were insignificant.

The other two reactions did show an increase in overall reaction rate with increasing stirrer speed. The effect was more pronounced at lower stirrer speeds and became less significant at higher speeds. The increased stirrer speed did have another effect, however. As the stirrer speed was increased, an increase of catalyst particle attrition was also observed leading to an increased rate of catalyst loss from the system. As a compromise for the other measurements, a stirrer speed of 1400 rpm was adopted — a value where catalyst attrition was still negligible.

As outer mass transfer effects can usually be seen as an indicator of even larger inner mass transfer limitations (due to slower mass transfer within the particle and higher concentration of catalytic sites), and since the Weisz criterion indicated internal mass transfer limitations as being rate limiting some experiments were performed with ground catalyst particles with different particle sizes. These experiments were only carried out with the cyclohexene esterification reaction. The results indicate that pore diffusion resistances have an effect on reaction rate down to about $90\ \mu\text{m}$ catalyst grain size.

It was decided not to pursue the inner mass transfer effects further as a later reactive distillation column will always be operated with the catalyst with the commercially available particle size distribution. Outer mass transfer within the column will presumably be worse than in the stirred tank reactor which will have to be taken into account when modeling the reactive distillation column system. It is expected that the catalyst efficiency will drop due to these additional mass transfer rate limitations.

3 Numerical Methods and Results

The simulation of chemical engineering systems is strongly dependent on numerical treatment of the large differential-algebraic equation systems that result from modeling these systems. Especially, very robust and fast solvers for stiff systems are needed. Luckily however, such solvers exist both in DIVA and Matlab (by The Mathworks, Inc.) — both of which were used to do simulations as part of this work.

Apart from the integrators capable of handling the differential algebraic equation systems occurring in this work, three other types of algorithms are needed in the framework of this thesis. These are global optimization algorithms especially needed for parameter estimation, appropriate objective functions needed to quantify the quality of solutions found and algorithms for rapid liquid-liquid phase splitting computations. Unluckily, these were not available as standard tools so that they had to be implemented as part of this work and are to be presented in the following sections.

3.1 Global Optimization Algorithm

One of the most important goals of many engineering activities lies in the optimization of devices or plants. This optimization usually tries to minimize or maximize some objective function like costs or profit, respectively. To allow for easier discussion, the following sections assume a minimum is being sought. Usually, the numerical algorithms being used for such purposes can be classified as optimizers that search for local optima. Many of them search for an extremum of the objective function which is mathematically defined as the location where the gradient with respect to the variables to be optimized is zero (and the second derivative larger than zero). Others use different criteria for their search. The

vast majority of optimization algorithms are based on the assumption that there is only one optimum to be found and independent of their optimization approach they will report this one best value found. However, the optimum these algorithms will report usually depends strongly on where they started searching in cases in which the objective function has multiple optima. Many modeling environments such as Matlab and DIVA already include the numerical algorithms to perform such local optimizations.

In some cases where the objective function is not convex over the definition range of the variables, however, many such points that show a gradient of zero can be found depending on where one starts the search. In these cases the value of the objective function that can be reached while trying to minimize it depends on the choice of the starting point. This behavior is very undesired as one would need to start sufficiently close to the global optimum to find it. In essence, one needs to know the location of the global optimum to choose the correct starting points to be able to find it.

To circumvent these problems, so-called global optimization algorithms have been developed. Unluckily, there are no simple mathematical criteria available that allow showing whether a local optimum is also the global optimum. For this reason one either has to assure that all local optima are found within the admissible range of the variables or that at least a sufficient number is found such that the global optimum is very likely to be included.

These two ways of finding the global optimum are referred to as deterministic and stochastic global optimizers. The deterministic global optimizers such as interval newton / generalized bisection proposed e.g. by Stadtherr et al. [56, 70] have the distinct disadvantage of requiring a high amount of computation time that rises exponentially with the number of variables. Their advantage however lies in the fact that they can mathematically guarantee finding the global optimum if given enough computation time to terminate. Due to the very high demand for computation time however, they are rarely used for systems containing more than five to ten variables.

The stochastic global optimizers on the other hand can not guarantee finding the global optimum within finite computation time. This drawback is compensated by the fact that their optimization behavior can typically be described as asymptotically approaching the global optimum [9]. This means that they will typically show a fast increase in quality

of the objective function at the beginning of the optimization and then slow down until the global optimum is reached. Since in many cases an optimum that is only marginally different from the globally attainable one is considered sufficiently good for practical applications, this approach has proven to be very useful.

The global evolution strategy presented here falls into this category. It is based on several analogies to phenomena that nature uses to attain (nearly) globally optimal solutions. In the following chapters the ideas behind Simulated Annealing and the associated Metropolis Criterion and Evolution Strategies are briefly introduced to allow to understand how they were combined to a Global Evolution Strategy for efficient global optimization purposes.

3.1.1 Simulated Annealing & Metropolis Criterion

Approaches of how to find global optima are fairly old. One of the first algorithms that was meant to achieve this goal was based on the following observation from nature: If one takes a molten piece of metal and cools it down very slowly — so-called annealing of the metal — it will end up being in the ideal crystal configuration which is the global energy minimum it can achieve.

The reason for it being able to attain the globally optimal configuration lies in the fact that the metal atoms or clusters of atoms have to pass intermediate states of higher energy to be able to switch configurations until the optimal configuration is reached. The energy that they have available for such changes depends on their temperature. Thus, if the metal is cooled too quickly — so-called quenching — the atoms or groups of atoms can no longer bypass intermediate high-energy states to attain the global optimum. The metal will be stuck in a local optimum. For this reason, the temperature has to be lowered very slowly and the cooling schedule plays an important role for annealing processes.

Using the idea behind the annealing process, the Simulated Annealing algorithms were initially suggested by Metropolis et al. [40]. The idea behind this class of algorithms lies in the modification of the variable vector, the evaluation of the objective function at this new location and the acceptance of any steps that lead to a quality increase. To be able to leave the region around one local minimum and reach another, however, it is

necessary to pass areas of significantly lower quality — just as the metal atoms have to pass higher-energy intermediate stages in search for the lowest possible configuration. For this reason steps that lead to quality decreases are not rejected as would be typical for local algorithms. Instead, the so-called Metropolis Criterion is evaluated:

$$\mathcal{P} = e^{\frac{f(z_k) - f(z_{k+1})}{T}} \quad (3.1)$$

In this equation, f is the objective function being evaluated at the old (index k) and the new (index $k + 1$) variable vector z . The \mathcal{P} being computed is the likelihood of the new variable vector being accepted. If a given evenly distributed random number in the range from zero to one happens to lie below \mathcal{P} , the new variable vector is accepted. The parameter T in equation 3.1 is the “temperature” in keeping with the annealing analogy. This parameter should have a high value at the beginning and then follow some “cooling schedule” to lower it until no further quality decreases are being accepted.

3.1.2 Evolution Strategies

Classical Evolution Strategies are optimization algorithms that will find local optima. They are based on the idea that the variables to be optimized can be seen just as genes can be seen for biological systems. Under this perspective, the variable vector plays the role of the genome of the individual. The fitness for some purpose can then be seen as the expression of these genes or as the function value of the objective function. Once the variables to be optimized are considered this way, all the ways nature has found to alter the genome to produce offspring that are better adapted to some objective function can also be applied to the variables. Methods here might include random mutation, recombination and others.

For a successful adaption of the individuals to a given environment, nature has also learned ways to control the step size of the changes it makes. In some genes, small changes will usually lead to very large effects in the resulting individual which will tend to be detrimental to its fitness. These genes are changed much more slowly than others where even large changes have little effect. The mechanism that can be described as evolution of step sizes is typically called adaptive step size control. An excellent overview of

evolution strategies of various kinds can be found in [50].

3.1.3 Global Evolution Strategy

Since classical Evolution Strategies are local optimization algorithms and typically show a slower convergence to the local optimum than deterministic approaches like e.g. Newton's method they are rarely used in technical applications. This becomes especially true for cases in which analytical gradients can be computed.

For global optimization however, Evolution Strategies can be combined very well with deterministic algorithms. The idea behind this combination is that Evolution Strategies are ideally suited to generate starting points for deterministic local optimizers. These starting points are to a certain extent randomly distributed around existing points and are then locally minimized using e.g. sequential quadratic programming (SQP) / Newton methods.

Since all the individuals within such an evolution strategic population are local minima, the overall definition range of the variables is somewhat discretized, as not all values or combinations of values can be obtained for the variables. Due to this, classical evolution strategies which typically know only one or a few individuals while searching for the local minimum had to be modified slightly as no continuous movement towards a goal is possible. To stay within the analogy, every local minimum of the objective function can be considered to be an ecological niche which is immediately found as soon as a starting point falls within the convex region around it. The Global Evolution Strategy now aims at filling all the niches or in analogy finding all minima. To do this, much larger populations are needed than in classical evolution strategies.

The resulting Global Evolution Strategy consists of the following eleven steps:

1. Initialization step: Compute value of objective function at starting point and set individual step sizes to 1/3 of the definition range of the variables. With this information generate first "individual" I consisting of variable vector z (the "genome"), its function value f , its generation g (which is 0 for the first individual) and the vector of individual step sizes ϑ . Thus, an individual can be represented by the

following vector:

$$I = \begin{pmatrix} z \\ f(z) \\ g \\ \vartheta \end{pmatrix} \quad (3.2)$$

The population is a list of individuals sorted by their function values f :

$$Population = (I_1, I_2, \dots, I_n) \quad (3.3)$$

Also, set the counter for the number of individuals to 1.

2. The index counting the current generation being generated g_{new} is incremented by 1. Also, the counter for the elder currently producing offspring is set to 1.
3. The Metropolis Criterion (Equation 3.1) is used to decide whether the current elder produces offspring or not. It is evaluated with the difference between the objective function values of the best individual and the current elder in the nominator of the exponential function. The number computed is compared to an evenly distributed random number generated between 0 and 1 and if the random number is smaller an offspring is generated by:

$$z_{offspring} = z_{elder} + \phi(0, 1) \vartheta_{elder} \zeta^{(g_{offspring} - g_{elder})} \varphi^\alpha \quad (3.4)$$

In this equation, $\phi(0, 1)$ is a vector of normally distributed random numbers with a mean of 0 and a standard deviation of 1. ζ is a factor smaller than 1 which will lead to the step size decreasing by a factor of 10^{-5} over the course of the optimization. φ is a scalar step scaling factor which was chosen to be 1.4 and α is -1 , 0 or 1 with equal likelihood (for reasons for this factor please refer to [50]).

Each variable in this new “genome” is then checked to lie within the definition range defined for it ($lb_i \leq z_i \leq ub_i$ with lb and ub as the respective lower and upper bounds) and in cases in which this is not given, z_i is reflected at the boundary.

4. A local optimizer (e.g. SQP / Newton) is used to optimize f with $z_{offspring}$ as the starting point to this optimization. If the local optimization does not terminate successfully, go to step 7.

5. Compute the new vector of individual step sizes $\vartheta_{offspring}$ using

$$\vartheta_{offspring} = \vartheta_{elder} \varphi^{\frac{\alpha}{\sqrt{dim}}} \zeta^{(g_{offspring} - g_{elder})} e^{\frac{\sqrt{\pi}|\vartheta| - \sqrt{2}}{dim \sqrt{\pi}}} \quad (3.5)$$

In this equation, dim is the dimension of the optimization problem which is equivalent to the number of variables. The equation was adapted from the approach presented in [50].

The resulting individual step sizes are then checked to lie below the width of the definition range of the according variables ($\vartheta_i \leq ub_i - lb_i$). If they are larger, they are restrained to this range.

6. If the optimized offspring thus generated has not been found before, assemble it as an individual according to equation 3.2 and add it into the population at the correct position according to its function value. Also increment the population size counter by 1.

If this leads to an increase in population size above what is permitted by the user, remove the last individual from the population and decrement the population size counter by 1.

7. Repeat steps three to seven for as many times as the user has set the number of offspring per generation.
8. Increment the counter of the elder currently producing offspring. Repeat steps three to eight until all elders have produced offspring in this generation. All individuals whose generation counter lies below g_{new} are considered to be elders.
9. Reduce the “temperature” parameter according to some cooling schedule chosen — e.g. by multiplying it with a constant factor below 1.
10. Remove any individuals from the population whose chance of producing any offspring in the remaining generations has fallen below 0.5. Should this still lead to a population size at the limit granted by the user, adjust “temperature”.
11. If the number of generations set by the user has not been reached, increment generation counter g_{new} and repeat steps two to eleven.

As each elder typically produces several offspring in every generation and the offspring themselves again produce further offspring in later generations this approach leads to an exponential increase in population size at the beginning. Due to the fairly large individual step sizes chosen at the beginning of the optimization this also leads to a dispersal of the population across the definition range of the variables initially.

To limit computational effort, some restrictions to population size or growth have to be imposed. These restrictions are a limit on the size of the population set by the user, the requirement of all individuals being unique and the Metropolis Criterion which becomes increasingly restrictive as the quality of the best individual increases and the “temperature” parameter is decreased. The effect this last criterion has is again based on an analogy to nature. As computational resources are plentiful at the beginning, all new individuals are accepted into the population to gain a maximum in diversity. As the bounds on computation time and memory come into sight, only the better individuals located at the better local optima are sufficiently well adapted to have a chance to create offspring which will be located relatively close to their successful elders thus concentrating the search on the more promising areas of the definition space.

For the algorithm to work well, a good choice of the “temperature” parameter and of an appropriate cooling schedule are very important. As a cooling schedule, a simple repetitive multiplication with a factor smaller than 1 was chosen. The choice of the initial “temperature” was delayed until population size has reached 100 and was then based on a multiple of the standard deviation associated with the function values achieved within the population. In the case that the Metropolis Criterion was not limiting enough leading to a population size at the limit permitted by the user, the “temperature” parameter was adjusted accordingly.

3.2 Objective Functions

Whenever trying to fit experimental measurement data to a function that is supposed to describe such data the question arises which parameter set describes the data best. Typically, the approach to finding such a parameter set is based on an optimization method

such as an SQP/Newton method or (in rather few cases so far) on global search methods like the global evolution strategy presented in Chapter 3.1.

Whenever using such techniques however the question of how the algorithm is to decide which parameter set leads to a better fit has to be addressed. Usually the approach here is to define an objective function to be minimized which is formulated as the sum of least squares:

$$\delta = \sum_{i=1}^{NP} (q_i^{exp} - q_i^{calc})^2 \quad (3.6)$$

In this equation, q denotes some (arbitrary) quantity, superscripts *exp* and *calc* denote experimentally measured and calculated values, i is an index that goes from 1 to the number of measurement points, NP .

If the measurement data were ideal — meaning without measurement error — the sum should be zero if the ideal parameter set is found and if the equation being fitted is capable of describing the phenomena measured completely (which is often assumed). Unluckily, ideal measurement data are rarely available. Instead, the measurements show a certain amount of scattering around the “true” values, which are not known. What is typically known however (or what can be estimated) is the standard deviation associated with the measurement. This becomes important, when different types of measurements are to be fitted simultaneously. The above terms on the right hand side of Equation 3.6 should then be normalized by dividing them through their variance before being summed up to weight them correctly:

$$\delta = \sum_{i=1}^{NP} \frac{(q_i^{exp} - q_i^{calc})^2}{\sigma_{q_i}^2} \quad (3.7)$$

The disadvantage of the above approach lies in the fact that typically one has to insert some measured quantities into the equation whose parameters are being optimized to be able to calculate the q_i^{calc} values. To demonstrate what is meant the Antoine Equation is chosen:

$$\log_{10} \left(\frac{P_i^{sat}}{Pa} \right) = A_i - \frac{B_i}{\frac{T}{K} + C_i} \quad (3.8)$$

In Equation 3.8, P_i^{sat} is the saturation pressure in Pa , T is the temperature in K and A_i , B_i and C_i are the parameters of substance i to be fitted to the data. The measurement

data will consist of several sets of pressure / temperature values. As both of these values are measured experimentally, they are not the true values (which are unknown) but are assumed to be normally distributed around the true values with estimated variances for the pressures of σ_p^2 and for the temperatures of σ_T^2 . In many cases, one of the two values (typically the temperature value) is inserted into Equation 3.8, the according pressure for the current parameter set is calculated and the sum of squares according to Equation 3.7 is computed using this calculated value considering only the variance of the pressure to weight the squared differences. What is being ignored is the fact that the *calculated* pressure has a variance of its own due to the temperature variance of the temperature measurement value inserted into the equation.

In many cases in which the accuracy of the temperature measurement is sufficiently high and the sensitivity of the calculated value with respect to the variance of the inserted measured temperature value is not too high, this will produce good results. Cases in which this is not the case can easily be constructed, however. To address this problem, the “true” temperature and pressure values are added into the fitting procedure as additional variables. The new objective function to be minimized for this case is now:

$$\delta = \sum_{i=1}^{NP} \frac{(P_i^{exp} - P_i^t)^2}{\sigma_{P_i}^2} + \frac{(T_i^{exp} - T_i^t)^2}{\sigma_{T_i}^2} \quad (3.9)$$

Superscripts t denote the “true” values. The equation to be fitted can now be seen as a set of equality constraints of the optimization, the parameters sought are the parameters of these equality constraints. As the “true” values have to exactly fulfill Equation 3.8, and the equation is easily solved for one value if the other is known, either the “true” temperature or pressure values can be calculated directly from the respective other value allowing to reduce the number of variables of the optimization. Whether such a reduction is possible depends on the nature of the equation to be fitted, though.

This second approach to defining the objective function to be minimized when searching for the best set of parameters has the drawback of usually requiring more computation time because of the additional variables to be optimized (the “true” values). In some cases, however, a significant improvement in the achieved fit was observed without having to resort to global optimization techniques.

3.3 Phase Splitting Calculations

If one wants to simulate reactive distillation with liquid-liquid phase splitting, the solution of the phase splitting subproblem has to be handled in a very efficient manner since this subproblem has to be solved many thousands of times.

In general, the phase splitting problem requires a global optimization approach because in the case that two phases coexist the Gibbs' enthalpy surface for a given overall composition has (at least) two local minima. These local minima correspond to the trivial solution where the compositions in both phases are equal (the actual one-phase solution) and to the sought-after two-phase solution where this is not the case. Whenever there is more than one solution, the solution with the lowest Gibbs enthalpy is the favored one.

Since it is not known a priori whether there exists a second minimum of the Gibbs enthalpy surface, this would usually lead to the necessity of finding all minima and in consequence necessitates a global minimum search. Known global minimizers such as those proposed e.g. by McDonald & Floudas [38] or by Tessier et al. [70] have shown fairly large computation times especially in cases with many components. Due to the fact that the global minimum search has to be carried out repetitively the high computational cost of a real global optimization is unacceptable.

For this reason several different approaches have been suggested in the literature (e.g. [41, 48]). However, these approaches can be shown to be unreliable under certain conditions. For this reason, three further approaches were investigated as part of this work. Two of these approaches are based on a homotopy continuation method proposed for exactly this purpose by Bausa and Marquardt [4] but which was modified slightly. A third approach is based on non-equilibrium thermodynamic considerations.

3.3.1 Homotopy Continuation

The homotopy method that was proposed by Bausa and Marquardt [4] is based on the following set of equations which have to be fulfilled for liquid-liquid equilibrium:

$$\beta x_i^{nonpolar} + (1 - \beta)x_i^{polar} = x_{i,tot} \quad (3.10)$$

$$\gamma_i^{nonpolar} x_i^{nonpolar} - \gamma_i^{polar} x_i^{polar} = 0 \quad (3.11)$$

$$\sum_{i=1}^{NC} (x_i^{nonpolar} - x_i^{polar}) = 0 \quad (3.12)$$

with NC as the number of components, i as the component index, tot indicating the overall composition, $nonpolar$ and $polar$ as superscripts denoting the non-polar and polar phases respectively, x as the component mole fraction, β as the mole fraction of the non-polar phase and the γ_i as the respective activity coefficients at the compositions of the respective phases. Equations 3.10 and 3.11 each lead to NC equations — one for each component. Equation 3.12 adds another equation leading to a total of $2NC + 1$ equations and variables. The formulation of Equation 3.12 might seem slightly unusual. It was chosen to assure that both summation equations ($\sum_{i=1}^{NC} x_i^{nonpolar} = 1$ and $\sum_{i=1}^{NC} x_i^{polar} = 1$) are fulfilled without needing more than one equation. One could have chosen one of the two summation equations instead but this would have led to one summation equation being explicitly stated whereas the other is fulfilled as a result of the overall equation set.

The homotopy continuation is based on these equations which are left unchanged except for Equation 3.10. This equation is slightly modified on the right hand side:

$$\beta x_i^{nonpolar} + (1 - \beta) x_i^{polar} = \lambda \cdot x_{i,tot} + (1 - \lambda) x_{i,start} \quad (3.13)$$

In Equation 3.13, λ is the continuation parameter that is increased from 0 to 1 during the continuation. The $x_{i,start}$ is a starting composition for which it is known that the algorithm will converge to a two-phase solution.

Since the overall shape of the two-phase region is usually not known at the beginning, Bausa and Marquardt suggest to use several starting points which are chosen to be in the middle of all binary mixing gaps in the multicomponent system under study. The homotopy then starts at the known two-phase solution and changes the overall composition slowly towards the final composition that is of interest. Should the binodal surface be crossed during this transition before λ reaches 1, the continuation is restarted at the next starting point or — in the case that the current continuation is already using the last starting point — the system is assumed to have only one liquid phase.

As was shown for Equations 3.10 to 3.12, the equation system in the formulation of Bausa and Marquardt has $2NC + 1$ equations and variables. The real number of degrees of freedom in such a system is NC , however, as can easily be seen from Gibbs' phase rule. From

the theoretical side this suggests that it should be possible to restate the equation system with only NC equations and variables. Since the solution of the equation system consisting of Equations 3.10 to 3.12 is typically achieved using a Newton approach the amount of computation necessarily rises with the third power of the number of equations or variables. Due to this it is highly desirable to reduce the amount of equations and variables. To achieve this goal, two sets of transformed variables were introduced.

3.3.1.1 Tie Line Coordinates

The first set of these transformed variables was suggested by D. Flockerzi at the Max Planck Institute in Magdeburg [62] and can be interpreted as trying to describe the tie lines in the phase diagram. As can easily be seen in e.g. a three component system that shows phase splitting, the tie line can be described by the difference in the composition of the two phases for two components and by its location with respect to the current (λ -dependent) overall composition.

This variable transformation can be written as:

$$\eta_i = x_i^{nonpolar} - x_i^{polar} \quad (3.14)$$

$$\xi_i = x_i^{nonpolar} + x_i^{polar} - 2x_{i,tot} \quad (3.15)$$

With these variables, the $x_i^{nonpolar}$ and x_i^{polar} can be expressed as

$$x_i^{nonpolar} = x_{i,tot} + \frac{\xi_i + \eta_i}{2} \quad (3.16)$$

$$x_i^{polar} = x_{i,tot} + \frac{\xi_i - \eta_i}{2} \quad (3.17)$$

The η_i can be interpreted as the length of the tie lines with respect to the different components. They have to lie within a range from -1 to 1 .

Replacing the $x_i^{nonpolar}$ and x_i^{polar} in Equation 3.10 with these definitions leads to the following expression:

$$\xi_i = (1 - 2\beta)\eta_i \quad (3.18)$$

which in turn gives:

$$x_i^{nonpolar} = x_{i,tot} + (1 - \beta)\eta_i \quad (3.19)$$

$$x_i^{polar} = x_{i,tot} - \beta\eta_i \quad (3.20)$$

Equation 3.18 allows to remove the ξ_i from the equation system reducing the overall amount of variables and equations to $NC + 1$. Furthermore, inserting η_i into Equation 3.12 the following equation can be derived:

$$\sum_{i=1}^{NC} \eta_i = 0 \quad (3.21)$$

This equation allows to reduce the number of variables and equations by 1. What is left are Equations 3.11. This reduces the problem to NC equations and NC variables — or roughly by a factor of two. Since computational effort for the Newton approach is cubic with respect to the number of variables or equations the computational effort is reduced by a factor of 8. However, Equation 3.11 has to be restated in terms of the first $i = 1 \dots NC-1$ η_i and β . To do this one first introduces a new variable vector called θ that contains exactly these variables, namely $\eta_1 \dots \eta_{NC-1}$ and β .

Denoting Equations 3.11 as $f(\theta)$, the general Newton approach to solving such an equation system is given by

$$\theta_{k+1} = \theta_k - J^{-1}(f(\theta_k))f(\theta_k) \quad (3.22)$$

In this equation, J^{-1} is the inverted Jacobian of $f(\theta)$. Obviously, one would use some more efficient approach than direct matrix inversion to solve the appropriate linear equation system for larger systems (e.g. by Gaussian Elimination).

Unluckily however the Jacobian has to be derived with respect to θ . The derivative of Equation 3.11 with respect to some arbitrary θ_j is

$$\begin{aligned} \frac{\partial f_i}{\partial \theta_j} = & \frac{\partial x_i^{nonpolar}}{\partial \theta_j} \gamma_i^{nonpolar} + \gamma_i^{nonpolar} \frac{\partial \ln(\gamma_i^{nonpolar})}{\partial \theta_j} x_i^{nonpolar} \\ & - \frac{\partial x_i^{polar}}{\partial \theta_j} \gamma_i^{polar} - \gamma_i^{polar} \frac{\partial \ln(\gamma_i^{polar})}{\partial \theta_j} x_i^{polar} \end{aligned} \quad (3.23)$$

To derive Equation 3.23 the product rule was applied. The logarithm in the derivative was included since the NRTL formulation of the activity coefficient calculation is often given as $\ln \gamma = \dots$ [53]. This is possible since $\partial \gamma = \gamma \cdot \partial \ln(\gamma)$. To avoid having to derive $\partial \ln(\gamma)/(\partial \theta)$ analytically, the following equation can be applied:

$$\frac{\partial \ln(\gamma_i)}{\partial \theta_j} = \sum_{l=1}^{NC} \frac{\partial \ln(\gamma_i)}{\partial x_l} \sum_{m=1}^{NC-1} \frac{\partial x_l}{\partial x_m} \frac{\partial x_m}{\partial \theta_j} \quad (3.24)$$

The superscripts *nonpolar* and *polar* were omitted here since the above equation is valid for both phases. Obviously one has to calculate the two separately.

The first term on the right hand side of Equation 3.24 is the analytically derived derivative of the NRTL equation with respect to the x_k . The derivation of this derivative is time consuming but fairly trivial.

The second term is necessary due to the fact that the x_k are not independent of each other since they have to add to 1. This derivative leads to a matrix that is composed of an $(NC - 1) \times (NC - 1)$ identity matrix and an additional line at the bottom containing -1 s due to the fact that one can write x_{NC} as $1 - x_1 - x_2 - \dots - x_{NC-1}$.

The third term finally is dependent on the phase currently being calculated. It is the derivative of the defining equations of $x_i^{nonpolar}$ or x_i^{polar} (Equations 3.19 and 3.20) with respect to the θ_j . For the whole equation system defined by Equations 3.11 the following matrix representation for the Jacobian can be derived:

$$J = \left[\text{diag}(\gamma^{nonpolar}) + \text{diag}(\gamma^{nonpolar}) \text{diag}(x^{nonpolar}) \Gamma^{nonpolar} \right] \tau \Theta^{nonpolar} - \left[\text{diag}(\gamma^{polar}) + \text{diag}(\gamma^{polar}) \text{diag}(x^{polar}) \Gamma^{polar} \right] \tau \Theta^{polar} \quad (3.25)$$

In this equation the term *diag* denotes a diagonal matrix where the diagonal elements are the elements of the vector given in brackets. Γ is the analytical Jacobian of the logarithmic version of the NRTL equation with respect to all x_j and evaluated at $x^{nonpolar}$ or x^{polar} respectively:

$$\Gamma^{phase} = \left. \frac{\partial \ln(\gamma_i)}{\partial x_j} \right|_{x=x^{phase}} \quad (3.26)$$

τ is an $NC \times (NC - 1)$ matrix and is identical to the matrix described as the second term of Equation 3.24. Finally, Θ is the matrix of derivatives of the first $i = 1 \dots (NC - 1)$ x_i with respect to all θ_j and is an $(NC - 1) \times NC$ matrix:

$$\Theta^{phase} = \begin{pmatrix} \frac{\partial x_1^{phase}}{\partial \theta_1} & \dots & \frac{\partial x_1^{phase}}{\partial \theta_{NC}} \\ \dots & \dots & \dots \\ \frac{\partial x_{NC-1}^{phase}}{\partial \theta_1} & \dots & \frac{\partial x_{NC-1}^{phase}}{\partial \theta_{NC}} \end{pmatrix} \quad (3.27)$$

The *nonpolar* and *polar* versions of Θ denote that the derivatives of $x^{nonpolar}$ or x^{polar} with respect to θ are meant. Obviously, this means that the two Θ matrices are different in their

analytical elements due to the different definitions of $x^{nonpolar}$ and x^{polar} in Equations 3.19 and 3.20.

3.3.1.2 Phase Partitioning Coefficients

Besides trying to describe the tie lines as was the case with the previous set of transformed variables, there are many other ways of variable transformation. One of these ways is to introduce so-called phase partitioning coefficients according to:

$$\theta_i = \frac{n_i^{nonpolar}}{n_i^{nonpolar} + n_i^{polar}} \quad (3.28)$$

The n_i are the molar amounts in the respective phases. These variables can be interpreted as distribution coefficients for every component between the two phases. For obvious physical reasons the θ_i have to lie within a range between 0 and 1 for any system with two liquid phases. To be more precise, they have to be strictly above 0 and below 1 (for thermodynamic reasons solubility is always nonzero).

It can be easily shown that if the LLE problem is restated in these new variables, Equations 3.10 and 3.12 are automatically fulfilled. What is left is Equation 3.11. This again reduces the problem to NC equations and NC variables.

As was the case for the tie-line coordinates, the remaining equations now have to be restated in terms of these new variables. To do this one first derives expressions for $x_i^{nonpolar}$ and x_i^{polar} :

$$x_i^{nonpolar} = \frac{\theta_i x_{i,tot}}{\sum_{j=1}^{NC} \theta_j x_{j,tot}} \quad (3.29)$$

$$x_i^{polar} = \frac{(1 - \theta_i) x_{i,tot}}{\sum_{j=1}^{NC} (1 - \theta_j) x_{j,tot}} \quad (3.30)$$

In combination with Equation 3.10 this leads to the following equation for β :

$$\beta = \sum_{j=1}^{NC} \theta_j x_{j,tot} \quad (3.31)$$

These new definitions can now be inserted into Equations 3.10 and 3.11. Again, the Newton iteration will need the Jacobian of this equation vector with respect to these new

θ_i . To derive this Jacobian the same approach was used as for the tie-line coordinates (Equations 3.22 to 3.25). Obviously, the contents of the Θ matrices are different as the definitions of the x_i with respect to the θ_i has changed. All of the definitions for the individual terms are the same as with the tie line coordinates, however, so that they will not be repeated here.

3.3.2 Rate-Based Approach

As was mentioned in the introduction to this section, three approaches were investigated for the phase splitting computations. Besides the two homotopy-based approaches presented above, a third approach first suggested by K. Sundmacher of the Max Planck Institute in Magdeburg based on non-equilibrium thermodynamic considerations was implemented. The idea behind this approach is to model what happens within a mixture that exhibits a local concentration inhomogeneity. As e.g. Kondepudi & Progovine [32] note, such a local inhomogeneity will lead the system to respond by moving back to the stable node in case that the one phase solution is stable. When a mixture crosses the phase boundary into the two phase realm, however, a local concentration inhomogeneity in an initially single phase system can grow into a full-fledged second phase as the one phase solution is no longer a stable node.

The model thus considers two liquid phases of different initial composition and then follows the evolution of the compositions of the two phases as they are brought into contact. In cases in which the one-phase solution is stable, the second liquid phase will either tend to dissolve and disappear or try to change its composition to match the first phase indicating that only one phase exists. In cases in which the one-phase solution is unstable, however, the initial disturbance will grow until phase equilibrium is reached.

The model can be formulated as follows:

$$\begin{aligned} \frac{dn_i^{nonpolar}}{dt} &= \frac{k}{RT} A_{int} (\mu_i^{polar} - \mu_i^{nonpolar}) \\ &= k A_{int} \ln \left(\frac{a_i^{polar}}{a_i^{nonpolar}} \right) \\ \frac{dn_i^{polar}}{dt} &= -\frac{k}{RT} A_{int} (\mu_i^{polar} - \mu_i^{nonpolar}) \end{aligned} \quad (3.32)$$

$$= -kA_{int} \ln \left(\frac{a_i^{polar}}{a_i^{nonpolar}} \right) \quad (3.33)$$

In these equations the interfacial area between the two phases is denoted as A_{int} and modeled as the mole fraction of the minor phase to the power of $2/3$ — essentially assuming spherical droplets within the continuous larger phase. The kinetic constant k describes the mass transfer rate across the phase boundary.

To determine the equilibrium solution, Equations 3.32 and 3.33 are simply integrated until steady state is reached. In cases in which two liquid phases exist, the steady state will reflect this. This is due to the fact that the one-phase solution mathematically represents an unstable node which will not be found as the steady state solution during integration if a two-phase solution exists. Only in the case of identical starting compositions in both phases will the unstable point be found.

In cases in which one is only interested in the equilibrium solution — and not in the trajectory leading there — there is the possibility of using Equations 3.32 and 3.33 and their integration trajectory as an increasingly accurate set of starting values for simple Newton solution attempts of e.g. Equations 3.10 to 3.12 or their transformed versions as described in the previous two chapters. In case that during one of these solution attempts a two-phase solution is found, this dramatically reduces computational effort.

The choice of the starting compositions of both phases is only restricted by the need to leave the overall composition unchanged and by the fact that the compositions in the two phases have to differ. The choice of starting compositions that are close to the final equilibrium solution will speed up the solution process however.

The integration of Equations 3.32 and 3.33 can also be used to describe the real composition change that an initially two-phase mixture is undergoing. In this case the equations would be solved simultaneously with any other system equations of the system being described. To achieve realistic results, the mass transfer coefficient k has to be chosen correctly and might actually be more complex as e.g. Maxwell-Stefan mass transfer theory might be used instead of the simple approach used here.

If such an approach is chosen to model the composition trajectories, intermediate Newton solution attempts do not make any sense any more. The simultaneous solution approach can be used however even in cases in which equilibrium compositions are desired. In

this case the mass transfer coefficient k only has to be raised to the point where the mass transfer is basically instantaneous. Care has to be taken, however, as raising k might lead to an increasingly stiff differential equation system which calls for appropriate solvers.

3.3.3 Numerical Considerations

The three approaches to phase splitting calculations presented in the previous chapters require very careful implementation if they are to be used in systems that exhibit extreme phase splitting phenomena as can be expected from systems with water and an olefin.

In the case of the rate based approach, the main source of numerical problems lies in the risk of arriving at negative molar amounts of individual substances due to step size / gradient combinations that lead to such results. To counteract this risk, two measures were taken. The first step was to integrate the phase boundary area into Equations 3.32 and 3.33. As the smaller phase increasingly dissolves within the larger phase, the rate at which the mass transfer takes place decreases, leading to smaller mass transfer streams and in turn reducing the risk of passing into the negative amount range.

In the case that only the equilibrium composition is of interest and that the equation system is integrated separately from the remaining system being simulated, there is a second measure that can be taken. This is based on the fact that it is known that any solutions with negative amounts of any substance do not make any sense. The integrator step size can thus be restrained such that these solutions will not be reached.

In the cases in which homotopy continuation approaches are being pursued, the main numerical difficulty lies in the limited computational accuracy associated with the typical 15-digit numerical number representation.

At the first moment this problem seems a bit far fetched as one would usually assume that 15 digits are enough accuracy for any real system. A simple example will be used to show that there are many cases in which this is not the case. Consider for example a mixture of cyclohexane and water. Let us assume that the water solubility in cyclohexane is 12 ppm. This means that in any case where the overall mole fraction of the water is above 12.1 ppm, the algorithm has to detect a second phase if the error in computing the water activity is to be less than roughly 1%. This in turn means that of the 12.1 ppm water, roughly

12 ppm will dissolve in the majority phase of almost pure cyclohexane. The remaining 0.1 ppm forms a second, aqueous phase whose phase fraction is also roughly 0.1 ppm. Obviously, this aqueous phase will be saturated with cyclohexane whose mole fraction in it will be assumed to be 376 ppm. In the case of the phase partitioning coefficients the fraction of the cyclohexene in the aqueous phase is thus 3.76×10^{-11} . If one now wants to solve the activity equality Equations 3.11 with 8-digit accuracy, the last digit needed is in the range of 10^{-18} . As long as the phase partitioning coefficient is defined by chance as being close to zero, this will not be a problem as the exponent can simply be changed leaving 15 significant digits of the mantissa. In case that the non-polar phase is the first phase however, the phase partitioning coefficient becomes a number very close to 1. This in turn means that too many significant digits are lost to be able to solve the phase splitting problem accurately.

To solve this numerical difficulty, the definition of the phase partitioning coefficients was changed:

$$\theta_i = \begin{cases} \frac{n_i^{nonpolar}}{n_i^{nonpolar} + n_i^{polar}} & : n_i^{nonpolar} \leq n_i^{polar} \Rightarrow \kappa_i = -1 \\ \frac{n_i^{polar}}{n_i^{nonpolar} + n_i^{polar}} & : n_i^{nonpolar} > n_i^{polar} \Rightarrow \kappa_i = 1 \end{cases} \quad (3.34)$$

As can be seen, the θ_i are now always in the range from 0 to 0.5, thus removing the numerical problem. The additional flag κ_i was introduced to store the information on which definition is currently valid.

The definitions of the $x_i^{nonpolar}$ and x_i^{polar} with respect to the θ_i now also depend on the κ_i . A similar approach can be formulated for the tie line coordinates. As these can be both positive and negative, this approach uses two such flags for each θ_i . The implementation of such case-dependent variables requires great care especially when computing the gradients as they have to always be formulated depending on the case that is currently valid.

3.3.4 Performance Comparison and Conclusions

Considering that all three approaches to phase splitting computations will converge towards the correct solution (if implemented correctly), the question arises as to which algorithm to select. Since the phase splitting computations have to be carried out frequently

Table 3.1: Parameterizations, number of variables and computation times for the example taken from [70] with the four components propanol, butanol, benzene and water using the NRTL parameters reported there. All algorithms found the same LLE solution. (“BM” - original Bausa & Marquardt algorithm, “Tie” - tie line approach, “Part” - phase partitioning coefficients, “Rate” - rate based approach)

Algorithm	Variables	Number of Variables	Computation Time
BM	$x_{i=1...NC}^{polar}, x_{i=1...NC}^{nonpolar}, \beta$	$2NC + 1$	1.4 ms
Tie	$\eta_{i=1...NC-1}, \beta$	NC	4.4 ms
Part	$\theta_{i=1...NC}$	NC	1.1 ms
Rate	$n_{i=1...NC}^{polar}, n_{i=1...NC-1}^{nonpolar}$	$2NC - 1$	0.58 ms

during a simulation run computation times are of paramount importance.

As a first step in comparing the different algorithms, the example given in [70] and used by Bausa & Marquardt [4] for rate comparisons of their homotopy continuation algorithm was used. As these authors have shown, their algorithm is already significantly faster than the other approaches shown there. To be able to compare to their results, a SPECfp2000 value of 128 was estimated for their computer based on the SPECfp95 value that they published.

Our own computations were performed on an AMD Athlon XP 2400+ processor using SuSe Linux kernel 2.4.22. The computer has a SPECfp2000 value of approximately 650. The algorithms were implemented under Fortran77 using g77 (gcc version 2.95.3) as a compiler. The algorithms use dgesv from the LAPACK library for solving the linear equation system of the Newton iterations. The computation times were measured using the “time” command under Linux (for most measurements multiple runs of the algorithm were used for time measurements).

The results of this comparison can be found in Table 3.1 and show that both the rate based and phase partitioning approaches were faster in this example. Further comparisons between the three newly suggested algorithms were carried out. A series of runs was performed using three to six component systems to gather information on the order with which the computation time increases with increasing numbers of substances. The

system used for these computations is the six component system under study here (cyclohexene, cyclohexanol, water, cyclohexane, formic acid cyclohexyl ester and formic acid) using the NRTL parameter set from Chapter 2.6. For a three component system, only the first three of these were used, for a four component system the first four were used and so on.

To study the algorithm performance under different situations, four cases were considered all of which were at 298 K. The first case is a situation where the overall composition is such that two phases exist. The location is chosen such that the computed point lies well inside of the two-phase region. This was achieved by setting the mole fraction of water to be 40 % and having the other components share the remaining 60 %. Table 3.2 shows the results of this comparison as well as the correct solution for all systems. As can be seen, there are significant differences between the three algorithms with respect to computation times. The rate based approach shows the best performance for all cases having computation times of less than 1 ms for the three and four component systems. The further tests will show whether this is only a case of having found a good starting point by chance. The tie line coordinates on the other hand show the poorest performance. The apparent orders in which the computation times increase with the number of components are 5.3, 2.6 and 2.3 for the three approaches. As a comparison: Newton's method is known to have an order of 3.

The second test case is at an overall composition where there is only one stable phase. This was achieved by setting the cyclohexanol mole fraction to 0.6 and having the other components share the remaining 0.4 equally. This point is well into the one phase region. Table 3.3 shows the measured computation times for this case. The most obvious change between this case and the previous one is the strong increase of computation times for all algorithms. This is due to the fact that before accepting a composition as having only one stable phase the algorithms give their best to find a suitable two phase solution whereas they are immediately satisfied with any solution that has two phases.

Apart from this general increase in computation time, the rate based approach is again shown to be the fastest one except in the three component case where the phase partitioning coefficient approach is marginally faster. The increase of computation time for the two homotopy based algorithms is also not as predictable as with the previous case.

Table 3.2: Computation times, overall composition (x^{tot}) and correct two phase solution ($x^{nonpolar}$ and x^{polar}) for the three algorithms (“Tie” - tie line approach, “Part” - phase partitioning coefficients, “Rate” - rate based approach) and the different number of components.

Components	Tie	Part	Rate	x^{tot}	$x^{nonpolar}$	x^{polar}
Cyclohexene	3.2 ms	1.6 ms	0.33 ms	0.3	0.4229	4.641×10^{-5}
Cyclohexanol				0.3	0.4215	0.003596
Water				0.4	0.1556	0.99636
Cyclohexene	19.1 ms	2.5 ms	0.65 ms	0.2	0.3175	2.530×10^{-5}
Cyclohexanol				0.2	0.3159	0.002814
Water				0.4	0.04899	0.99715
Cyclohexane				0.2	0.3176	7.988×10^{-6}
Cyclohexene	24.5 ms	4.1 ms	1.1 ms	0.15	0.2361	1.649×10^{-5}
Cyclohexanol				0.15	0.2348	0.002265
Water				0.4	0.05699	0.99757
Cyclohexane				0.15	0.2361	5.660×10^{-6}
FCE				0.15	0.2360	1.384×10^{-4}
Cyclohexene	126 ms	9.9 ms	1.6 ms	0.12	0.2084	3.260×10^{-4}
Cyclohexanol				0.12	0.2020	0.008939
Water				0.4	0.09997	0.8063
Cyclohexane				0.12	0.2085	1.817×10^{-4}
FCE				0.12	0.2076	0.001382
Formic Acid				0.12	0.07358	0.1829

This is due to the different number of starting points needed according to Bausa and Marquardt [4] (two in the three component case, three in the four component case, four in the five component case and six in the six component case) for the different number of components which leads to an additional increase in computational demand. The apparent orders of computation time increase with the number of components are 4.6, 4.0 and 2.3 respectively.

To check whether the algorithms reliably detect a two phase case in close proximity to the binodal surface, a third case was measured. In this case the mole fraction of water was set to be 0.00153, the mole fraction of cyclohexene was set to be 0.99847 and the mole fraction of all other components was zero. The correct solution to this problem has two

Table 3.3: Computation times, and overall composition (x^{tot}) for the three algorithms (“Tie” - tie line approach, “Part” - phase partitioning coefficients, “Rate” - rate based approach) and the different number of components. Correct solution shows only one phase.

Components	Tie	Part	Rate	x^{tot}
Cyclohexene Cyclohexanol Water	39.3 ms	10.5 ms	11.7 ms	0.2 0.6 0.2
Cyclohexene Cyclohexanol Water Cyclohexane	277 ms	40.8 ms	21.8 ms	0.13333 0.6 0.13334 0.13333
Cyclohexene Cyclohexanol Water Cyclohexane FCE	473 ms	69.0 ms	38.2 ms	0.1 0.6 0.1 0.1 0.1
Cyclohexene Cyclohexanol Water Cyclohexane FCE Formic Acid	947 ms	167 ms	57.2 ms	0.08 0.6 0.08 0.08 0.08 0.08

liquid phases with a water mole fraction of 0.0015296 and an overall mole fraction of the smaller phase of less than 4×10^{-7} . Table 3.4 shows the measured computation times.

When compared with the first case, the computation times again generally increased even though more moderately than in case 2. All algorithms show the correct solution, but again the rate based approach was by far the fastest. The orders of computation time increase are 5.1, 2.7 and 2.2 respectively.

Finally, to assure oneself that the algorithms also detect the one phase solution when the overall composition is very close to the binodal surface, a fourth case was measured. The water mole fraction was set to be 0.00152, the cyclohexene mole fraction was set to 0.99848 and again the remaining mole fractions were set to zero. The result can be seen

Table 3.4: Computation times for the three algorithms (“Tie” - tie line approach, “Part” - phase partitioning coefficients, “Rate” - rate based approach) and the different number of components. The overall composition was $x_{Water} = 0.00153$, $x_{Cyclohexene} = 0.99847$, all other components had zero mole fraction. The correct solution found by all algorithms is $x_{Water}^{nonpolar} = 0.0015296$ and $x_{Cyclohexene}^{polar} = 4.6043 \times 10^{-5}$ with a mole fraction of the small phase of less than 4×10^{-7} .

Components	Tie	Part	Rate
Cyclohexene Cyclohexanol Water	14.7 ms	5.3 ms	0.45 ms
Cyclohexene Cyclohexanol Water Cyclohexane	31.5 ms	12.5 ms	0.80 ms
Cyclohexene Cyclohexanol Water Cyclohexane FCE	46.3 ms	19.4 ms	1.3 ms
Cyclohexene Cyclohexanol Water Cyclohexane FCE Formic Acid	493 ms	33.6 ms	2.0 ms

in Table 3.5. This is one case in which the rate based approach is clearly beaten by the phase partitioning coefficients for three and four components. Again, the computation times have increased significantly when compared to the similar two-phase case. The tie line approach is again shown to be by far the worst approach. The computational effort increases with the number of components with an order of 8.4, 4.3 and 2.1 (tie line approach, phase partitioning coefficients and rate based approach, respectively).

To conclude, it can be said that all algorithms are capable of reliably finding the correct number of phases. Their computational demands however are very different and the rate

Table 3.5: Computation times for the three algorithms (“Tie” - tie line approach, “Part” - phase partitioning coefficients, “Rate” - rate based approach) and the different number of components. The overall composition was $x_{Water} = 0.00152$, $x_{Cyclohexene} = 0.99848$, all other components had zero mole fraction. The correct solution found by all algorithms has only one phase with the same composition.

Components	Tie	Part	Rate
Cyclohexene Cyclohexanol Water	25.8 ms	5.0 ms	11.4 ms
Cyclohexene Cyclohexanol Water Cyclohexane	155 ms	14.6 ms	19.8 ms
Cyclohexene Cyclohexanol Water Cyclohexane FCE	434 ms	29.0 ms	32.7 ms
Cyclohexene Cyclohexanol Water Cyclohexane FCE Formic Acid	8755 ms	95.8 ms	49.9 ms

based approach has been shown to be the best under most conditions followed by the phase partitioning coefficient approach. When doing simulations, the rate based approach should thus be favored typically.

The differences found can be attributed to different phenomena. When comparing the rate based approach with both homotopy based approaches, the latter approaches have the disadvantage of requiring the solution from several starting points. This number of starting points also increases with the number of components which leads to the significantly higher order for the one phase cases where all starting points have to be explored.

A second reason lies in the lower number of Newton solution approaches which enable the rate based approach to consistently have an order below three.

The large difference between the two homotopy based approaches can have two reasons. One might be that the tie line approach still has an implementation error even though great care was taken during the implementation. There exists, however, a second more physical interpretation of the large difference found. This explanation is based on what happens to the transformed variables as the algorithm traverses the two-phase region. In the case of the phase partitioning coefficients this actually leads to a rather minor change which is also mostly linear as long as the binodal surface is not too close. The tie line coordinates, however, do not have this very favorable behavior and thus make the solution more tedious resulting in smaller steps and more computations needed.

4 Process Design

When designing complex integrated systems like reactive distillation columns, the question arises where to start such a design process. There are almost infinite possibilities for column configurations as the locations and size of feed streams, the catalyst distribution and others have to be taken into account.

To help alleviate these problems, a preliminary design tool called residue curves was developed by Doherty and Perkins [13, 2] initially meant for pure distillation column design. Subsequent efforts have expanded the original idea to include reaction [73] and recent efforts by Huang et al. have shown residue curves to be applicable to systems with mass transfer limitations as e.g. in reactive membrane reactors [27].

In general, residue curves or the plot of multiple residue curves into so-called residue curve maps give a good overview of both phase behavior and reaction. The interpretation of singular points helps to identify potential top and bottom products of such columns and explains in some cases why certain pure products can not be achieved. The following chapter will give a short introduction into the formulation of residue curves. The subsequent chapter will show the results obtained for the system under study.

4.1 Residue Curves

The idea behind residue curves is to answer the question of what happens to the concentration of the liquid residue in a batch reactor undergoing slow, open evaporation. For obvious reasons, the light boiling components will have a higher mole fraction in the vapor leaving the vessel and the contents of the vessel will contain an increasing fraction of high boiling components. On the other hand, reaction changes the composition in the

liquid which might increase this change or counteract it. A more general formulation of the according mass balances also includes a liquid feed stream making the model one of a continuously stirred tank reactor (CSTR):

$$\frac{dn_{tot}}{dt} = \underline{n}_{tot,in} - \underline{n}_{tot,out} + m_{cat} \sum_{r=1}^{NR} v_{tot,r} r_r^{het} + n_{tot} \sum_{r=1}^{NR} v_{tot,r} r_r^{hom} \quad (4.1)$$

$$\frac{dn_i}{dt} = \underline{n}_{i,in} - \underline{n}_{i,out} + m_{cat} \sum_{r=1}^{NR} v_{i,r} r_r^{het} + n_{tot} \sum_{r=1}^{NR} v_{i,r} r_r^{hom} \quad (4.2)$$

These are the total and component molar mass balances for such a system in which multiple reactions take place. The assumption being made is that there are heterogeneously catalyzed reactions as well as homogeneous reactions. The reaction rates of the homogeneous reactions are assumed to be proportional to the overall molar reactor content.

The concentration changes associated with the evaporation and reaction phenomena can be seen better by inserting the overall molar mass balance into the component molar mass balance:

$$\begin{aligned} n_{tot} \frac{dx_i}{dt} &= \underline{n}_{tot,in} (x_{i,in} - x_i) - \underline{n}_{tot,out} (x_{i,out} - x_i) \\ &+ m_{cat} \sum_{r=1}^{NR} (v_{i,r} - x_i v_{tot,r}) r_r^{het} + n_{tot} \sum_{r=1}^{NR} (v_{i,r} - x_i v_{tot,r}) r_r^{hom} \end{aligned} \quad (4.3)$$

The whole equation can be made dimensionless by introducing the following definition for dimensionless time

$$d\tau = \frac{\underline{n}_{tot,out}}{n_{tot}} dt \quad (4.4)$$

The result obtained when inserting this dimensionless time into Equation 4.3 is the following:

$$\begin{aligned} \frac{dx_i}{d\tau} &= \frac{\underline{n}_{tot,in}}{\underline{n}_{tot,out}} (x_{i,in} - x_i) - (x_{i,out} - x_i) \\ &+ \frac{m_{cat}}{\underline{n}_{tot,out}} \sum_{r=1}^{NR} (v_{i,r} - x_i v_{tot,r}) r_r^{het} + \frac{n_{tot}}{\underline{n}_{tot,out}} \sum_{r=1}^{NR} (v_{i,r} - x_i v_{tot,r}) r_r^{hom} \end{aligned} \quad (4.5)$$

The terms for the specific reaction rates r_j^{het} and r_j^{hom} can be split into two parts, namely the kinetic constant of the reaction and an expression containing products of activities. Since the activity expression is dependent on the reaction under study we will denote it

as α_j . The reaction terms can thus be expressed as $r_j = k_{f,j} \cdot \alpha_j$. The reaction terms were split to allow to define two dimensionless Damköhler (Da) numbers — one for the heterogeneous and one for the homogeneous reaction:

$$Da_r^{het} = \frac{m_{cat} k_{f,r}^{het}(T)}{\underline{n}_{tot,out}} \quad (4.6)$$

$$Da_r^{hom} = \frac{n_{tot} k_{f,r}^{hom}(T)}{\underline{n}_{tot,out}} \quad (4.7)$$

To be able to allow simulations with a constant Da number, it is necessary to fix the temperature for which the reaction rate constant is computed to T^{ref} which is usually chosen to be the lowest boiling point within such a system under the pressure given. Since the real boiling temperature changes during the integration, an additional correction term is needed. Besides a fixed temperature, a constant Da^{het} requires a constant outflow rate $\underline{n}_{tot,out}$ because the catalyst mass will not change during the course of the simulation.

If the homogeneous reaction is also to be simulated with a constant Da number, it is necessary to fix n_{tot} , the overall molar amount in the reactor. Fixing both the size of an outflow (to a number larger than zero) and the holdup requires a source or feed term. As the reactions are unlikely to exactly counter the outflow a feed term is needed. This is why the original equations by Ung and Doherty [73] were expanded to include the feed. The feed is now adjusted such that n_{tot} is constant over time. Since the feed should not distort the concentrations in the reactor, it is set such that its composition matches that of the reactor contents ($x_{i,in} = x_i$). Inserting these changes into Equation 4.5 leads to

$$\begin{aligned} \frac{dx_i}{d\tau} = & (x_i - x_{i,out}) + \sum_{r=1}^{NR} (v_{i,r} - x_i v_{tot,r}) Da_r^{het} \frac{k_{f,r}^{het}(T)}{k_{f,r}^{het}(T^{ref})} \alpha_r^{het} \\ & + \sum_{r=1}^{NR} (v_{i,r} - x_i v_{tot,r}) Da_r^{hom} \frac{k_{f,r}^{hom}(T)}{k_{f,r}^{hom}(T^{ref})} \alpha_r^{hom} \end{aligned} \quad (4.8)$$

This equation is valid for multiple reactions which can each be heterogeneous and / or homogeneous. It was used for the simulations presented in the following chapters.

4.2 Column Design for Cyclohexene Esterification

When designing a reactive distillation column, certain considerations should be made prior to making the extensive residue curve simulation studies needed for a detailed feasibility examination. One of these considerations lies in the pressure at which such a column will be operated later. Usually, ambient pressure operation is preferred unless there are reasons to deviate from ambient pressure.

As formic acid is not stable in contact with Amberlyst 15 at temperatures above 333 K (see Chapter 2.6.6.1 and [55]), it was decided to reduce pressure in the column to 10 kPa to enlarge the concentration range in which this criterion is met. Still some parts of the concentration range remain inadvisable for catalyst placement, as pure FCE still has a boiling point above 363 K at this pressure.

4.2.1 Residue Curve Map Studies

To allow comparing between the ambient pressure and reduced pressure residue curve maps for the non-reactive case, Figure 4.1 shows residue curve maps for 100 kPa and 10 kPa. Even though there are some quantitative differences, the qualitative behavior in both cases is very similar. As can be seen, in both cases the mixing gap is fairly limited and at both pressure levels FCE is obtained as the desired bottom product.

Since formic acid is both reactant in the reaction and catalyst, the non-reactive residue curves in Figure 4.1 are only a theoretical consideration as reaction will always take place. One practically feasible option is to carry out the reaction without the heterogeneous catalyst present. The simulation results obtained under this assumption can be seen in Figure 4.2 for four different Damköhler numbers.

As reaction rates increase with increasing Damköhler number, the stable node in the FCE corner shifts out of the corner because FCE can split into its two constituents. At low Damköhler numbers, the reaction thus counteracts the distillation effects leading to Damköhler number dependent locations of the stable node. The faster the reaction rate becomes, the further the stable node is pushed away from the corner until – at a critical

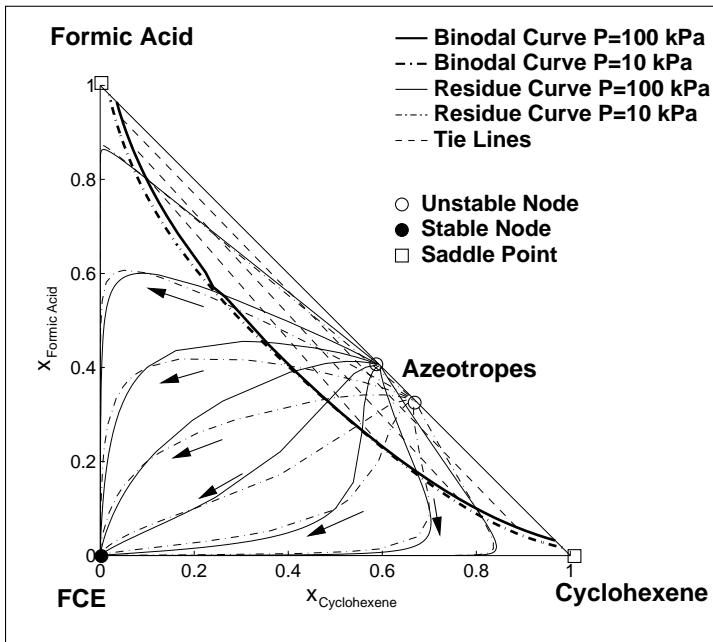


Figure 4.1: Non-reactive residue curves for cyclohexene esterification system at $P=100$ kPa and $P=10$ kPa

Damköhler number – the stable node in the FCE corner disappears altogether and formic acid is the expected bottom product.

The changing location of the stable node as a function of increasing Damköhler number can be seen in Figure 4.3. It was calculated using a one parameter continuation method. To introduce the heterogeneous reaction rate into these considerations, a further dimensionless number – the heterogeneity h – was introduced as the homogeneous reaction rate will always be present. It was defined as:

$$h = \frac{Da^{het}}{Da^{het} + Da^{hom}} \quad (4.9)$$

The ratio can be interpreted as the fraction of the overall reaction rate which can be attributed to the heterogeneous reaction at the reference point. The diagrams shown in Figure 4.2 were computed with a heterogeneous Damköhler number of $Da^{het} = 0$ and, as a result, at $h = 0$.

Since the amount of heterogeneous catalyst present throughout the residue curve computation is fixed whereas the amount of formic acid varies with location in composition space, the precise trajectories making up the residue curve map will differ slightly with different values of h . However, the computations show no visible deviation between the continuation results shown in Figure 4.3 for the shape of the stable node trajectory. Only the location on the trajectory depends on the heterogeneity. The critical Damköhler num-

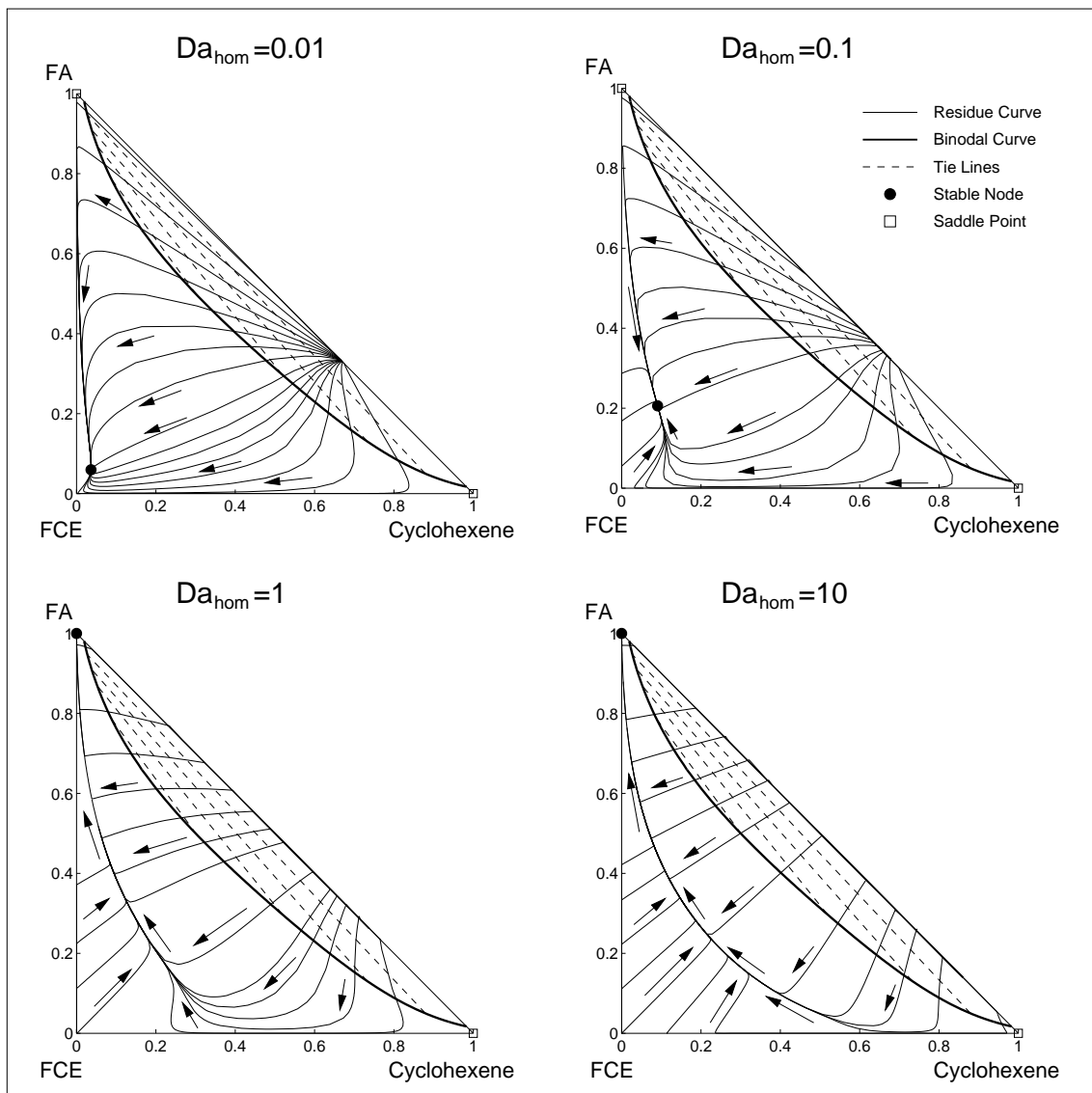


Figure 4.2: Reactive residue curve maps for cyclohexene esterification system at $P=10$ kPa and different values of the homogeneous Damköhler number

ber at which the stable node in the FCE corner disappears thus varies from 0.79 to 1.49 as h increases from 0 to 1.

4.2.2 Column Design Consequences

Figures 4.2 and 4.3 show that an ideal column configuration would need to have a very low overall Damköhler number towards the bottom of the column to allow for fairly pure FCE as the bottom product. The presence of formic acid as a homogeneous catalyst will

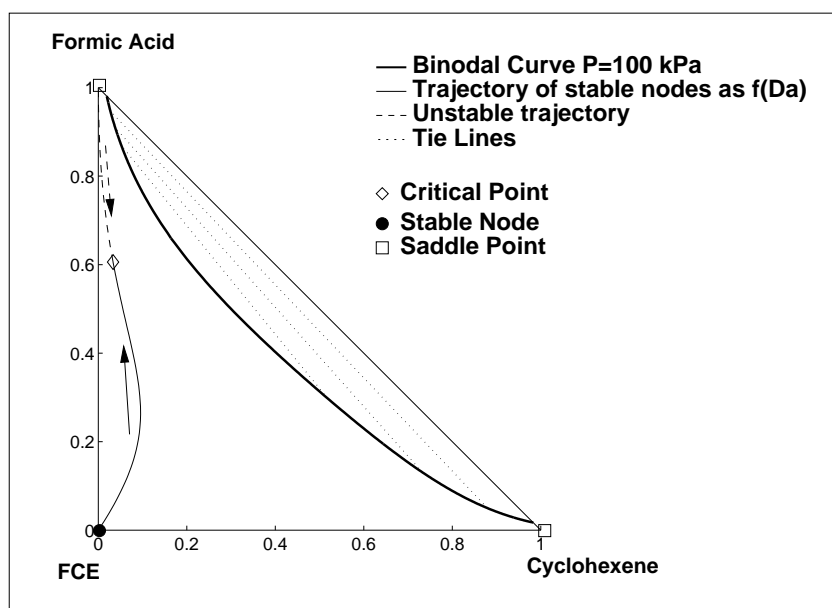


Figure 4.3: Changing location of the stable node as a function of Damköhler number for the cyclohexene esterification system at $P=10$ kPa.

not allow completely non-reactive column sections. For this reason, it is suggested not to raise the overall Damköhler number towards the bottom of the column by introducing heterogeneous catalyst.

On the other hand, column productivity depends on an appreciable amount of reaction taking place. For this reason, the top part of the column is suggested to be as reactive as possible which leads to the conclusion that this is where the heterogeneous catalyst should be placed. The length of this highly reactive section should be designed in such a way that it ends before FCE decomposition starts taking place after the reaction / separation has reached the chemical equilibrium curve as seen in the last diagram of Figure 4.2.

This catalyst placement has the additional advantage of locating the catalyst in the colder part of the column where its lifetime will be increased and where formic acid decay will not play a significant role.

Such a combined heterogeneously / homogeneously catalyzed reactive distillation column is depicted in Figure 4.4. The column concentration profiles were derived by combining two partial residue curves that were chosen such that they meet at the same concentration at the lower end of the heterogeneously catalyzed zone. The lower part of the curve was

computed at a Damköhler number of 0.001 as this part of the column is not heterogeneously catalyzed. The upper part was computed from a starting point at the cyclohexene / formic acid azeotrope which is the unstable node of the reactive residue curve map. It was computed for a Damköhler number of 1 taking the heterogeneous catalyst into account. In this case, the combined residue curve was not plotted in the usual composition space. Instead, the concentration changes along the residue curve are plotted along the column height coordinate. When considering this combined profile, the reader should

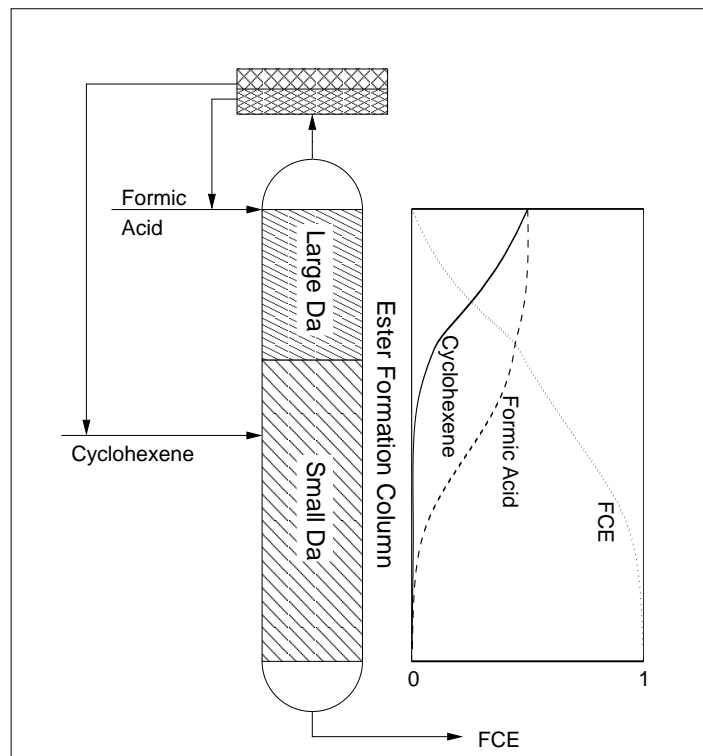


Figure 4.4: Suggested reactive distillation column configuration for cyclohexene esterification.

Shown concentration profiles are based on combined residue curve computations and do not consider feed point locations

keep in mind that residue curves only accurately describe columns of infinite length at total reflux. The placement of the feed locations for the two reactants shown in the column configuration were chosen to allow contacting the reactants in a counter-current manner. Since the concentration profiles are based on residue curve computations, naturally, they do not reflect feed point locations.

4.3 Column Design for FCE Splitting

The FCE splitting reaction system is a typical ester splitting reaction. As such, it has four reactants, namely water, formic acid (the acid), cyclohexanol (the alcohol) and FCE (the ester). As in many esterification reactions, the mixture shows significant composition ranges where liquid-liquid phase splitting occurs. The quaternary system exhibits three low boiling azeotropes: between water and cyclohexanol, between water and FCE and between cyclohexanol and FCE. Additionally, there is a high boiling azeotrope between water and formic acid and a ternary azeotrope between water, formic acid, and FCE. Furthermore, there are two binary mixing gaps.

As was the case in the cyclohexene esterification reaction, a reduced pressure of 10 kPa was chosen for carrying out the reaction to lower the range of temperatures within the column.

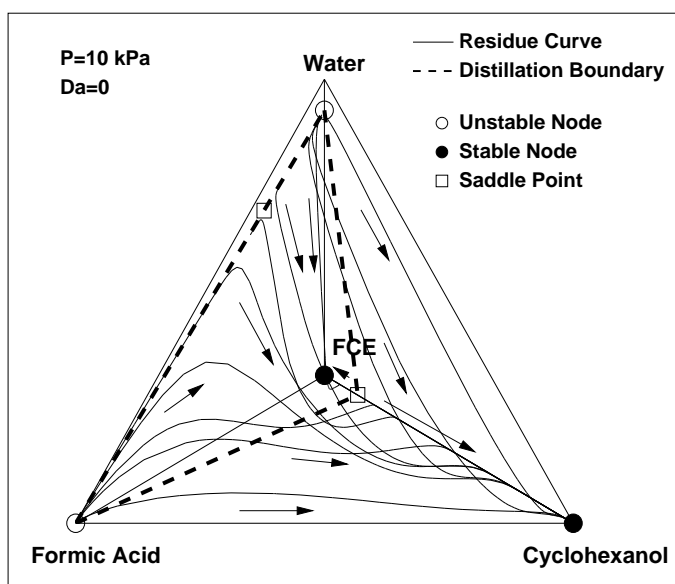
4.3.1 Residue Curve Map Studies

Formic acid and the azeotrope between water and FCE are the light boiling, unstable nodes in the reaction system. They are the potential top products of the distillation column. Since the column is also used for regaining formic acid as the reactive entrainer, formic acid would be the top product of choice given these options. The non-reactive residue curve map can be seen in Figure 4.5.

Water, the azeotrope between FCE and cyclohexanol and a ternary point consisting of FCE, water and formic acid can be seen to be saddle points within this system. Finally, there are two stable nodes at the pure cyclohexanol and FCE corners which constitute potential bottom products of the distillation. The residue curves within a small composition range above the range showing the residue curves in Figure 4.5 was omitted for presentation clarity.

The purely non-reactive distillation behavior of the system is such that it preferentially removes the two light boiling components (water and formic acid) until only a binary mixture of cyclohexanol and FCE remains. Once this binary edge of composition space has been reached, the further behavior depends on the side of the cyclohexanol / FCE

Figure 4.5: Non-reactive residue curves for the FCE splitting reaction system at $P=10$ kPa



azeotrope the system is at. As this binary azeotrope is low boiling, either one of the pure high boiling reactants (FCE or cyclohexanol) will be the bottom product of the column. From the perspective of pure cyclohexanol production, it is advantageous that the binary azeotrope is located more towards the FCE corner as this enlarges the composition range ultimately leading to pure cyclohexanol as the bottom product.

Since once again formic acid is both a reactant and a catalyst within this system, the non-reactive residue curve maps shown in Figure 4.5 are a purely theoretical simulation result. The other extreme is the case of chemical reaction equilibrium. The residue curve map for this second case can be seen in Figure 4.6. As the reaction equilibrium condition reduces the degrees of freedom of the system by one, the residue curve map is forced onto the chemical reaction equilibrium plane. Interestingly, the qualitative system behavior remains unchanged. As was the case in the non-reactive system, the two low boiling reactants water and formic acid are preferentially removed until only cyclohexanol and FCE remain. Since these two are incapable of reacting without their low boiling reaction partners, the non-reactive behavior is regained and the two components are potential bottom products.

The fact that reaction equilibrium reduces composition space to the chemical reaction equilibrium plane allows using the transformed composition variables X_i and Y_i as suggested by Barbosa [2] for a two dimensional projection of the remaining composition space which can be seen in Figure 4.7. The reference component used for calculating this

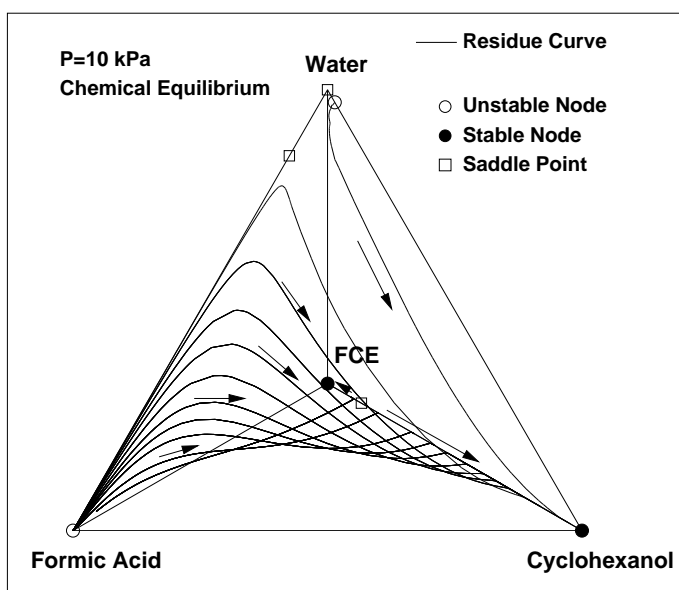


Figure 4.6: Residue curves for the FCE splitting reaction system at chemical equilibrium and $P=10$ kPa

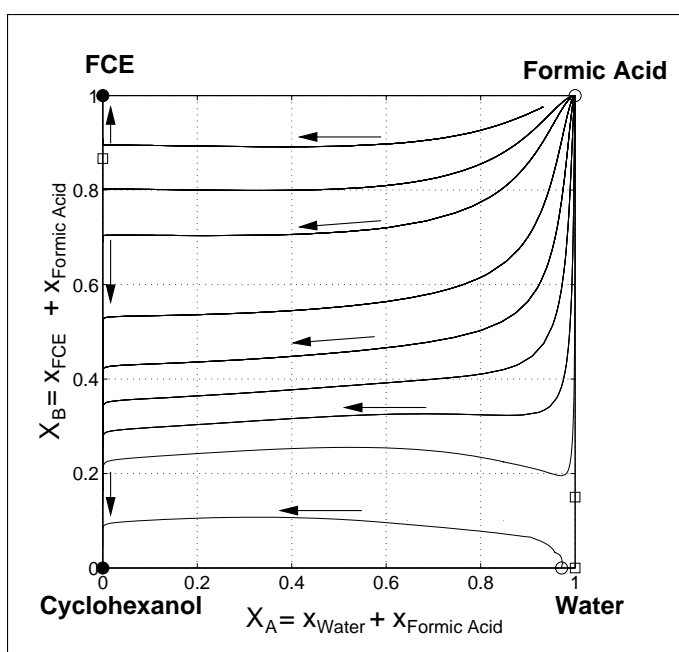


Figure 4.7: Residue curve map for the FCE splitting reaction system at chemical reaction equilibrium using transformed composition variables [2] at $P=10$ kPa

projection was chosen to be formic acid.

As can be seen in the figure the vast majority of composition space will ultimately lead to cyclohexanol as the bottom product just as it was desired. The figure also shows that a significant part of the composition space will lead to formic acid as the top product of the column. The residue curves connecting formic acid with cyclohexanol are the ideal case in which the column is fed with the reactants and produces only the pure desired products.

4.3.2 Column Design Consequences

Figure 4.7 is also an example as to why reactive residue curve maps are not always easy to interpret for column design. When deviating even slightly from the complete reflux considerations underlying the residue curve / column analogy, one can see that the residue curve starting in the water / cyclohexanol binary azeotrope and ending in the cyclohexanol corner can never be a realistic column profile. The reason for this is that when feeding the column with the reactants FCE and water and expecting cyclohexanol as the bottom product and cyclohexanol / water as the top product, the formic acid group introduced as part of the ester cannot leave the column. Obviously, such a breach of the mass balance over the complete column could never be a steady state of a real column. Thus, the restrictions with respect to the interpretation of residue curve maps have to be kept in mind when using them to consider column configurations and their feasibility.

Used carefully, residue curve maps do allow to do preliminary column design, however. When considering Figures 4.5 to 4.7, one can see that in all cases pure cyclohexanol can be achieved as the bottom product of such a column as long as the system ends on the right side of the binary azeotrope between FCE and cyclohexanol. Since this is the case for many starting compositions, attaining pure cyclohexanol as a bottom product seems to be an easy task.

However, there are several additional considerations to take into account. First, there are the fairly high boiling points found near the binary edge of composition space between FCE and cyclohexanol. At the high temperatures encountered there, even at 10 kPa formic acid would decompose at a significant rate in the presence of Amberlyst 15 as the heterogeneous catalyst. This would suggest not placing any catalyst in the lower, hotter part of the column.

Then there is the consideration of catalyst lifetime. It is known from MTBE production that Amberlyst 15 is stable below 343 K for several years within an RD column, if sufficient water is available. Even though it is specified for temperatures up to 393 K in non-aqueous media, catalyst lifetime will surely increase at lower temperatures, again suggesting catalyst placement towards the top of the column especially as the reaction mixture does contain water, reducing catalyst stability.

Finally, since catalyst amount has an influence on overall column setup costs, it should be reduced while assuring sufficient catalyst reserves to be able to compensate for catalyst deactivation during column operation. As in the cyclohexene esterification case, it should be noted that column productivity is coupled to reaction amount which is dependent on catalyst amount. This can be seen when considering that no cyclohexanol is initially introduced into the column while still expecting it as the main product.

On the other hand, inserting more catalyst into the column beyond a certain point will lead to diminishing returns on the investment and should be avoided. The determination of the economically favorable catalyst amount taking into account catalyst deactivation and unfavorable mass transfer in catalytic bales in the column will lead to a similar hybrid design as was suggested for cyclohexene esterification and which can be seen in Figure 4.8: The

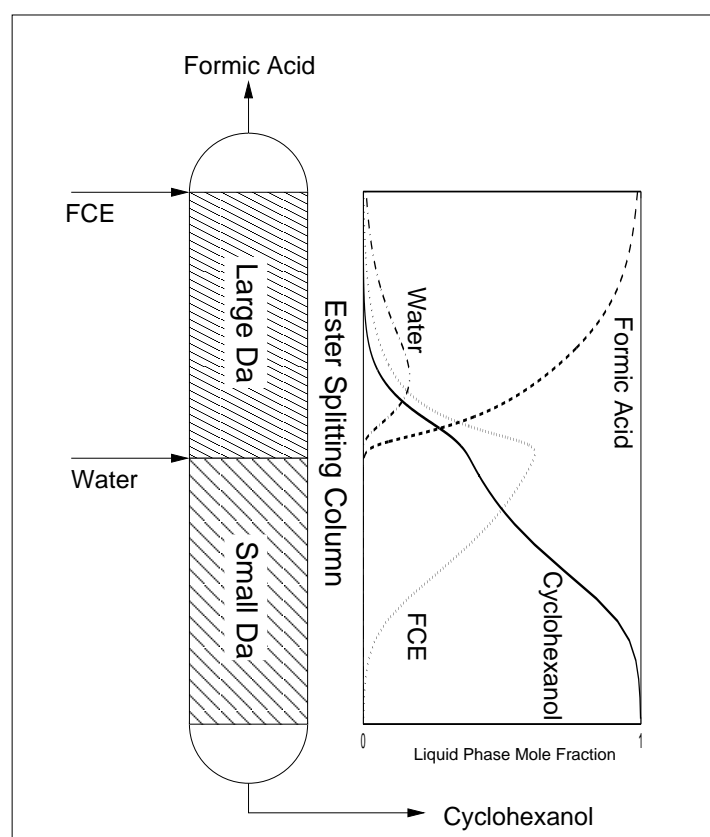


Figure 4.8: Suggested reactive distillation column configuration for FCE splitting. Shown concentration profiles are based on combined residue curve computations and do not consider feed point locations.

concentration profiles shown in the figure were again computed by combining residue curves for homogeneously and heterogeneously catalyzed column sections and plotting the composition changes along the column height coordinate. The same limitations of interpretation apply as were stated for the cyclohexene esterification case.

5 Conclusions and Outlook

As the previous chapters have shown, the two-step reactive distillation process initially proposed in Figure 1.5 seems to be a realistic option for the production of cyclohexanol from cyclohexene. Figures 4.4 and 4.8 give additional details as to the ideal configuration of the two columns involved. The overall flow sheet derived from this analysis can be seen in Figure 5.1. The basic feasibility of this configuration was demonstrated based on calculated residue curve maps and their analysis. Unless a significantly better catalyst is

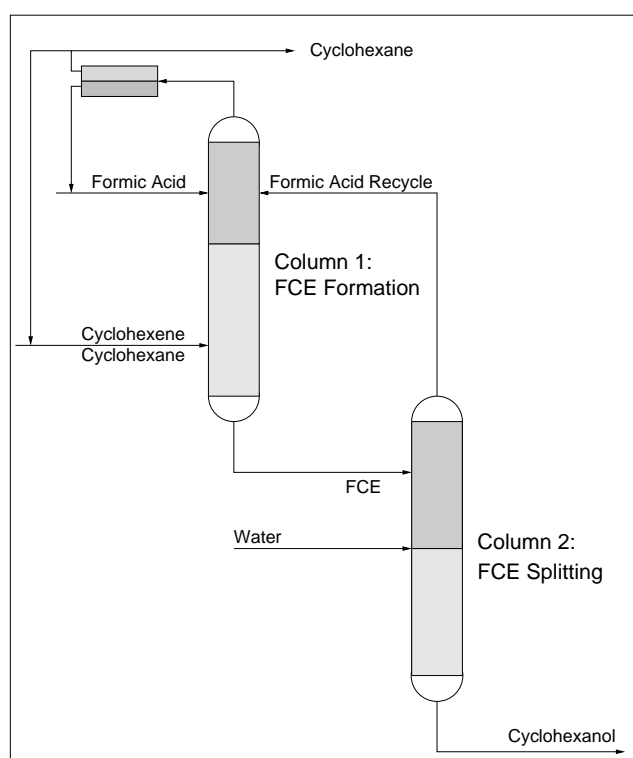


Figure 5.1: Suggested flow sheet for a new indirect cyclohexene hydration process for the production of cyclohexanol using two reactive distillation columns.

found for the direct hydration route, this seems to be an economically favorable approach as the reaction rates allow for a realistically sized plant with good productivity.

5.1 Further Work

Based on the results of this work, detailed process simulations including simulations of the individual and coupled columns have recently been carried out [31].

The results obtained so far indicate that the overall behavior of the process — especially of the ester splitting column where all reactions take place simultaneously — is challenging but stable and feasible solutions with high cyclohexanol yields have been found. It remains to be seen to what extent the liquid-liquid phase splitting behavior has to be taken into account during column simulations especially with respect to catalyst activity and differing liquid flow rates of the different phases.

From the experimental side, the column simulations have been validated by experimental data obtained from a miniplant [34]. The experiments have been carried out in a stainless steel reactive distillation mini-plant which was set up during the course of this work. As predicted by the feasibility studies presented here, FCE was readily produced in the ester formation column and split producing cyclohexanol in the ester splitting column.

It will be interesting to see to what extent fluid dynamic effects due to phase splitting lead to unexpected results. There is a strong likelihood that Amberlyst 15 as a strongly polar catalyst will prefer immersion in the polar phase which could lead to a significant reduction in catalyst efficiency. Combining simulation and experimental studies will lead to some new insights on these effects.

5.2 Process Variations

An alternative use of the first column and the ester formation within it could lie in a highly selective separation of cyclohexene from cyclohexane and benzene similar to the one suggested for the separation isobutene from its isomers by Stein et al. [60]. Cyclohexene, cyclohexane and benzene can be expected to be part of any partial hydrogenation reactor

outlet (e.g. to produce cyclohexene). As they share a very similar boiling point, their separation by direct distillation would be fairly difficult.

If such a separation is desired, one would operate a second column just like the ester formation column but in reverse, feeding FCE and regaining formic acid and pure cyclohexene. Cyclohexane and benzene would leave the process at the top of the ester formation column and will not be present in the second column due to the fact that the FCE at the bottom of the first column will contain practically no cyclohexane or benzene due to the high difference in boiling point.

A step towards further integrating the reaction and separation steps currently being carried out in two separate columns as shown in Figure 5.1 could be to integrate both reactions into one column. The suggested configuration can be seen in Figure 5.2. From an academic standpoint, such an integrated column is an interesting challenge. There is no obvious thermodynamic or reaction kinetic reason that would rule out such an overall configuration. When looking at the overall flow sheet, the “ideal” column configuration suggested in Figure 1.3 in the Introduction (Chapter 1.1) is regained — with a more complex internal structure, two catalysts and numerous additional azeotropes and phase splitting challenges.

Whether such a highly integrated process can work in a practical production setting and whether this has significant advantages when compared with the two column solution remains to be seen. The hardware costs of the one column solution would seem to be lower and only one column would need heating and cooling.

Finally, there seems to be some motivation for looking into the use of acetic acid as the reactive entrainer instead of using formic acid as was done in this work. Some simple preliminary tests in this direction have been carried out as part of this work as mentioned in Chapter 2.6.6.1. At the time these experiments were carried out, the higher reaction rates of formic versus acetic acid suggested using formic acid as the reactive entrainer. This choice was made after having been forced to abandon the direct hydration route due to its reaction kinetic limitations.

When taking into account the limited stability of formic acid in the presence of Am-

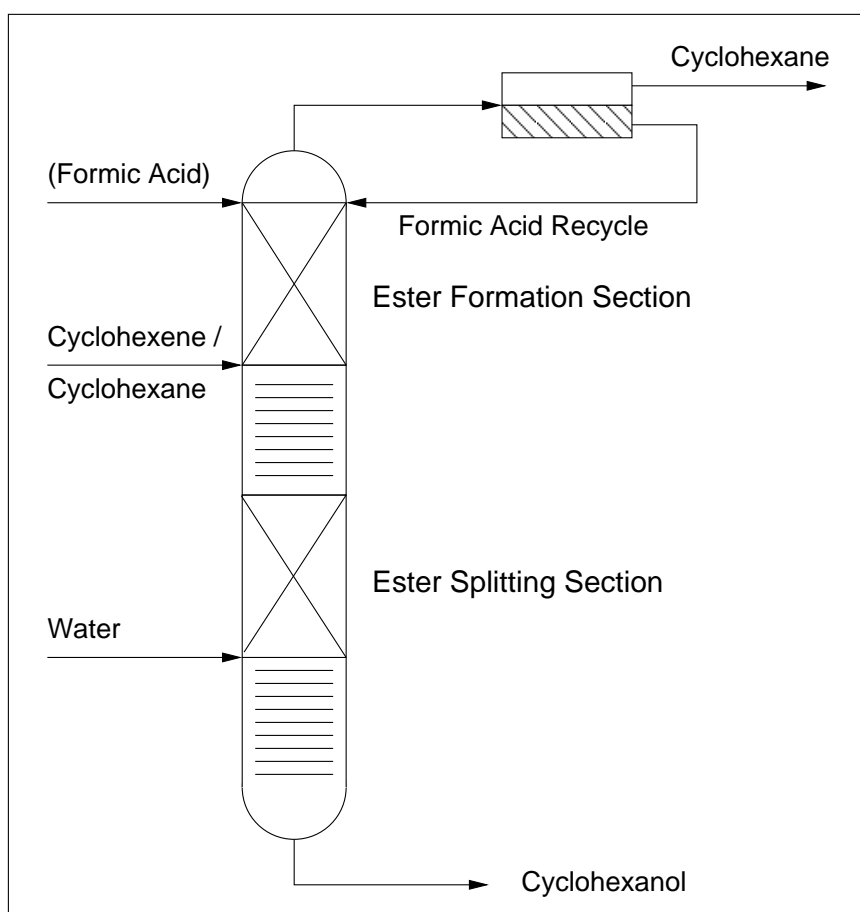


Figure 5.2: Column integrating both reaction steps into one column with two catalytic zones. Formic acid as the reactive entrainer is trapped in the column and only needs to be replenished to compensate for losses.

berlyst 15, the high boiling azeotrope between water and formic acid, the very similar boiling points of FCE and cyclohexanol and their azeotrope, and the very aggressive nature of formic acid, it might seem justified to review this a priori decision. An additional factor could be the lower price of acetic acid even though little acid is consumed during the process.

Bibliography

- [1] K. Adachi, H. Suga, and S. Seki. Phase changes in crystalline and glassy-crystalline cyclohexanol. *Bull. Chem. Soc. Japan*, 41:1073–1087, 1968.
- [2] D. Barbosa and M.F. Doherty. Design and minimum-reflux calculations for single-feed multicomponent reactive distillation columns. *Chem. Eng. Sci.*, 43:1523–1537, 1988.
- [3] A. F. M. Barton and A. S. Kertes, editors. *Alcohols with Water*, volume 15 of *IUPAC-NIST Solubility Data Series*. Pergamon Press: Oxford, 1984.
- [4] J. Bausa and W. Marquardt. Quick and reliable phase stability test in VLLE flash calculations by homotopy continuation. *Comput. Chem. Eng.*, 24:2447–2456, 2000.
- [5] C.W. Beckett, N.K. Freeman, and K.S. Pitzer. The thermodynamic properties and molecular structure of cyclopentene and cyclohexene. *J. Am. Chem. Soc.*, 70:4227–4230, 1948.
- [6] A. Behr et al. *Winnacker · KÜCHLER Chemische Technik*, volume 5, chapter Cyclohexanol und Cyclohexanon., pages 70–74. Wiley-VCH: Weinheim, 2005.
- [7] A. Behr, M. Urschey, and V.A. Brehme. Aqueous biphasic catalysis as a powerful tool for catalyst recycling in telomerization and hydrogenation chemistry. *Green Chem.*, 5:198–204, 2003.
- [8] S. Brüggemann, J. Oldenburg, P. Zhang, and W. Marquardt. Robust dynamic simulation of three-phase reactive batch distillation columns. *Ind. Eng. Chem. Res.*, 43:3672–3684, 2003.

- [9] C. J. P. Bélisle. Convergence theorems for a class of simulated annealing algorithms on Rd. *J. Appl. Probab.*, 29:885–895, 1992.
- [10] J. Chao and B.J. Zwolinski. Ideal-gas thermodynamic properties of methanoic and ethanoic acids. *J. Phys. Chem. Ref. Data*, 7:363–377, 1978.
- [11] M.W. Chase. NIST-JANAF thermochemical tables, fourth edition. *J. Phys. Chem. Ref. Data*, pages 1–1951, 1998.
- [12] J.D. Cox, D.D. Wagman, and V.A. Medvedev. *CODATA Key Values for Thermodynamics*. Hemisphere Publishing Corp., New York, 1984.
- [13] M.F. Doherty and J.D. Perkins. On the dynamics of distillation processes – I. the simple distillation of multicomponent non-reacting, homogeneous liquid mixture. *Chem. Eng. Sci.*, 33:281–301, 1978.
- [14] S.-J. Dong, Q.-J. Chi, B. Saha, and M.M. Sharma. Esterification of formic acid, acrylic acid and methacrylic acid with cyclohexene in batch and distillation column reactors: ion-exchange resins as catalysts. *Reac. Func. Polym.*, 28:263–278, 1996.
- [15] S.-J. Dong, Q.-J. Chi, B. Saha, and M.M. Sharma. Esterification of formic acid, acrylic acid and methacrylic acid with cyclohexene in batch and distillation column reactors: Ion-exchange resins as catalysts. *React. Funct. Polym.*, 28:263–278, 1996.
- [16] T. Frey and J. Stichlmair. Review. thermodynamic fundamentals of reactive distillation. *Chem. Eng. Technol.*, 22:11–18, 1999.
- [17] J. Gangadwala, A. Kienle, E. Stein, and S. Mahajani. Production of butyl acetate by catalytic distillation: Process design studies. *Ind. Eng. Chem. Res.*, 43:136–143, 2004.
- [18] M.M. Gilburd, F.B. Moin, Y.A. Pazderskii, V.D. Zadvorniyak, and B.N. Yurkevich. Liquid-vapor phase-equilibrium in the water-formic acid system at elevated pressures. *J. Appl. Chem. USSR*, 57:851–852, 1984.
- [19] J. Gmehling, J. Menke, J. Krafczyk, and K. Fischer. *Azeotropic Data*. Wiley-VCH: Weinheim, 1st edition, 1994.

- [20] J.Ya. Gorodetsky and V.M. Olevsky. Vapor-liquid equilibrium data collection: Tables and diagrams of data of binary and multicomponent mixtures up to moderate pressures. In J. Gmehling, U. Onken, and W. Arlt, editors, *Part I: Aqueous-Organic Systems*, page 514. DECHEMA: Frankfurt am Main, 1991.
- [21] S. Grüner, K.-D. Mohl, A. Kienle, E.-D. Gilles, G. Fernholz, and M. Friedrich. Nonlinear control of a reactive distillation column. *Contr. Eng. Pract.*, 11:915–925, 2003.
- [22] Z.H. Gumus and A.R. Ciric. Reactive distillation column design with vapour/liquid/liquid equilibria. *Comput. Chem. Eng.*, 21(Suppl.):S983–S988, 1997.
- [23] J.P. Guthrie. Hydration of carboxamines. evaluation of the free energy change for addition of water to acetamide and formamide derivatives. *J. Am. Chem. Soc.*, 96:3608–3615, 1974.
- [24] J. M. Harrison and L. Berg. Vapor-liquid equilibria of binary hydrocarbon systems. *Ind. Eng. Chem.*, 38:117–120, 1946.
- [25] A. Higler, R. Krishna, and R. Taylor. Nonequilibrium modeling of reactive distillation: A dusty fluid model for heterogeneously catalyzed processes. *Ind. Eng. Chem. Res.*, 39:1596–1607, 2000.
- [26] A. Higler, R. Taylor, and R. Krishna. Modeling of a reactive separation process using a nonequilibrium stage model. *Comput. Chem. Eng.*, 22:S111–S118, 1998.
- [27] Y.-S. Huang, K. Sundmacher, Z. Qi, and E.-U. Schlünder. Residue curve maps of reactive membrane separation. *Chem. Eng. Sci.*, 59:2863–2879, 2004.
- [28] H. Ishida, Y. Fukuoka, O. Mitsui, and M. Kono. Liquid-phase hydration of cyclohexene with highly siliceous zeolites. *Stud. Surf. Sci. Catal.*, 83:473–480, 1994.
- [29] M. Ivanova, Z. Qi, E.U. Schlünder, and K. Sundmacher. Analysis of potential singular point surface of reactive stripping processes. *Chem. Eng. Sci.*, 61:1901–1912, 2006.

- [30] R.J. Jakobsen, Y. Mikawa, and J.W. Brasch. Far infrared studies of hydrogen bonding in carboxylic acids. I. Formic and acetic acids. *Spectrochim. Acta Part A*, 23:2199–2209, 1967.
- [31] A. Katariya, H. Freund, and K. Sundmacher. Two-step reactive distillation process for cyclohexanol production from cyclohexene. *Ind. Eng. Chem. Res.*, 48:9534–9545, 2009.
- [32] D. Kondepudi and I. Prigogine. *Modern Thermodynamics: From Heat Engines to Dissipative Structures*. Wiley: Chichester, 1998.
- [33] A.A. Kozyro, A.V. Blokhin, G.J. Kabo, and Y.U. Paulechka. Thermodynamic properties of some cyclohexyl esters in the condensed state. *J. Chem. Thermodynamics*, 33:305–331, 2001.
- [34] R. Kumar, A. Katariya, H. Freund, and K. Sundmacher. Development of a novel reactive distillation process for cyclohexanol production: Mini plant experiments. In *GPE-EPIC - 2nd International Congress on Green Process Engineering - 2nd European Process Intensification Conference, Venice, Italy, 2009*.
- [35] P.J. Linstrom and W.G. Mallard, editors. *NIST Chemistry WebBook, NIST Standard Reference Database*, volume 69. National Institute of Standards and Technology, Gaithersburg MD, (<http://webbook.nist.gov/chemistry/>), July 2001.
- [36] S. Löning, C. Horst, and U. Hoffmann. Theoretical investigations on the quaternary system n-butanol, butyl acetate, acetic acid and water. *Chem. Eng. Tech.*, 23:789–794, 2000.
- [37] G.T.P. Mabande, G. Pradhan, W. Schwieger, M. Hanebuth, R. Dittmeyer, T. Selvam, A. Zampieri, H. Baser, and R. Herrmann. A study of Silicalite-1 and Al-ZSM-5 membrane synthesis on stainless steel supports. *Micropor. Mesopor. Mater.*, 75:209–220, 2004.
- [38] C.M. McDonald and C.A. Floudas. GLOPEQ: A new computational tool for the phase and chemical equilibrium problem. *Comput. Chem. Eng.*, 21:1–23, 1997.

- [39] J. Mesnage and A. A. Marsan. Vapor-liquid equilibrium at atmospheric pressure. *J. Chem. Eng. Data*, 16:434–439, 1971.
- [40] N. Metropolis, A. W. Rosenbluth, and A. H. Teller. Equation of state calculations by fast computer machines. *J. Chem. Phys.*, 21:1087–1092, 1953.
- [41] M.L. Michelsen. The isothermal flash problem. Part I. stability. *Fluid Phase Equilibria*, 9:1–19, 1982.
- [42] O. Mitsui and Y. Fukuoka. Process for producing cyclic alcohol. United States Patent 4,588,846, 1986.
- [43] K.-D. Mohl, A. Kienle, E.-D. Gilles, P. Rapmund, K. Sundmacher, and U. Hoffmann. Steady-state multiplicities in reactive distillation columns for the production of fuel ethers MTBE and TAME: theoretical analysis and experimental verification. *Chem. Eng. Sci.*, 54:1029–1043, 1999.
- [44] K.D. Mohl, A. Kienle, E.D. Gilles, P. Rapmund, K. Sundmacher, and U. Hoffmann. Nonlinear dynamics of reactive distillation processes for the production of fuel ethers. *Comput. Chem. Eng.*, 21(Suppl.):S989–S994, 1997.
- [45] T.M. Musser. *Industrial Organic Chemicals: Starting Materials and Intermediates*, volume 10, ullmann’s encyclopedia Cyclohexanol and Cyclohexanone., pages 279–290. Wiley-VCH: Weinheim, 2003.
- [46] H.-J. Panneman and A.A.C.M. Beenackers. Solvent effects in the liquid phase hydration of cyclohexene catalyzed by a macroporous strong acid ion exchange resin. *Chem. Eng. Sci.*, 47:2635–2640, 1992.
- [47] Y.U. Paulechka, D.H. Zaitsau, and G.J. Kabo. On the difference between isobaric and isochoric heat capacities of liquid cyclohexyl esters. *J. Mol. Liq.*, 115:105–111, 2004.
- [48] H.N. Pham and M.F. Doherty. Design and synthesis of heterogeneous azeotropic distillations I. Heterogeneous phase diagrams. *Chem. Eng. Sci.*, 45:1823–1836, 1990.

- [49] Z.W. Qi, A. Kolah, and K. Sundmacher. Residue curve maps for reactive distillation systems with liquid-phase splitting. *Chem. Eng. Sci.*, 57:163–175, 2002.
- [50] I. Rechenberg. *Evolutionsstrategie '94*. Frommann-Holzboog, Stuttgart, 1994.
- [51] F. Reepmeyer, J.-U. Repke, and G. Wozny. Time optimal start-up strategies for reactive distillation columns. *Chem. Eng. Sci.*, 59:4339–4347, 2004.
- [52] A. Rehfinger. *Reaktionstechnische Untersuchungen zur Flüssigphasensynthese von Methyl-tert.-butylether (MTBE) an einem starksauren makroporösen Ionenaustauscherharz als Katalysator*. PhD thesis, Clausthal Technical University, Clausthal-Zellerfeld, Germany, 1988.
- [53] H. Renon and J. M. Prausnitz. Local compositions in thermodynamic excess functions for liquid mixtures. *AIChE J.*, 14:135–144, 1968.
- [54] J.-U. Repke and G. Wozny. Experimental investigations of three-phase distillation in a packed column. *Chem. Eng. Tech.*, 25:513–519, 2002.
- [55] W. Reutemann and H. Kieczka. *Industrial Organic Chemicals: Starting Materials and Intermediates*, volume 5, Ullmann's encyclopedia, Formic Acid, page 2713. Wiley-VCH, Weinheim, 1999.
- [56] C. A. Schnepfer and M. A. Stadtherr. Robust process simulation using interval methods. *Comput. Chem. Eng.*, 20:187–199, 1996.
- [57] B. Seliger. Inbetriebnahme eines Versuchstands und Vermessung erster reaktionskinetischer Parameter im Stoffsystem Wasser / Cyclohexanol / Cyclohexen. Master's thesis, Otto-von-Guericke University, Magdeburg, Germany, 2003.
- [58] D. G. Shaw and A. S. Kertes, editors. *Hydrocarbons with Water and Seawater*, volume 37, Part I of *IUPAC-NIST Solubility Data Series*. Pergamon Press: Oxford, 1989.
- [59] W.V. Steele, R.D. Chirico, S.E. Knipmeyer, A. Nguyen, N.K. Smith, and I.R. Tasker. Thermodynamic properties and ideal-gas enthalpies of formation for cyclohexene,

- (2,5-dihydrobenzo-3,4-furan), isoxazole, octylamine, dioctylamine, trioctylamine, phenyl isocyanate, and 1,4,5,6-tetrahydropyrimidine. *J. Chem. Eng. Data*, 41:1269–1284, 1996.
- [60] E. Stein, A. Kienle, and K. Sundmacher. Separation using coupled reactive distillation columns. *Chem. Eng.*, 107:68–72, 2000.
- [61] H. Stephen and T. Stephen, editors. *Solubilities of inorganic and Organic Compounds*, volume 1, Part I. Pergamon Press: Oxford, 1963.
- [62] F. Steyer, D. Flockerzi, and K. Sundmacher. Equilibrium and rate-based approaches to liquid-liquid phase splitting calculations. *Comput. Chem. Eng.*, 30:277–284, 2005.
- [63] F. Steyer, H.-J. Freund, and K. Sundmacher. A novel reactive distillation process for the indirect hydration of cyclohexene to cyclohexanol using a reactive entrainer. *Ind. Eng. Chem. Res.*, 47:9581–9587, 2008.
- [64] F. Steyer, Z. Qi, and K. Sundmacher. Synthesis of cyclohexanol by three-phase reactive distillation: influence of kinetics on phase equilibria. *Chem. Eng. Sci.*, 57:1511–1520, 2002.
- [65] F. Steyer and K. Sundmacher. VLE and LLE data for the system cyclohexane + cyclohexene + water + cyclohexanol. *J. Chem. Eng. Data*, 49:1675–1681, 2004.
- [66] F. Steyer and K. Sundmacher. VLE and LLE dataset for the system cyclohexane + cyclohexene + water + cyclohexanol + formic acid + formic acid cyclohexyl ester. *J. Chem. Eng. Data*, 50:1277–1282, 2005.
- [67] F. Steyer and K. Sundmacher. Cyclohexanol production via esterification of cyclohexene with formic acid and subsequent hydration of the ester — reaction kinetics. *Ind. Eng. Chem. Res.*, 46:1099–1104, 2007.
- [68] K. Sundmacher and U. Hoffmann. Multicomponent mass and energy transport on different length scales in a packed reactive distillation column for heterogeneously catalyzed fuel ether production. *Chem. Eng. Sci.*, 49:4443–4464, 1994.

- [69] S. Takagi. Pt. 1 : Aqueous-organic systems. In J. Gmehling, U. Onken, and W. Arlt, editors, *Vapor-Liquid Equilibrium Data Collection: Tables and Diagrams of Data of Binary and Multicomponent Mixtures up to Moderate Pressures.*, page 17. DECHEMA: Frankfurt am Main, 1991.
- [70] S.R. Tessier, J.F. Brennecke, and M.A. Stadtherr. Reliable phase stability analysis for excess Gibbs energy models. *Chem. Eng. Sci.*, 55:1785–1796, 2000.
- [71] E.K. Tunik and V.T. Zharov. Pt. 1 : Aqueous-organic systems. In J. Gmehling, U. Onken, and W. Arlt, editors, *Vapor-Liquid Equilibrium Data Collection: Tables and Diagrams of Data of Binary and Multicomponent Mixtures up to Moderate Pressures.*, page 18. DECHEMA: Frankfurt am Main, 1991.
- [72] S. P. Tunik, T.M. Lesteva, and V. I. Chernaya. Phase equilibria in the water-alcohols-formaldehyde systems. I. The liquid-vapour equilibria in the systems water — C6 and C7 alcohols. *Russ. J. Phys. Chem.*, 51:751, 1977.
- [73] S. Ung and M.F. Doherty. Synthesis of reactive distillation systems with multiple equilibrium chemical reactions. *Ind. Eng. Chem. Res.*, 34:2555–2565, 1995.
- [74] J.M. van Baten, J. Ellenberger, and R. Krishna. Hydrodynamics of reactive distillation tray column with catalyst containing envelopes: experiments vs. cfd simulations. *Catal. Today*, 66:233–240, 2001.
- [75] VDI. *VDI Wärmeatlas*. Springer: Berlin, 1997.
- [76] J.E.S. Venart. Flixborough: The explosion and its aftermath. *Process Saf. Environ. Prot.*, 82:105, 2004.
- [77] G. Venimadhavan, M.F. Malone, and M.F. Doherty. A novel distillate policy for batch reactive distillation with application to the production of butyl acetate. *Ind. Eng. Chem. Res.*, 38:714–722, 1999.
- [78] E.Q. Wang, C.Y. Li, L.Y. Wen, and E. Min. Study on suspension catalytic distillation for synthesis of linear alkylbenzene. *AIChE J.*, 51:845–853, 2005.

-
- [79] P.B. Weisz and C.D. Prater. Interpretation of experiments in experimental catalysis. *Adv. Catal.*, 6:143–196, 1954.
- [80] K.B. Wiberg, D.J. Wassermann, E.J. Martin, and M.A. Murcko. Enthalpies of hydration of alkenes. 3. Cycloalkenes. *J. Am Chem. Soc.*, 107:6019–6022, 1985.
- [81] H. Zhang, S.M. Mahajani, M.M. Sharma, and T. Sridhar. Hydration of cyclohexene with solid acid catalysts. *Chem. Eng. Sci.*, 57:315–322, 2002.
- [82] L. K. Zharikov, K. S. Krylova, G. M. Kopylevich, N. K. Tikhonova, G. K. Oparina, and L. A. Serafimov. Phase equilibria in systems water-aniline, water-cyclohexanol, ethanol-aniline, and ethanol-cyclohexanol. *J. Appl. Chem. USSR*, 48:1306–1308, 1975.
- [83] Y. Zhicai, C. Xianbao, and G. Jing. Esterification-distillation of butanol and acetic acid. *Chem. Eng. Sci.*, 53:2081–2088, 1998.
- [84] H.H.Y. Ünveren and R. Schomäcker. Hydroformylation with rhodium phosphine-modified catalyst in a microemulsion: comparison of organic and aqueous systems for styrene, cyclohexene and 1,4-diacetoxy-2-butene. *Catal. Lett.*, 102:83–89, 2005.

Appendices

A GC Measurement Method

method: H:\DATEN\AGIGC208\METHODS\OLD\7MIX.M
Modified on: 11/12/2003 at 11:33:33 PM

Method Information

Method: H:\DATEN\AGIGC208\METHODS\OLD\7MIX.M
Modified: 11/12/2003 at 11:33:33 PM

Method to demo HP 6890 parameter editing for Split/Splitless & Purged Packed inlets plus FID and TCD. This method is for the purpose of OFFLINE demos only!

In order to load this method use the macro "6890demo.mac" or copy the file 'IQ1.MTH' from this methods' subdirectory to the instrument subdirectory and rename it 'IQ1.cfg'. The method can then be loaded and will show appropriate parameters.

Method Audit Trail

Operator : Steyer
Date : 10.10.2002 14:26:54
Change Info:

Operator : Seliger
Date : 10.10.2002 15:54:39
Change Info:

Operator : Seliger
Date : 11.10.2002 10:29:13
Change Info:

Operator : Seliger
Date : 11.10.2002 10:32:22
Change Info:

Operator : Seliger
Date : 11.10.2002 10:34:40
Change Info:

Operator : Seliger
Date : 11.10.2002 10:38:55
Change Info:

Operator : Seliger
Date : 11.10.2002 13:08:07
Change Info:

Operator : Seliger
Date : 11.10.2002 13:19:07
Change Info:

Operator : Seliger
Date : 11.10.2002 13:35:14
Change Info:

Operator : Seliger
Date : 17.10.2002 12:46:31

Instrument 1 12/21/2009 8:29:01 AM ikert

method: H:\DATEN\AGIGC208\METHODS\OLD\7MIX.M
Modified on: 11/12/2003 at 11:33:33 PM
Change Info:

Operator : Stein
Date : 14.11.2002 14:52:33
Change Info:

Operator : Stein
Date : 15.11.2002 11:30:35
Change Info:

Operator : Stein
Date : 19.11.2002 12:39:26
Change Info:

Operator : Stein
Date : 19.11.2002 13:01:11
Change Info:

Operator : Stein
Date : 19.11.2002 13:04:26
Change Info:

Operator : Stein
Date : 20.11.2002 11:16:33
Change Info:

Operator : Stein
Date : 26.03.2003 14:40:09
Change Info: 1:100 Splitt

Operator : Seliger
Date : 09.04.2003 14:12:32
Change Info:

Operator : Seliger
Date : 09.04.2003 14:56:10
Change Info:

Operator : Seliger
Date : 16.04.2003 10:46:48
Change Info:

Operator : Wasan
Date : 12.05.2003 11:15:49
Change Info:

Operator : steyer
Date : 26.05.2003 15:18:32
Change Info: This method was created at 26.05.2003 15:18:32 and based on
method H:\DATEN\AGIGC208\METHODS\5MIX.M

Operator : steyer
Date : 26.05.2003 15:18:34
Change Info:

Operator : steyer
Date : 26.05.2003 15:20:00
Change Info:

method: H:\DATEN\AGIGC208\METHODS\OLD\7MIX.M
Modified on: 11/12/2003 at 11:33:33 PM
Operator : steyer
Date : 26.05.2003 17:36:37
Change Info:

Operator : steyer
Date : 27.05.2003 10:22:44
Change Info:

Operator : steyer
Date : 28.05.2003 14:13:42
Change Info:

Operator : steyer
Date : 02.06.2003 10:18:43
Change Info:

Operator : steyer
Date : 02.06.2003 17:09:07
Change Info:

Operator : steyer
Date : 02.06.2003 18:29:07
Change Info:

Operator : steyer
Date : 03.06.2003 08:14:16
Change Info:

Operator : steyer
Date : 04.06.2003 15:30:46
Change Info:

Operator : Stein
Date : 06.06.2003 13:59:24
Change Info:

Operator : Stein
Date : 06.06.2003 16:48:47
Change Info:

Operator : Seliger
Date : 30.06.2003 14:55:56
Change Info:

Operator : Steyer
Date : 16.07.2003 16:59:59
Change Info:

Operator : Steyer
Date : 16.07.2003 17:16:12
Change Info:

Operator : Huang
Date : 08.08.2003 09:15:48
Change Info:

Operator : Felsch
Date : 09.09.2003 08:19:09

method: H:\DATEN\AGIGC208\METHODS\OLD\7MIX.M
Modified on: 11/12/2003 at 11:33:33 PM
Change Info:

Operator : Felsch
Date : 19.09.2003 17:21:21
Change Info:

Operator : Steyer
Date : 12.11.2003 14:33:33
Change Info:

Run Time Checklist

Pre-Run Cmd/Macro: off
Data Acquisition: on
Standard Data Analysis: on
Customized Data Analysis: off
Save GLP Data: off
Post-Run Cmd/Macro: off
Save Method with Data: off

Injection Source and Location

Injection Source: GC Injector
Injection Location: Front

=====
6890 GC METHOD
=====

OVEN

Initial temp: 50 'C (On) Maximum temp: 260 'C
Initial time: 2.00 min Equilibration time: 0.00 min
Ramps:
 # Rate Final temp Final time
 1 50.00 130 3.90
 2 0.0(Off)
Post temp: 0 'C
Post time: 0.00 min
Run time: 7.50 min

FRONT INLET (SPLIT/SPLITLESS) BACK INLET (UNKNOWN)
Mode: Split
Initial temp: 210 'C (On)
Pressure: 108.4 kPa (On)
Split ratio: 100:1
Split flow: 142.0 mL/min

method: H:\DATEN\AGIGC208\METHODS\OLD\7MIX.M
Modified on: 11/12/2003 at 11:33:33 PM
Total flow: 145.9 mL/min
Gas saver: On
Saver flow: 20.0 mL/min
Saver time: 2.00 min
Gas type: Helium

COLUMN 1
Capillary Column
Model Number: HP 19091N-133
HP-INNOWax Polyethylene Glycol
Max temperature: 260 'C
Nominal length: 30.0 m
Nominal diameter: 250.00 um
Nominal film thickness: 0.25 um
Mode: constant flow
Initial flow: 1.4 mL/min
Nominal init pressure: 108.4 kPa
Average velocity: 33 cm/sec
Inlet: Front Inlet
Outlet: Front Detector
Outlet pressure: ambient

COLUMN 2
(not installed)

FRONT DETECTOR (FID)
Temperature: 250 'C (On)
Hydrogen flow: 40.0 mL/min (On)
Air flow: 450.0 mL/min (On)
Mode: Constant makeup flow
Makeup flow: 45.0 mL/min (On)
Makeup Gas Type: Helium
Flame: On
Electrometer: On
Lit offset: 2.0

BACK DETECTOR (TCD)
Temperature: 250 'C (On)
Reference flow: 20.0 mL/min (On)
Mode: Constant makeup flow
Makeup flow: 7.0 mL/min (On)
Makeup Gas Type: Helium
Filament: On
Negative polarity: Off

SIGNAL 1
Data rate: 20 Hz
Type: front detector
Save Data: On
Zero: 5.0 (Off)
Range: 0
Fast Peaks: Off
Attenuation: 0

SIGNAL 2
Data rate: 20 Hz
Type: back detector
Save Data: On
Zero: 0.0 (Off)
Range: 0
Fast Peaks: Off
Attenuation: 0

COLUMN COMP 1
Derive from front detector

COLUMN COMP 2
Derive from back detector

POST RUN
Post Time: 0.00 min

TIME TABLE
Time Specifier Parameter & Setpoint

GC Injector

Front Injector:
Sample Washes 2
Sample Pumps 3

method: H:\DATEN\AGIGC208\METHODS\OLD\7MIX.M

Modified on: 11/12/2003 at 11:33:33 PM

Injection Volume	1.00 microliters
Syringe Size	5.0 microliters
PreInj Solvent A Washes	0
PreInj Solvent B Washes	0
PostInj Solvent A Washes	4
PostInj Solvent B Washes	4
Viscosity Delay	7 seconds
Plunger Speed	Fast
PreInjection Dwell	0.00 minutes
PostInjection Dwell	0.00 minutes
Sampling Depth	-2.0 mm

Back Injector:

No parameters specified

method: H:\DATEN\AGIGC208\METHODS\OLD\7MIX.M
 Modified on: 11/12/2003 at 11:33:33 PM

=====
 Integration Events
 =====

 Non signal specific Integration Events

Event	Value
Tangent Skim Mode	Standard

 Default Integration Event Table "Event"

Event	Value	Time
Initial Slope Sensitivity	1.000	Initial
Initial Peak Width	0.040	Initial
Initial Area Reject	1.000	Initial
Initial Height Reject	1.700	Initial
Initial Shoulders	OFF	Initial

 Detector Default Integration Event Table "Event_ADC"

Event	Value	Time
Initial Slope Sensitivity	20.000	Initial
Initial Peak Width	0.040	Initial
Initial Area Reject	1.000	Initial
Initial Height Reject	1.000	Initial
Initial Shoulders	OFF	Initial

 Detector Default Integration Event Table "Event_ECD"

Event	Value	Time
Initial Slope Sensitivity	100.000	Initial
Initial Peak Width	0.080	Initial
Initial Area Reject	1.000	Initial
Initial Height Reject	1.000	Initial
Initial Shoulders	OFF	Initial

method: H:\DATEN\AGIGC208\METHODS\OLD\7MIX.M
Modified on: 11/12/2003 at 11:33:33 PM

Detector Default Integration Event Table "Event_NPD"

Event	Value	Time
Initial Slope Sensitivity	500.000	Initial
Initial Peak Width	0.040	Initial
Initial Area Reject	1.000	Initial
Initial Height Reject	1.000	Initial
Initial Shoulders	OFF	Initial

Detector Default Integration Event Table "Event_FPD"

Event	Value	Time
Initial Slope Sensitivity	50.000	Initial
Initial Peak Width	0.040	Initial
Initial Area Reject	1.000	Initial
Initial Height Reject	1.000	Initial
Initial Shoulders	OFF	Initial

Detector Default Integration Event Table "Event_uECD"

Event	Value	Time
Initial Slope Sensitivity	500.000	Initial
Initial Peak Width	0.080	Initial
Initial Area Reject	1.000	Initial
Initial Height Reject	1.000	Initial
Initial Shoulders	OFF	Initial

Detector Default Integration Event Table "Event_TCD"

Event	Value	Time
Initial Slope Sensitivity	100.000	Initial
Initial Peak Width	0.040	Initial
Initial Area Reject	1.000	Initial
Initial Height Reject	1.000	Initial
Initial Shoulders	OFF	Initial

method: H:\DATEN\AGIGC208\METHODS\OLD\7MIX.M
Modified on: 11/12/2003 at 11:33:33 PM

Detector Default Integration Event Table "Event_FID"

Event	Value	Time
Initial Slope Sensitivity	50.000	Initial
Initial Peak Width	0.040	Initial
Initial Area Reject	1.000	Initial
Initial Height Reject	1.000	Initial
Initial Shoulders	OFF	Initial

Signal Specific Integration Event Table "Event_FID1A"

Event	Value	Time
Initial Slope Sensitivity	1.738	Initial
Initial Peak Width	0.025	Initial
Initial Area Reject	0.215	Initial
Initial Height Reject	10.000	Initial
Initial Shoulders	OFF	Initial
Baseline at Valleys	ON	1.200

Signal Specific Integration Event Table "Event_TCD2B"

Event	Value	Time
Initial Slope Sensitivity	28.705	Initial
Initial Peak Width	0.022	Initial
Initial Area Reject	2.576	Initial
Initial Height Reject	0.973	Initial
Initial Shoulders	OFF	Initial
Area Sum	ON	3.100
Area Sum	OFF	3.500

Apply Manual Integration Events: No

=====
Calibration Table
=====

Calib. Data Modified : 08.09.2003 13:25:01

Rel. Reference Window : 5.000 %
Abs. Reference Window : 0.000 min
Rel. Non-ref. Window : 5.000 %
Abs. Non-ref. Window : 0.000 min
Uncalibrated Peaks : not reported
Partial Calibration : No recalibration if peaks missing

Curve Type : Linear

method: H:\DATEN\AGIGC208\METHODS\OLD\7MIX.M

Modified on: 11/12/2003 at 11:33:33 PM

Origin : Forced
Weight : Equal

Recalibration Settings:

Average Response : Average all calibrations
Average Retention Time: Floating Average New 75%

Calibration Report Options :

Printout of recalibrations within a sequence:
Calibration Table after Recalibration
Normal Report after Recalibration
If the sequence is done with bracketing:
Results of first cycle (ending previous bracket)

Signal 1: FID1 A,

Signal 2: TCD2 B,

RetTime	Lvl	Amount	Area	Amt/Area	Ref Grp Name
[min]	Sig	[nmol]			
1.583	2 16	1.29400e-1	5.36984	2.40976e-2	Cyclohexan
	15	2.58900e-1	10.41057	2.48690e-2	
	14	4.86000e-1	10.52336	4.61830e-2	
	13	1.18150	23.43576	5.04144e-2	
	12	2.32500	43.36783	5.36112e-2	
	11	4.78700	93.29000	5.13131e-2	
	10	10.52800	205.80048	5.11563e-2	
	9	18.53600	336.87350	5.50236e-2	
	1	92.68100	1833.91028	5.05374e-2	
	7	185.36000	3509.82227	5.28118e-2	
1.624	1 18	3.07500e-2	13.48548	2.28023e-3	Cyclohexan
	17	3.69110e-2	22.54941	1.63689e-3	
	16	1.29400e-1	61.03391	2.12013e-3	
	15	2.58900e-1	152.61090	1.69647e-3	
	14	4.86000e-1	273.07867	1.77971e-3	
	13	1.18150	630.26703	1.87460e-3	
	12	2.32500	1255.54907	1.85178e-3	
	11	4.78740	2777.41040	1.72369e-3	
	10	10.52850	6288.39795	1.67427e-3	
	9	18.53600	1.02981e4	1.79994e-3	
	1	92.68100	5.60650e4	1.65310e-3	
	7	185.36000	1.10242e5	1.68139e-3	
1.857	1 18	3.07500e-2	7.39448	4.15851e-3	Cyclohexen
	17	3.69100e-2	12.75023	2.89485e-3	
	16	1.29400e-1	39.69197	3.26011e-3	
	15	2.58900e-1	103.28600	2.50663e-3	
	14	4.86000e-1	219.53000	2.21382e-3	
	13	1.18150	523.28300	2.25786e-3	
	12	2.32500	1104.67000	2.10470e-3	
	11	4.78700	3324.27588	1.44001e-3	
	10	10.52800	6561.87598	1.60442e-3	
	9	18.53600	1.03958e4	1.78302e-3	
	1	98.60000	5.75300e4	1.71389e-3	
	6	197.20000	1.15347e5	1.70963e-3	
1.899	2 15	2.58900e-1	5.14646	5.03064e-2	Cyclohexen
	14	4.86000e-1	8.08664	6.00991e-2	
	13	1.18100	16.14398	7.31542e-2	
	12	2.32500	31.79327	7.31287e-2	

method: H:\DATEN\AGIGC208\METHODS\OLD\7MIX.M
 Modified on: 11/12/2003 at 11:33:33 PM

RetTime [min]	Lvl Sig	Amount [nmol]	Area	Amt/Area	Ref Grp Name	
11		4.78700	133.69771	3.58047e-2		
10		10.52800	223.98242	4.70037e-2		
9		18.53600	338.68277	5.47297e-2		
1		98.60000	1881.90759	5.23936e-2		
6		197.20000	3715.37744	5.30767e-2		
2.532	1	10	56.06700	1.24923e4	4.48814e-3	Isopropanol
		11	96.26400	2.15502e4	4.46696e-3	
		12	113.50500	2.55590e4	4.44091e-3	
		13	121.51100	2.70950e4	4.48462e-3	
		14	126.38000	2.80325e4	4.50834e-3	
		15	127.97000	2.85716e4	4.47892e-3	
		16	128.87760	2.88230e4	4.47134e-3	
		17	129.52500	2.89925e4	4.46753e-3	
		18	129.56800	2.90703e4	4.45706e-3	
		1	129.78000	2.89763e4	4.47884e-3	
		8	259.57000	5.72096e4	4.53718e-3	
2.540	2	10	56.06700	780.50311	7.18344e-2	Isopropanol
		11	96.26400	1348.11694	7.14063e-2	
		12	113.50500	1603.72266	7.07760e-2	
		13	121.51100	1698.48242	7.15409e-2	
		14	126.38000	1763.14868	7.16786e-2	
		15	127.97000	1795.54883	7.12707e-2	
		16	128.88000	1812.18091	7.11187e-2	
		17	129.52500	1826.32959	7.09209e-2	
		18	129.56800	1823.56311	7.10521e-2	
		1	129.78000	1838.91333	7.05743e-2	
		8	259.57000	3591.75806	7.22682e-2	
3.301	2	18	7.70000e-3	9.24949	8.32478e-4	Wasser
		17	9.24200e-3	6.81576	1.35597e-3	
		16	3.24000e-2	7.49050	4.32548e-3	
		15	6.48000e-2	2.71380	2.38780e-2	
		14	1.21700e-1	8.03460	1.51470e-2	
		13	2.95800e-1	11.50298	2.57151e-2	
		12	5.82200e-1	10.96830	5.30802e-2	
		11	1.19880	15.07476	7.95237e-2	
		10	2.63633	20.26961	1.30063e-1	
		9	4.65130	25.03505	1.85792e-1	
		1	555.56000	2645.68470	2.09987e-1	
		4	1111.10000	5290.11523	2.10033e-1	
4.677	2	16	1.29480e-1	4.43405	2.92013e-2	ACE
		15	2.59000e-1	7.24988	3.57247e-2	
		14	4.86300e-1	13.63005	3.56785e-2	
		13	1.18200	31.77195	3.72026e-2	
		12	2.32600	58.33202	3.98752e-2	
		11	4.79000	117.90058	4.06275e-2	
		10	10.53400	269.63208	3.90681e-2	
		9	18.54600	485.98349	3.81618e-2	
		1	77.96900	1898.92603	4.10595e-2	
		3	155.94000	3768.10596	4.13842e-2	
4.750	1	18	3.07700e-2	17.35130	1.77335e-3	ACE
		17	3.69300e-2	35.86851	1.02959e-3	
		16	1.29476e-1	113.77967	1.13795e-3	
		15	2.59000e-1	208.99777	1.23925e-3	
		14	4.86300e-1	375.77814	1.29411e-3	
		13	1.18200	878.72644	1.34513e-3	

method: H:\DATEN\AGIGC208\METHODS\OLD\7MIX.M

Modified on: 11/12/2003 at 11:33:33 PM

RetTime [min]	Lvl Sig	Amount [nmol]	Area	Amt/Area	Ref Grp Name
		12 2.32600	1606.09106	1.44824e-3	
		11 4.78990	3286.36572	1.45751e-3	
		10 10.53400	7495.43506	1.40539e-3	
		9 18.54600	1.34929e4	1.37450e-3	
		1 77.96900	5.20329e4	1.49845e-3	
		3 155.94000	1.04371e5	1.49409e-3	
5.147	1 18	5.33400e-2	25.46947	2.09427e-3	Cyclohexanol
		17 6.40300e-2	53.58487	1.19493e-3	
		16 2.24484e-1	170.28719	1.31827e-3	
		15 4.49000e-1	310.51953	1.44596e-3	
		14 8.43100e-1	562.06146	1.50001e-3	
		13 2.05000	1313.39758	1.56084e-3	
		12 4.03330	2401.13525	1.67975e-3	
		11 8.30470	4901.24512	1.69441e-3	
		10 18.26400	1.11694e4	1.63518e-3	
		9 32.15500	2.01337e4	1.59707e-3	
		1 93.85000	5.69441e4	1.64811e-3	
		2 187.70000	1.17260e5	1.60071e-3	
5.162	2 16	2.24480e-1	6.60958	3.39628e-2	Cyclohexanol
		15 4.49000e-1	9.91586	4.52810e-2	
		14 8.43100e-1	18.46092	4.56695e-2	
		13 2.05000	42.07404	4.87236e-2	
		12 4.03300	77.19681	5.22431e-2	
		11 8.30500	159.38667	5.21060e-2	
		10 18.26400	363.66867	5.02215e-2	
		9 32.15500	657.81793	4.88813e-2	
		1 93.85000	1892.34949	4.95944e-2	
		2 187.70000	3873.94507	4.84519e-2	
6.045	2 10	3.48150	3.38421	1.02875	Ameisensäure
		9 6.12950	19.23995	3.18582e-1	
		1 265.04000	2531.39502	1.04701e-1	
		5 530.09000	5216.38770	1.01620e-1	

More compound-specific settings:

Compound: Cyclohexan

Time Window : From 1.499 min To 1.749 min

Compound: Cyclohexan

Time Window : From 1.549 min To 1.799 min

Compound: Cyclohexen

Time Window : From 1.800 min To 1.996 min

Compound: Cyclohexen

Time Window : From 1.800 min To 2.028 min

Compound: Isopropanol

Time Window : From 2.383 min To 2.595 min

Compound: Isopropanol

Time Window : From 2.384 min To 2.604 min

Compound: Wasser

Time Window : From 2.834 min To 3.734 min

method: H:\DATEN\AGIGC208\METHODS\OLD\7MIX.M
Modified on: 11/12/2003 at 11:33:33 PM

Compound: ACE
Time Window : From 4.426 min To 4.845 min

Compound: ACE
Time Window : From 4.510 min To 4.931 min

Compound: Cyclohexanol
Time Window : From 4.846 min To 5.450 min

Compound: Cyclohexanol
Time Window : From 4.849 min To 5.400 min

Compound: Ameisensäure
Time Window : From 5.500 min To 6.612 min

1 Warnings or Errors :

Warning : Overlapping peak time windows at 4.75 min, signal 1

=====
Peak Sum Table
=====

No Entries in table
=====

=====
Sample related custom fields
=====

Custom Field	Type	Mand.	Default Value

None defined			

=====
Compound related custom fields
=====

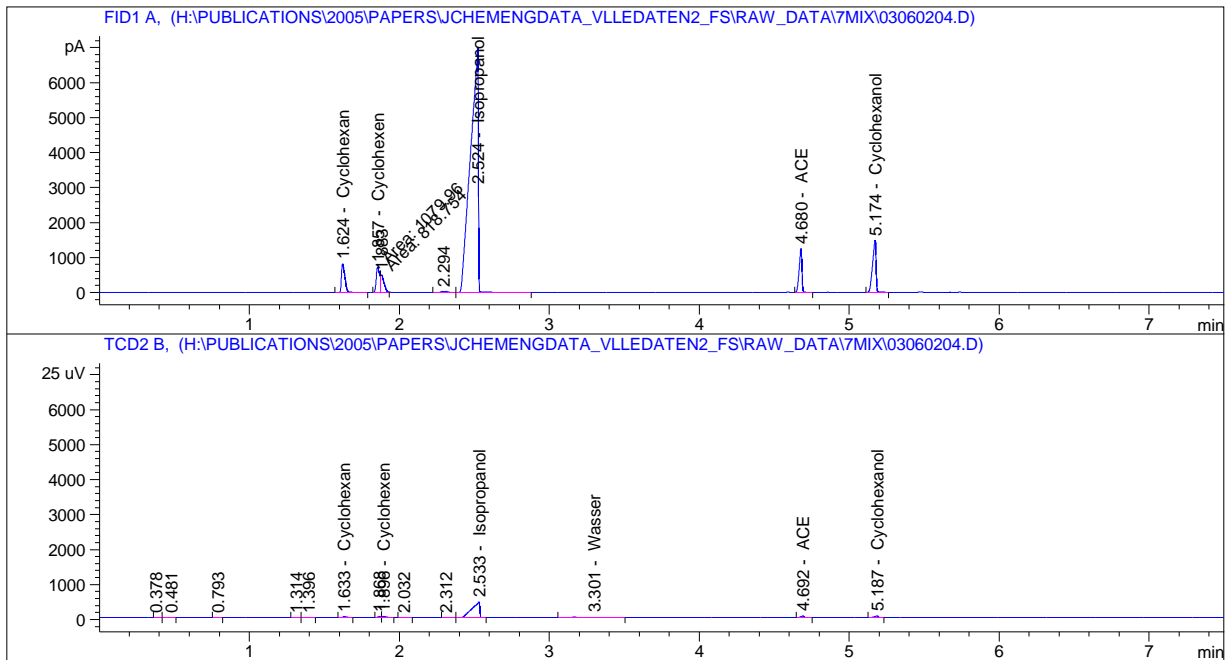
Custom Field	Type	Mand.	Default Value

None defined			

B Sample Chromatogram

=====
Acq. Operator : fan Seq. Line : 4
Acq. Instrument : Instrument 1 Location : Vial 29
Injection Date : 02.06.2003 13:42:03 Inj : 1
Inj Volume : 1 µl
Acq. Method : H:\DATEN\AGIGC208\METHODS\7MIX.M
Last changed : 6/2/2003 7:18:43 PM by steyer
Analysis Method : H:\DATEN\AGIGC208\METHODS\OLD\7MIX.M
Last changed : 12/21/2009 8:37:32 AM by ikert
(modified after loading)
Method Info : Method to demo HP 6890 parameter editing for Split/Splitless & Purged
Packed inlets plus FID and TCD. This method is for the purpose of OFFLINE
demos only!

In order to load this method use the macro "6890demo.mac" or copy the file
'IQ1.MTH' from this methods' subdirectory to the instrument subdirectory
and rename it 'IQ1.cfg'. The method can then be loaded
and will show appropriate parameters.



=====
External Standard Report
=====

Sorted By : Signal
Calib. Data Modified : 08.09.2003 13:25:01
Multiplier: : 1.0000
Dilution: : 1.0000
Use Multiplier & Dilution Factor with ISTDs

Signal 1: FID1 A,

RetTime [min]	Type	Area [pA*s]	Amt/Area	Amount [nmol]	Grp	Name
1.624	BB	1255.54919	1.67661e-3	2.10507		Cyclohexan
1.857	MF	1079.96094	1.71061e-3	1.84739		Cyclohexen
2.524	BB	2.55590e4	4.49426e-3	114.86859		Isopropanol
4.680	BB	1606.09180	1.49311e-3	2.39808		ACE
5.174	BB	2401.13550	1.61000e-3	3.86582		Cyclohexanol

Totals : 125.08496

Signal 2: TCD2 B,

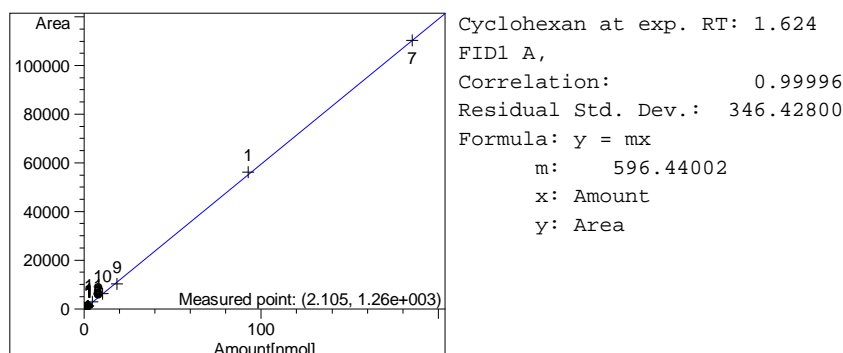
RetTime [min]	Type	Area [25 uV*s]	Amt/Area	Amount [nmol]	Grp	Name
1.633	VV	43.36860	5.23572e-2	2.27066		Cyclohexan
1.896	VB	54.68837	5.29259e-2	2.89443		Cyclohexen
2.533	VV	1603.72241	7.15103e-2	114.68261		Isopropanol
3.301	VVA+	29.81979	2.10022e-1	6.26283		Wasser
4.692	VB	58.33168	4.12712e-2	2.40742		ACE
5.187	BB	77.19748	4.86978e-2	3.75935		Cyclohexanol
6.045		-	-	-		Ameisensäure

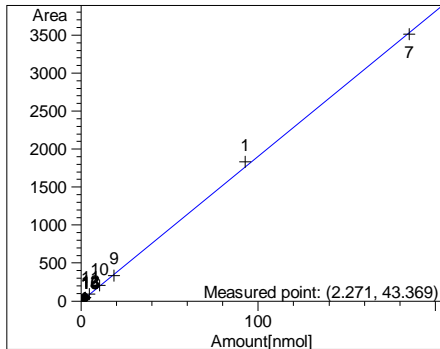
Totals : 132.27729

3 Warnings or Errors :

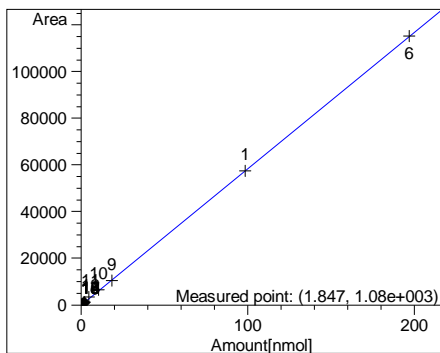
- Warning : Calibration warnings (see calibration table listing)
- Warning : Calibrated compound(s) not found
- Warning : Elution order of calibrated compounds may have changed

=====
 Calibration Curves
 =====

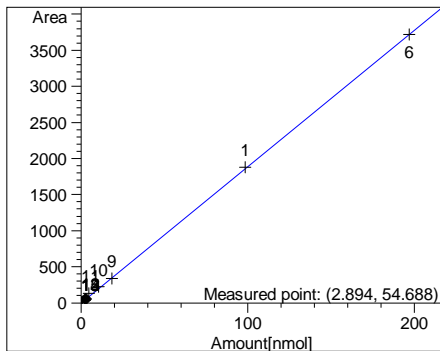




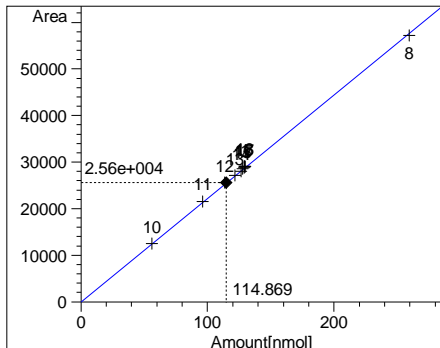
Cyclohexan at exp. RT: 1.583
 TCD2 B,
 Correlation: 0.99983
 Residual Std. Dev.: 24.38935
 Formula: $y = mx$
 m: 19.09959
 x: Amount
 y: Area



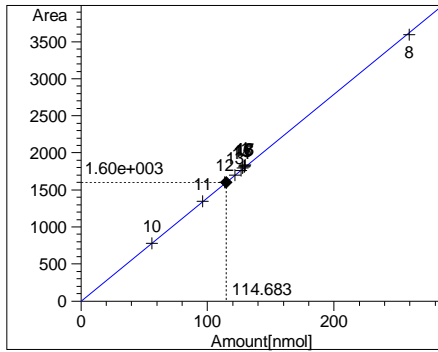
Cyclohexen at exp. RT: 1.857
 FID1 A,
 Correlation: 0.99998
 Residual Std. Dev.: 261.70889
 Formula: $y = mx$
 m: 584.58639
 x: Amount
 y: Area



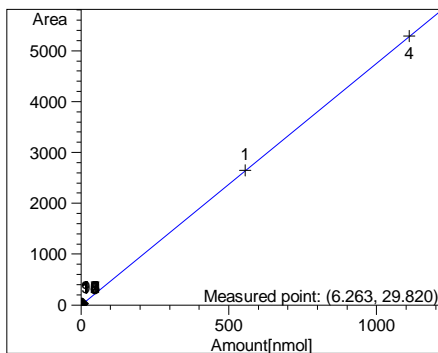
Cyclohexen at exp. RT: 1.899
 TCD2 B,
 Correlation: 0.99991
 Residual Std. Dev.: 20.27579
 Formula: $y = mx$
 m: 18.89433
 x: Amount
 y: Area



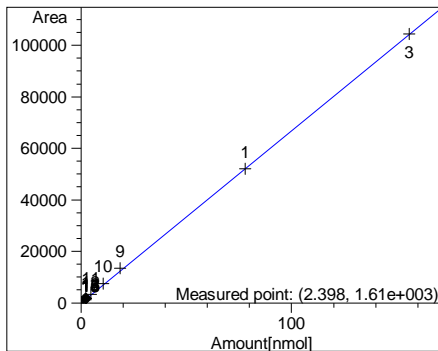
Isopropanol at exp. RT: 2.532
 FID1 A,
 Correlation: 0.99997
 Residual Std. Dev.: 234.01937
 Formula: $y = mx$
 m: 222.50602
 x: Amount
 y: Area



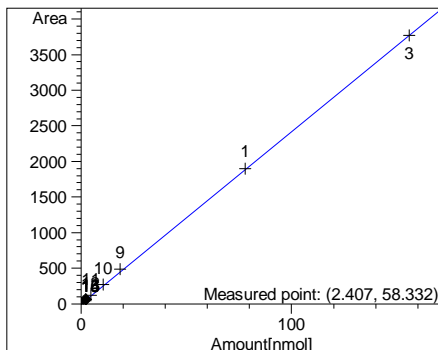
Isopropanol at exp. RT: 2.540
 TCD2 B,
 Correlation: 0.99996
 Residual Std. Dev.: 16.82755
 Formula: $y = mx$
 m: 13.98401
 x: Amount
 y: Area



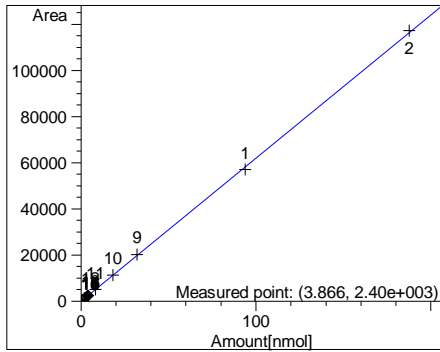
Wasser at exp. RT: 3.301
 TCD2 B,
 Correlation: 0.99999
 Residual Std. Dev.: 7.20415
 Formula: $y = mx$
 m: 4.76140
 x: Amount
 y: Area



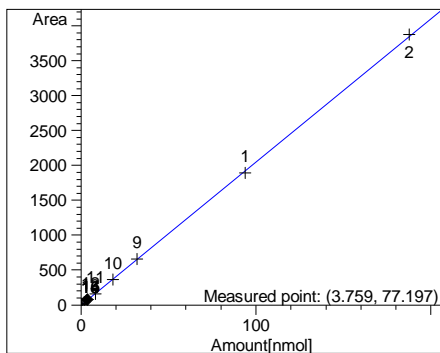
ACE at exp. RT: 4.750
 FID1 A,
 Correlation: 0.99995
 Residual Std. Dev.: 357.12371
 Formula: $y = mx$
 m: 669.74191
 x: Amount
 y: Area



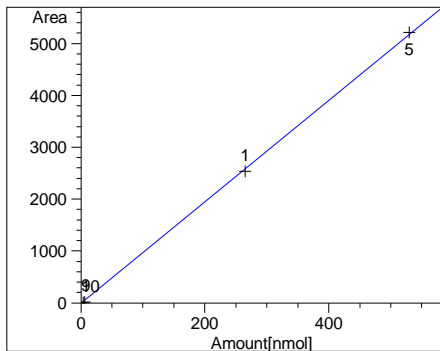
ACE at exp. RT: 4.677
 TCD2 B,
 Correlation: 0.99995
 Residual Std. Dev.: 14.03246
 Formula: $y = mx$
 m: 24.22997
 x: Amount
 y: Area



Cyclohexanol at exp. RT: 5.147
FID1 A,
Correlation: 0.99993
Residual Std. Dev.: 468.34115
Formula: $y = mx$
m: 621.11865
x: Amount
y: Area



Cyclohexanol at exp. RT: 5.162
TCD2 B,
Correlation: 0.99995
Residual Std. Dev.: 14.50703
Formula: $y = mx$
m: 20.53482
x: Amount
y: Area



Ameisensäure at exp. RT: 6.045
TCD2 B,
Correlation: 0.99989
Residual Std. Dev.: 49.36709
Formula: $y = mx$
m: 9.78164
x: Amount
y: Area

=====
*** End of Report ***

C Own Publications

Peer reviewed full papers:

- F. Steyer, Z. Qi, and K. Sundmacher. Synthesis of cyclohexanol by three-phase reactive distillation: influence of kinetics on phase equilibria. *Chem. Eng. Sci.*, 57:1511-1520, 2002.
- F. Steyer and K. Sundmacher. VLE and LLE data for the system cyclohexane + cyclohexene + water + cyclohexanol. *J. Chem. Eng. Data*, 49:1675-1681, 2004.
- F. Steyer and K. Sundmacher. VLE and LLE dataset for the system cyclohexane + cyclohexene + water + cyclohexanol + formic acid + formic acid cyclohexyl ester. *J. Chem. Eng. Data*, 50:1277-1282, 2005.
- F. Steyer, D. Flockerzi, and K. Sundmacher. Equilibrium and rate-based approaches to liquid-liquid phase splitting calculations. *Comput. Chem. Eng.*, 30:277-284, 2005.
- F. Steyer and K. Sundmacher. Cyclohexanol production via esterification of cyclohexene with formic acid and subsequent hydration of the ester — reaction kinetics. *Ind. Eng. Chem. Res.*, 46:1099-1104, 2007.
- F. Steyer, H.-J. Freund, and K. Sundmacher. A novel reactive distillation process for the indirect hydration of cyclohexene to cyclohexanol using a reactive entrainer. *Ind. Eng. Chem. Res.*, 47:9581-9587, 2008.

Public Oral Presentations:

- F. Steyer, Z. Qi, and K. Sundmacher. Synthesis of cyclohexanol by three-phase reactive distillation : kinetics and phase equilibria. *ISMR-2 (International symposium on multifunctional reactors)*, Nuremberg, Germany, June 26-28, 2001.
- F. Steyer, Z. Qi, and K. Sundmacher. Selective Separation by Reactive Distillation Applied to Close Boiling Mixtures Undergoing Phase Splitting. *ACHEMA 2003*, Frankfurt am Main, Germany, May 19-24, 2003.
- F. Steyer, H. Freund, and K. Sundmacher. Einsatz eines reaktiven Entrainers zur Synthese von Cyclohexanol in einem Prozess gekoppelter Reaktivdestillationskolonnen. *GVC/DECHEMA-Jahrestagungen*, Wiesbaden, Germany, September 26-28, 2006. Also appeared in: *Chemie Ingenieur Technik* 78/9:1200, 2006.

Contributions to Posters and Oral Presentations:

- G. Radulescu, J. Gangadwala, A. Kienle, F. Steyer, and K. Sundmacher. Dynamic Simulation of Reactive Distillation Processes with Liquid-Liquid Phase Splitting. *5th International Symposium on Process Control*, Ploiesti, Romania, May 18-19, 2006.
- J. Gangadwala, G. Radulescu, A. Kienle, F. Steyer, and K. Sundmacher. New Process for Recovery of Acetic Acid from Waste Water. *(Oral) 17th International Congress of Chemical and Process Engineering*, Prague, Czech Republic, August 27-31, 2006.
- M. Ivanova, Z. Qi, F. Steyer, P. Aghalayam, S. Mahajani, and K. Sundmacher. Coupling of Chemical Reactions in a Reactive Distillation Process. *(Poster) 6th International Symposium on Catalysis in Multiphase Reactors (CAMURE-6) and 5th International Symposium on Multifunctional Reactors (ISMR-5)*, Pune, India, January 14-17, 2007.

- H. Freund, A. Katariya, R. Kumar, F. Steyer, and K. Sundmacher. Application of Catalytic Distillation in a Novel Process Concept for the Production of Cyclohexanol. (*Poster*) *DGMK International Conference*, Hamburg, Germany, October 10-12, 2007.
- A. Katariya, F. Steyer, H. Freund, and K. Sundmacher. Process Intensification in Cyclohexanol Production: A Novel Integrated Process Scheme. (*Oral*) *18th International Congress of Chemical and Process Engineering CHISA 2008*, Prague, Czech Republic, August 24-29, 2008.

D Lebenslauf

Persönliche Angaben

Name: Frank Steyer
Geboren am: 27.02.1974
Familienstand: verheiratet

Berufserfahrung

seit 10/2005: Gründer und Geschäftsführer metraTec GmbH (2005 als ADEMICS Sensor Technology GmbH gegründet).

Ausbildung

05/2000 - 09/2005: Doktorand am Max-Planck-Institut für Dynamik komplexer technischer Systeme, Magdeburg. Thema: Reaktivdestillation und Phasenzерfall.
10/1993 - 05/2000: Technische Universität Berlin. Abschluss: Dipl.-Ing. Verfahrens- und Energietechnik (sehr gut).
09/1998 - 05/1999: Stanford University, USA. Abschluss: Master of Industrial Engineering and Engineering Management.
08/1984 - 06/1993: Johanneum zu Lübeck. Abschluss: Abitur (Jahrgangsbester).
02/1981 - 07/1984: Montclair Elementary School, USA (Englisch als zweite Muttersprache).
08/1980 - 02/1981: Janusz-Korczak-Schule, Göttingen.